

AD625179

Prepared under  
DSR 8841  
Project NR 083-157  
Office of Naval Research

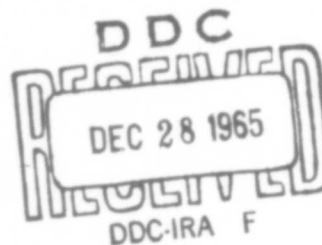
## ION FRACTIONATION IN DROPS FROM BREAKING BUBBLES

by

Ferren MacIntyre

CLEARINGHOUSE FOR FEDERAL SCIENTIFIC AND TECHNICAL INFORMATION			
Hardcopy	Microfiche	275	as
\$6.00	\$1.50	pp	
ARCHIVE COPY			

Department of Chemistry *Code 1*  
Massachusetts Institute of Technology  
Cambridge, Massachusetts 02139



September 1965

ION FRACTIONATION IN DROPS FROM BREAKING BUBBLES

by

Ferren MacIntyre

B.A.  
University of California at Riverside  
(1960)

SUBMITTED IN PARTIAL FULFILLMENT OF THE  
REQUIREMENTS FOR THE DEGREE OF  
DOCTOR OF PHILOSOPHY

at the

MASSACHUSETTS INSTITUTE OF TECHNOLOGY

September 1965

Signature of Author. . . *Ferren MacIntyre* . . . . .  
Department of Chemistry, 15 September 1965

Certified by . . . . . *John W. Winchester* . . . . .  
Thesis Supervisor

Certified by . . . . . *Raymond E. Casutt* . . . . .  
Thesis Supervisor

Certified by . . . . . *George A. Satchard* . . . . .  
Thesis Co-Supervisor

Accepted by . . . . . *C. W. Garland* . . . . .  
Chairman, Departmental Committee  
on Graduate Students

**BLANK PAGE**

## ION FRACTIONATION IN DROPS FROM BREAKING BUBBLES

by

Ferren MacIntyre

Submitted to the Department of Chemistry on 15 September 1965 in partial fulfillment of the requirements for the degree of Doctor of Philosophy.

## ABSTRACT

Available data for ion ratios in precipitation are analyzed and shown to be consistent with the hypothesis of a distinctive marine aerosol in which all reported ions are enriched with respect to Na, compared with sea water values.

Experiments with bubble-produced aerosols from a  $^{22}\text{Na}$ - $^{32}\text{PO}_4$  solution show that the fractionation ratio

$$F = \frac{(\text{PO}_4^{3-}/\text{Na}^+)_{\text{aerosol}}}{(\text{PO}_4^{3-}/\text{Na}^+)_{\text{solution}}}$$

is greater than 1 for all drop sizes from 0.5 to 50 microns, and may be as high as 700 for 15-micron drops.

Drops formed by the central jets of small bubbles show enrichment ratios  $E (=F-1)$  below 10 which are independent of drop size, while drops from the film caps of large bubbles frequently show an additional high peak,  $\hat{E}$ , log-normal and centered on 15- $\mu$  drops, with a standard deviation (about the geometric mean) of log 1.75.

It is suggested that small bubbles form an efficient surface microtome which selectively ejects only the uppermost 1- $\mu$  layer of the solution into the aerosol phase, and that this selectivity is responsible for the anomalous ion ratios reported in marine precipitation.

(As an analytical tool, the "bubble microtome" permits investigation of surface concentrations far lower than those which can be reached by other techniques.)

To explain the two types of phosphate enrichment, it is proposed that a single chemical mechanism is at work, involving adsorption with surface excesses  $\Gamma_i$  as low as  $10^6$  ions/cm<sup>2</sup>. This is responsible for the uniformly present low enrichment  $\bar{E}$ . The peak enrichment, related to  $\hat{E}$  by

$$\log \hat{E} = 2.4 \log(\bar{E}/0.8)$$

with a correlation of 0.6, is not explained, but would appear to be caused by a physical mechanism, concentrating the surface phosphate into a small region at the point of subsequent film cap rupture.

A preliminary solution of the Navier-Stokes equation for flow around a rising bubble (hard sphere model) provides tentative values of the streamlines and transit times for near-surface flow within the region of molecular diffusion.

Thesis Supervisor: John W. Winchester  
Title Associate Professor of Geochemistry

Thesis Supervisor: Dayton E. Carritt  
Title Professor of Chemical Oceanography

Thesis Co-Supervisor: George Scatchard  
Title Professor of Physical Chemistry,  
Emeritus

This thesis has been examined by:

... John A. Winchester ...

... Dayton J. Covert ...

... George Scatchard ...

... W. Garland ...

... David P. Shonker ...

To Carol

this work of my  
head and hands.

## TABLE OF CONTENTS

Abstract	2
List of figures and tables	8
Statement of the problem	10
Plan of the work	11
I. ION RATIOS IN THE MARINE ATMOSPHERE	13
Introduction	14
Ion ratios from Junge & Werby	17
Chlorine	20
Excess sodium	22
Potassium	22
Calcium	23
Sulfate	23
Other data	24
Discussion	25
Aeolian organic matter	27
"Surface thickness" from Dean's hypothesis	29
II. BUBBLE MECHANICS	31
The generalized bubble	32
Bubble rupture	
Jet formation	32
Reversible flow	33
Experimental support	37
Jet-drop diameter vs. bubble diameter	41
Surface thickness incorporated into jet drops	41
Uniformity of jet-drop formation at a clean surface	46
The film cap of a bubble	
Area estimation	52
The mechanism of film cap rupture	53
Comparison with experimental results	57
Discussion	62
Further examples of drop formation	63
III. THE BAYLOR EFFECT	67
The Baylor effect	68
Early experiments	69
Extent of reaction	72
The bubble as a micelle	74
Particulate matter	
Amount formed	75
Inorganic particles	76
Organic particles	77
Survey of possible reactions	79
Bubbles and the marine phosphate cycle	81

IV. EXPERIMENTAL RESULTS	85
The basic experiment	86
Apparatus	86
Sample counting	92
Raw data	95
Data reduction	95
Description of runs	
Runs with no surfactant added	97
Inorganic salts present	98
Ionic surface-active agents	99
Non-ionic surfactants	99
"Maypon"	99
"STRactan"	100
Experimental results	
Nomenclature and derivations	101
Sodium results	102
Particle number	103
8-micron volume minimum	107
The constancy of the sodium/water ratio	110
High-wind aerosol distributions in nature	111
Phosphate results	117
Additional nomenclature	117
Excess phosphate data from jet-drop runs	120
Peak enrichment $\bar{E}$ from film-drop runs	126
Discussion	
Interpretation of runs	138
Maypon runs	140
Sea water runs	141
STRactan runs	142
Summary	142
Interpretation of $E$	143
The drop-volume excess phosphate	144
Concentration dependence of the linear enrichment	145
The 15-micron $\bar{E}$ maximum	148
Correlation between $\bar{E}$ and $\hat{E}$	151
Error analysis	154
Counting errors	155
Systematic errors	157
Conclusions	
Jet-drop enrichment $\bar{E}$	158
Film-drop enrichment $\hat{E}$	159
Enrichment of other marine ions	160
V. SUPPORTING WORK	161
High-precision counting of eccentric radioactive	
samples	162
Conclusions	183
The making of bubbles	185
Film-drop bubbles	185
Gas source	186
Jet-drop bubbles	189
Capillary bubbles	190
Orifice plates	195



## LIST OF FIGURES

2.1	The generalized small bubble	35
2.2	Flow patterns in surface cavities	39
2.3	Jet drop diameter vs. bubble diameter	43
2.4	Salt stalactite formed by jet drops	49
2.5	Radius and number of initial film drops	59
2.6	Film drop production	61
3.1	Time dependence of phosphate removal	71
4.1	Experimental apparatus	89
4.2	The micro-ocean	91
4.3	Volume of aerosol collected	105
4.4	Particle number distribution	109
4.5	Oceanic aerosol distribution	113
4.6	Laboratory aerosol distribution	115
4.7	Phosphate content of aerosol	119
4.8	Drop-surface excess phosphate	123
4.9	Enrichment of jet-drop runs	125
4.10	Enrichment of film-drop runs	129
4.11	Enrichment of film-drop runs	131
4.12	Maypon runs	133
4.13	Sea water runs	135
4.14	STRactan runs	137
4.15	Concentration dependence of the linear enrichment	147
4.16	Correlation between $\bar{E}$ and $\bar{E}$	153
5.1	Eccentric sample free to rotate	165
5.2	Eccentric sample constrained	167
5.3	Response of various sensitivity surfaces	173
5.4	Response of non-eccentric trough	175
5.5	Response of eccentric trough	177
5.6	Experimental data	179
5.7	Response contour map of detector surface	181
5.8	Bubbles generated by capillary whip	193
5.9	Aerosol impactor	203
5.10	Assumed collection efficiency of aerosol impactor	211
6.1	Coordinate system used in difference equations	225
6.2	Near-surface interpolation scheme	229
6.3	Near-surface streamlines and transit time	233

## LIST OF TABLES

1-1	Ion ratios in precipitation	18
3-1	Distribution of phosphate after bubbling	69
3-2	Transformation of phosphate by bubbles	73
4-1	Radiochemical data for nuclides used	94
4-2	Summary of runs	139
5-1	Correction factors for eccentric sources	184
5-2	Cut-off diameters for aerosol impactor	204

## STATEMENT OF THE PROBLEM

The primary objective of this study is the evaluation of the influence of surface chemistry upon the composition of aerosol particles produced by breaking bubbles. The secondary objective is the elucidation of the mechanisms whereby bubbles collect, alter, and transport material from bulk solution to atmospheric aerosol.

The importance of this study lies here: Bubbles breaking at the surface of the ocean must disperse some  $2 \times 10^9$  tons of "salt" into the atmosphere per year ( $1 \times 10^{12}$  g/cm<sup>2</sup>-day), for this amount returns to earth in precipitation (Eriksson 1958). Though the downward process and the composition of precipitation have been thoroughly documented, little is known of the upward process, and the minor constituents of the "salt" are inadequately known. Rossby (1959) has observed that the chemical constituents of precipitation "leave the sea in different proportions than those characteristic of sea water", and suggested the importance of surface chemistry in this process.

Concomitantly with production of aerosols, bubbles are responsible for phase transitions of organic material from solute to colloidal micelle or interfacial monolayer, and there is reason to suspect that chemical reactions of positive  $\Delta G$  may occur during bubble rupture. These processes may have been important in biogenesis, and are certainly important in marine ecology.

In any event, without a molecular description of the interface and of the hydrodynamic flow patterns during rupture, little can be predicted about the composition of the ejected droplets save that it is not necessarily identical with the parent liquid. Conversely, the nature of the droplets can provide insight into the molecular detail.

Sea water is too complex a solution to yield meaningful physicochemical data. In the hope that studies of simpler solutions could lead to an understanding of factors which are important in large-scale oceanological processes, sea water was approximated by a simple solution containing radioactive P-32 and Na-22. The present work reports on the  $PO_4/Na$  ratio of the spray from bubbles breaking on such simple solutions.

#### PLAN OF THE WORK

Chapter I calls attention to a problem little appreciated outside the small coterie of atmospheric chemists, which is that ion ratios in the marine atmosphere are not identical to those of sea water, and relates this fact to a number of surface-chemical phenomena which can change ion ratios in the (molecular) surface of the ocean.

Chapter II proposes a mechanism whereby bubbles breaking at the surface of the sea can take the molecular surface--with a minimum of bulk liquid--and eject it as droplets into the atmosphere.

Chapter III discusses the particular interaction of phosphate and bubbles in sea water, and suggests that more than one type of reaction is possible.

Chapter IV describes experiments designed to elucidate the physical and chemical mechanism of phosphate enrichment.

Chapter V reports on incidental supporting work.

Chapter VI gives the details of flow around a rising bubble needed for an analysis (not undertaken) of molecular diffusion in a previously not-well-characterized region of Reynolds numbers.

## CHAPTER I

## ION RATIOS IN THE MARINE ATMOSPHERE

The transport of salts from sea to air is  
by no means a simple mechanical process.

C.-G. Rossby

## ION RATIOS IN THE MARINE ATMOSPHERE

## INTRODUCTION

The atmospheric chemist seeking to disentangle the sources and reactions of the trace constituents of the atmosphere is faced with a quandary.

Clearly, the two primary sources of "foreign" material in the air are the continents and the oceans. (Secondary sources include meteoritic accretion from above the atmosphere, vulcanism, volatile organic material from vegetation, and human activities. None of these is unimportant locally, but all of them are small compared to the major sources.) To a first approximation, the ocean contributes material whose ion ratios are those of sea water; the continents contribute finely divided material which is highly siliceous, and far lower in sodium than sea water.

The presumptive origin of raindrop nuclei has oscillated from continent to sea to continent, and each swing has been marked by data supporting the chosen source. In such matters, ion ratios have been important factors, and the abandonment of the ocean as the major theoretical source of nuclei was brought about largely by the observation that the observed ion ratios in rainfall demanded the presence of

continental dust. Lately it has become evident that there are some anomalies in purely marine environments, and that a second look at the ion ratios in areas over the ocean which are free of continental contamination is in order.

The traditional approach to the study of atmospheric constituents has been the examination of what comes down at isolated stations. This method has been broadened to continent-wide long-term studies which are of much greater value, since now it is possible to pinpoint local and regional sources of particular ions. For North America, Junge & Werby (1958) have given yearly-average isopleths of ion ratios for the more common ions, and from these it is possible to make some estimate of the "background" ion ratios which would obtain in the absence of land masses. These maps do not extend over the oceans, and our marine data is dependent upon such places as Bermuda, Hawaii, and New Zealand, plus selected coastal stations with favorable wind-circulation patterns which minimize contamination by continental dust.

However, ion ratios at these near-shore stations become indistinguishable from sea water during storms, and this effect persists in both time and distance. Yearly averages of points tens of kilometers from the shore still reflect the addition of bulk sea water to the atmosphere (Miller 1961). Our interpretation of the "background" oceanic contribution to the atmosphere is based largely upon measurements which are known to be contaminated by

quantities of bulk sea water.

It is becoming increasingly clear that an important mechanism for the transport of material from sea to air is a quieter phenomenon than breaking surf and storm-driven spray. Most material which remains airborne is derived from the breaking of whitecap bubbles in moderate winds over immense areas of the ocean (Blanchard 1963, Moore & Mason 1954).

And this is the quandary: There are no ion ratio data from precipitation which are characteristic of the major portion of the earth's surface. From the data which are available, it is difficult to assess the undisturbed marine component.

The approach taken in this work represents one way out of the quandary. It proposes to study what goes up--in this case from the surface of simple artificial solutions, but in principle from the surface of the ocean. The idea is not new, for Köhler & Båth (1952) have attempted to measure ion ratios in spray with similar intentions, Sugawara (1959) has reported on halogen ratios in spray, and Komabayasi (1964) has studied Ca, Sr, and Ba in spray. Gast (1959) has examined the evaporation of boric acid from the surface of the sea, and Miyake & Tsunogai (1963) have examined the possibility of the photo-oxidation of iodine directly from the sea surface.

The importance of this type of work is best brought out by comparing the situation with that of a chemist who is

given the products of a reaction and asked to describe the reaction mechanisms, without having knowledge of the reactants. The models and assumptions of atmospheric chemists are greatly influenced by the reactants which they postulate.

As an example of differing interpretations of the same data (obtained from precipitation studies), the data of Junge & Werby will be analyzed with a set of basic assumptions different from those the authors used. It will be seen, in this analysis, that the choice of reactants modifies the conclusions reached by examining the products. The authors' set of assumptions included one which made the ion ratios of the marine contribution be the ion ratios of sea water, whereas the assumption made herein will be that this is not necessarily so; and an attempt will be made to estimate the supramarine ion ratios.

#### ION RATIOS FROM JUNGE & WERBY

The necessary data are collected in Table 1-1, which is an abridgement of the original data. Many points not germane to the ensuing discussion, and are ignored. The data are expressed as mg/l of the respective ions, and represent concentrations averaged over a year's precipitation.

The data of Table 1-1 are divided into two main groups. The first are near-shore, high-concentration stations, which should most nearly reflect the marine contribution. The

Table 1-1. Ions in precipitation, mg/liter (from Junge &amp; Werby)

Location	Cl	Na	Cl/Na	Excess Na	K	K/Na	Ca	Ca/Na
<b>Coastal, High concentration</b>								
Bermuda	12.41	7.23	1.72	0.43	0.36	0.050	2.91*	0.40
Newfoundland	8.85	5.16	1.71	0.31	0.32	0.062	0.78	0.15
Cape Cod	5.89	3.36	1.75	0.13	0.20	0.060	0.30	0.089
Cape Hatteras	9.90	4.49	1.54	0.71	0.24	0.053	0.44	0.098
Olympic Pen.	22.58	14.30	<u>1.58</u>	<u>1.93</u>	<u>0.44</u>	<u>0.041</u>	<u>0.73</u>	<u>0.051</u>
Average			1.66	0.70	0.44	0.053	----	(0.051)
<b>Coastal, Low concentration</b>								
San Diego	3.31	2.17	1.53	0.36	0.21	0.097*	0.83	0.38
Miami	2.44	1.62	1.51	0.17	0.11	0.062	0.56	0.35
Boston	1.19	0.71	<u>1.68</u>	<u>0.06</u>	<u>0.13</u>	<u>0.183</u>	<u>0.29</u>	<u>0.41</u>
Average			1.57	0.20	0.16	-----	----	----
Mid-continent average	0.17	0.30	0.61	0.19	0.20	0.67	----	5.87
Sea water ratios			1.80			0.036		0.038

\*Obvious influence by local sources.

second are near-shore, low-concentration stations which are more subject to continental contamination. The mid-continent average includes 26 stations from the Rocky Mountains to the Mississippi River which lie inside the steep slopes of the isopleths in a more or less uniformly flat region--which is as typical of continental ratios as can be found. Finally, sea water ion ratios are included for comparison.

Examining the Cl/Na data, we find them uniformly below the sea water value of 1.80. This can be explained either as loss of chlorine or as gain of sodium, and it appears that Junge has wavered between the two interpretations at various times. In the present instance, the authors attribute the low ratio to a gain of sodium by contamination with continental dust, with a Cl/Na ratio of approximately 0.61. This clearly moves the ratio in the right direction.

Closer examination, however, suggests that it is asking for extraordinary amounts of Midwestern dust in the rainfall on the Olympic Peninsula and Bermuda, where the absolute values are high, to bring the ratio down from 1.80 to the observed 1.66 average. The next problem which arises is that other locations with less rainfall show the same 1.66 value; according to the dust hypothesis, the ratio should have been reduced even further by similar amounts of contamination.

It is not possible to duplicate exactly the recorded ratios by simply adding dust with the average mid-continent

ratio to sea water, but it is instructive to show where such an approach would lead. For example, the Bermuda ratio can be gotten if about 6% of the chloride is continental. However, 6% of Bermuda's chloride is 0.72 mg/l, which must be compared with the mid-continent average composition of 0.17 mg/l. In other words, with this method we find that there is approximately 5 times as much continental dust in the rain of Bermuda as there is in the rain of Kansas.

This line of thought suggests an alternative explanation, which is that the insular and coastal value of 1.66 is a true estimate of the supramarine value and has not been appreciably contaminated. (The effect of contamination of the marine ratio is then seen in the 1.57 average of the low-concentration coastal stations.) The problem then becomes one of explaining why this ratio is not identical with the ion ratio of sea water.

## CHLORINE

The problem is further complicated by some additional observations of Junge (1957), who reports that approximately 50% of the chlorine content of the Hawaiian atmosphere is not in the aerosol phase, but is gaseous. This observation has been confirmed by Duce et al. (1965) and found to hold true for bromine also. It does not change the fact that we must explain a difference in ion ratios, but it changes the sign of the discrepancy, since the gaseous chlorine component presumably does not enter the atmosphere as a gas

from the sea surface, but is expelled from aerosol particles after chemical reactions in the atmosphere (Rossby & Egner 1955). This means that the extra chlorine has to enter the atmosphere in a small droplet ejected from the sea surface--and a small droplet in which the ion ratio is twice the value which is observed for the aerosol when it comes down as rain. That is, the Cl/Na ratio of the material leaving the sea surface must, under these assumptions, be 2 X 1.66, or 3.32. This is 1.7 times its sea water value.

This figure is implausibly high, and may be reduced by noting that most aerosol particles smaller than 0.5  $\mu$  escaped measurement in Duce's work (Duce, personal communication). These small particles contain an appreciable fraction of the total chlorine, and their inclusion in the particulate fraction would reduce the 50% gaseous component to perhaps 30%, lowering the Cl/Na ratio to 2.16 (assuming that the Cl/Na of the small particles is equal to 1.66 also). The ratio could be lowered by finding another route for gaseous chlorine to enter the atmosphere, or by finding continental contamination to be enriched in chlorine.

The burden of this thesis is that of making some increase in the Cl/Na ratio over the ocean appear less implausible than it does at present. We shall continue with an analysis of further data from Junge & Werby.

## EXCESS SODIUM

Explaining the observed deviation of the Cl/Na ratio by an excess of Na added from soil, the authors plot isopleths of "excess Na" (=observed Na - observed Cl/1.80). This plot (column 4 of the Table) has the curious feature of requiring concentrations of continental dust in the rainfall over Bermuda, Newfoundland, and the Pacific Northwest, greater than that over Oklahoma. This is a serious drawback, and not at all in accord with experience; it disappears completely if one accepts the oceanic excess as a real marine phenomenon.

It is true that the percentage of excess sodium is high in mid-continent, where some 60 to 70% of the sodium present has come from the land, but this is largely due to the washout of marine sodium with increasing distance from the sea. A high percentage of excess over the land is quite a different matter from a high absolute amount of terrestrial dust over the ocean!

## POTASSIUM

The potassium distribution parallels the excess sodium distribution faithfully, and is subject to the same interpretations. The K concentration is uniform across the continent, except for small local sources, at a value of 0.20 mg/l. But the oceanic value is roughly twice this. It is again unreasonable to ask the continent to export more dust than it keeps. This difficulty disappears if oceanic

aerosols have a K/Na ratio of 0.053 instead of the 0.036 value of sea water.

#### CALCIUM

The Ca/Na ratio data are not easily interpreted. There is clearly a major source of  $\text{CaCO}_3$  in the arid soil of the Southwest, and presumably a local source in the limestone island of Bermuda. Of all the coastal stations, only the Olympic Peninsula shows any sign of not being grossly contaminated by continental calcium, and it is hardly worth noting that this one point also shows a greater Ca/Na ratio than sea water. (However, there is greater reason to expect differences in ratio between Ca and Na than between K and Na, and Ca/Na ratio measurements over the undisturbed ocean would be of great interest.)

Miyake and Tsunogai (1965) have begun such measurements, sampling from an island station near Japan. They attribute the excess Ca to soil contamination on the basis of Ca/Fe data. On the other hand, Sugiura (1965) finds a twofold enrichment of Ca in the aerosol from sea water enriched with "sea weed extract". Much work remains to be done with calcium.

#### SULFATE

The one remaining ion discussed by Junge & Werby is sulfate. Their interest clearly lies with industrial

pollution, and they regard the oceanic excess as being unimportant. However, they do compute, from additional "unpolluted" data, an average value of 0.53 mg/l of excess sulfate which can be attributed to the oceans. (This is an excess referred to that most uncertain of indicators, the chloride ion, and therefore of dubious reliability. Nonetheless, 0.53 mg/l is about one quarter of the total excess sulfate in the atmosphere--which is an appreciable contribution from the oceans.)

#### OTHER DATA

Unfortunately, Junge & Werby do not discuss phosphate. Equally unfortunately, the data from the European precipitation network (Eriksson 1959) are of uncertain value for estimating the marine contribution to ion ratios, since they all lie leeward of industrial Britain. Nor do they report phosphate.

Eriksson's Hawaiian rainfall data from Project Shower (1957) appear to corroborate strongly the hypothesis of a marine enrichment. However, he emphasizes that the chief interest in Project Shower was the assessment of the total salt content of rain, and not ion ratios. His collectors were left uncovered for 24 hour periods, apparently on the ground near a road, and it would appear that a large part of the enrichment seen is in fact terrestrial dust. (Eriksson observes that this is indeed true for one set of samples collected near an unpaved road, and did not publish ion

ratios for that set.) It should be mentioned in this connection that the collectors employed by Junge & Werby were kept closed except during precipitation.

Finally we cite Oddle (1962) who found enrichment of K, Mg, and Ca in precipitation at cloud level which was reportedly not contaminated by land. His values for the fractionation ratios of these ions,

$$\frac{(M/Na)_{\text{sample}}}{(M/Na)_{\text{sea w.}}}$$

are respectively 12.5, 3, and 75, all of which seem remarkably high.

#### DISCUSSION

It appears from the foregoing that all ions are enriched with respect to sodium, and indeed one can find a theoretical justification for this in almost any given case. Calcium and magnesium, for instance, are known to be adsorbed with 50- to 200-fold preference to sodium as the counter ion on surfactant solution (Judson et al. 1953, Walling et al. 1957, Shinoda & Ito 1961); and the effect is purely electrostatic (van Voorst Vader 1960), and in fact is as familiar as hard-water scum. Anions are accepted more easily than cations by the surface dipole structure of water (Guest & Lewis 1939, Randles 1957); iodine exists in large organic molecules which show surface activity; and specific ion interactions and mechanisms can always be invoked to explain individual peculiarities.

In seeking a unifying principle for all marine atmospheric ion ratios, Komabayasi (1962) has taken the data of Sugawara (1958, 1961) and found a logarithmic enrichment of heavy ions which is correlated strongly with the ionic weight, appearing to hold true for  $\text{Na}^+$ ,  $\text{Mg}^{++}$ ,  $\text{K}^+$ ,  $\text{Ca}^{++}$ ,  $\text{CO}_3^{--}$ ,  $\text{Sr}^{++}$  and  $\text{I}^-$ . This is most unexpected, and has led Komabayasi to speculate that "Some isotopic fractionation mechanism like thermo-gravitational effect is suggested to be important for the ionic enrichment at the air-sea surface." He considered several alternative mechanisms also, which were: (1) Selective negative surface adsorption of cations at the surface; (2) Biological material--which appeared to him unlikely in view of the uniformity of the fractionation effect and the wide variability of biological activity in the sea; (3) Electrophoretic motion in the gravitational field; (4) Fractional crystallization during dehydration in the atmosphere; (5) Gas phase fractionation of volatile materials; and (6) Sugawara's (1959) unexplained "synfractionation".

Komabayasi's skepticism toward the contribution of organic material to this process is not widely shared, and perhaps the prevailing belief is the one held by Eriksson (1959): "Some fractionation process seems to take place at the sea surface (possibly involving organic matter derived from surface films)."

Probably the truth lies somewhere between these views, with both organic and inorganic effects contributing. The

one common denominator is the agreement that some surface mechanism is at work.

It is perhaps difficult to see how a physicochemical surface phenomenon, acting only over molecular distances, could affect the large scale transfer of matter from sea to air. An equivalent difficulty is that of visualizing the "surface" of the ocean as having a different composition from that of bulk sea water. This is particularly true among classical oceanographers, to whom "surface" has meant any sample collected in an open bucket instead of a Nansen bottle.

Nevertheless, we hope to show herein that such microscopic effects completely dominate this transfer, and that it does indeed take place in such a way that the composition of the molecular surface is of importance. We begin by considering some of the evidence for organic material of marine origin in the atmosphere.

#### AEOLIAN ORGANIC MATTER

Evidence for a marine contribution to the organic content of the atmosphere is growing. Woodcock (1948) noted that sufficient quantities of the pigmented product of the dinoflagellate Gymnodinium were found in the air in times of "red tide" to cause distress to sensitive people. From studies of snow in New Zealand, Wilson (1959) concluded that the only probable source of the organic nitrogen was the sea surface. Munckzak (1960) has found atmospheric amino

acid-like material of unknown origin. The highest altitude life zone of barren mountains forms an ecological region known as the "aeolian" zone, since it produces no primary food of its own, but supports a considerable arthropod population with a food chain based upon wind-blown material and the organic material from melting snow. Much of this nutrient may come from the sea surface.

Blanchard (1964) has observed surface active organic material in the aerosol downwind from breaking surf, and Goetz (1965) reports that kelp leaves exposed to sunlight metabolically produce bubbles to form a "distinct foam" which ejects a "prolific quantity of organic material" into the atmosphere.

Dean (1963) assumes that the chloride in New Zealand rain is derived from sea water, but that the iodine comes from the debris of plankton and algae which can be seen microscopically in the rainwater. On this assumption, he estimates that the rain contains 0.5 ml of sea water, and 4 mg of dry plankton and algae per liter, and finds that this accurately duplicates both the organic nitrogen and the phosphate content of New Zealand rains.

This is a remarkable result, and suggests that any discussion of the significance of ion ratios in the atmosphere must consider the probability that many marine anomalies arise from the injection of biological material into the atmosphere. Since the K/Na, Ca/Na, and Mg/Na ratios of biological material differ appreciably from sea

water, one might expect that Dean's approach, extended to these ions, would help explain the observed anomalies.

A closer look at this raises question. Ordinarily sea water contains ca. 4 mg/l of dissolved plus particulate organic matter (Duursma 1960). Dean's recipe calls for no less than 8 grams per liter, or 2000 times as much organic matter as expected. A discrepancy of this magnitude often suffices to relegate an hypothesis to the limbo of lost causes, but it need not do so here if we require that the airborne component be removed from the organically enriched surface of the sea.

#### "SURFACE THICKNESS" FROM DEAN'S HYPOTHESIS

In fact, we can obtain an order-of-magnitude estimate of the thickness  $dt$  of the "surface" by assuming that in this surface one half of the organic material is particulate and one half is dissolved. (This is a higher ratio of particulate to organic than is commonly found in deeper water, but is partially justified by Dean's microscopic observation of planktonic debris in rain.) We will suppose that the "dissolved" material has a molecular weight of 100, and forms a monolayer at the surface containing  $2.5 \times 10^{14}$  molecules/cm<sup>2</sup>. We wish to put 4 grams or  $2.5 \times 10^{22}$  molecules of the monolayer into a liter of drops, with another 4 grams of particulate matter being carried aloft by the same mechanism.

Thus we have

$$\frac{2.5 \times 10^{22} \text{ molec/l}}{2.5 \times 10^{14} \text{ molec/cm}}$$

of surface per liter of ejected sea water, or

$$dt = (10^3 \text{ cm}^3/\text{l}) / (10^8 \text{ cm}^2/\text{l}) = 10^{-5} \text{ cm} = 0.1 \text{ micron.}$$

This is a rough approximation indeed, but in the next chapter we shall try to show that this thickness is at most one order of magnitude too small, and may actually be a rather good estimate for the surface thickness ejected by a breaking bubble. In Chapter IV we shall argue that there are additional mechanisms for enrichment of certain ions which make the thickness requirement less stringent.

CHAPTER II

BUBBLE MECHANICS

All at once and nothing first  
Just like a bubble when it bursts

Oliver Wendell Holmes  
The Deacons's Masterpiece

## THE GENERALIZED BUBBLE

A view of a 1 mm bubble, and the two types of drops which it produces when it breaks, is shown in Figure 2.1. The numbers are intended as background information, and are to be understood as order-of-magnitude values.

The two kinds of drops made by the bubble are quite distinct, and arise from different mechanisms, which will be discussed in detail. However, not all bubbles make both kinds of drops. Film drop production ceases below 300 micron bubble diameter, while jet drops from bubbles larger than about 2 mm are too large to remain airborne. Thus it is possible to separate the two kinds of drops by avoiding bubble sizes near 1 mm.

### BUBBLE RUPTURE

#### JET FORMATION

No adequate theoretical treatment of the collapse of the bubble cavity under the influence of surface tension and gravity is available. A remotely similar cavity was considered by Naude & Ellis (1961) in their examination of the collapse of a hemisphere of vapor against a flat plate. Studying cavitation, in which the driving force is largely hydrostatic pressure, they were able to ignore surface tension and arrive at an analytic solution which predicted

the existence and energy of the resulting jet. They made no effort to describe flow patterns during this process.

Nor is there much experimental evidence relating to flow patterns during bubble rupture; the best work is that of Worthington & Cole (1898, 1900) who took spark photographs of the cavities formed by falling drops and solid spheres impacting on a liquid surface. There are noteworthy features of their work which bear on the collapse of the bubble cavity.

When they dropped milk into water, they observed that the tip of the jet which resulted from the collapse of the cavity contained nearly all of the original milk. This indicates that little mixing took place, and that the entire process up to this point is largely reversible.

#### REVERSIBLE FLOW

This observation does not indicate that the drop retained its geometric integrity during descent into the liquid and return in a process which might be likened to elastic rebound. It does indicate that whatever flow the drop underwent was reversed midway through the cycle, so that the input material (aside from some inevitable mixing at the interface) was returned with energy and mass conserved and momentum reversed. In particular, it may mean that the drop flattens out while also forming a cavity in the substrate liquid, and that the filling-in of the cavity also causes the original drop to reform to some extent.

Figure 2.1. The generalized small bubble. A summary of relevant information about bubbles and the drops they produce.



Consider the impact of a drop with a rigid plane. The flow pattern after impact is that of a spreading disc running radially and horizontally as in the cross section shown in Figure 2.2-a. This flow is clearly irreversible. Photographs by Professor Edgerton show that if the plate is covered by a thin layer of liquid, the disc flow of the rigid plate is deflected upward into "cup" flow, forming a thin corona of film which again irreversibly breaks up into drops. However, a portion of the flow reverses to form a central jet. "Cup" flow before any reversal occurs is indicated in Figure 2.2-b. If the depth of the liquid is increased, we come finally to the pattern found by Worthington & Cole, and it is reasonable to propose that there is a continuum of flow patterns connecting the irreversible disc flow to the highly reversible flow which returns the input drop at the top of the jet. This proposal leads to a picture such as Figure 2.2-c, which shows the maximum spreading of the drop before flow reversal begins.

Qualitative non-photographic experiments, dropping ink into water of varying depth, tend to support this conclusion. The distribution of colored drops from the corona, which travel radially and upward and may be examined by capture on a cylinder of paper, indicates that there is always some material lost by irreversible flow into the corona, but that this loss decreases with increasing water depth. There is no sudden transition from "disc-flow" to rebound.

The implication is that in deep liquid, the drop does spread in laminar flow outward and up the sides of the cavity it is creating. This must be followed by a similar flow in the reverse direction down the slope of the crater, reforming most of the original drop, as shown in Figure 2.2-d.

This is an unexpected implication, and one which requires corroboration. (However, consider the behavior of waves on an ideal liquid. Here one normally expects energy to propagate without frictional dissipation, to reflect reversibly from solid interfaces, and to leave behind an unmixed liquid.) Some experimental support is given by the second feature of Worthington & Cole's work, this time from observations of the cavity made by solid spheres.

#### EXPERIMENTAL SUPPORT

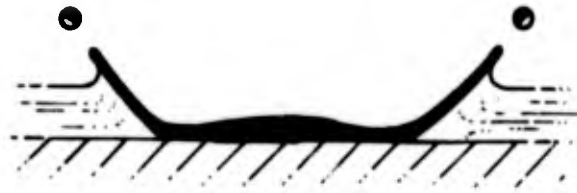
When dropping solid spheres into a liquid, they arranged to have two streams of very small bubbles (small enough to follow but not disturb flow patterns) rising near the sides of the cavity. It can be seen (more clearly on their original plates than on the published reproductions, according to the authors) that these streams of small bubbles turn downward near the cavity and begin to follow the flow down the slope as in Figure 2.2-e.

The drop- and sphere-cavities are not identical, nor can they be held to be overly similar to a bubble-cavity. Nonetheless, both the drop- and the sphere-cavities reach

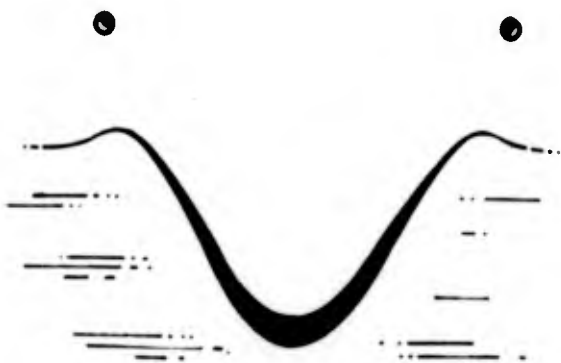
Figure 2.2. Flow patterns in surface cavities. (A) through (D) represent the cavity formed by a falling liquid drop, (E) that by a solid sphere, and (F) by a bubble.



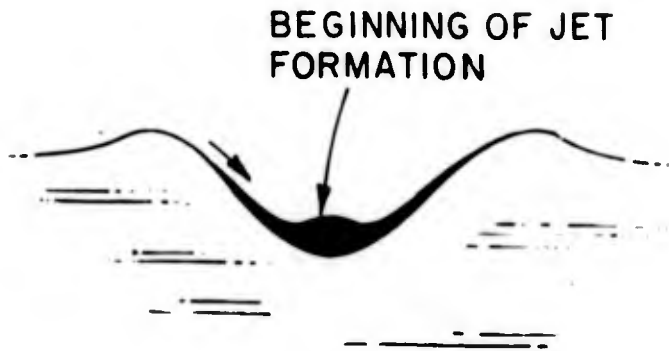
(A) KNOWN PATTERN ON RIGID PLANE



(B) KNOWN PATTERN IN THIN LIQUID FILM



(C) HYPOTHETICAL PATTERN IN DEEP LIQUID AT POINT OF MAXIMUM PENETRATION



(D) HYPOTHETICAL REVERSE FLOW REFORMING ORIGINAL DROP



(E) OBSERVED REVERSE FLOW DOWN SIDE OF CRATER LEFT BY SOLID SPHERE



(F) HYPOTHETICAL REVERSE FLOW DOWN SIDE OF CAVITY FORMED BY BREAKING BUBBLE

FLOW PATTERNS IN CAVITIES IN LIQUIDS

configurations in which the shape and the energy distribution are similar. When the cavity made by the drop is at its maximum depth, the kinetic energy of the system is at its lowest, and the potential energy at a maximum. Similarly, when the cavity closes behind the solid sphere, it may be considered no longer to belong to the system, and the energy distribution of the cavity alone is quite like the drop cavity. The situation in a hubble-cavity is a little different but perhaps can be made to look like the others (Figure 2.2-f) if one notes that while the mode of formation of the cavity is quite different, the amount of energy which has gone kinetically into spreading the walls of the sphere is probably about the same as that imparted by the falling object, while the potential energy is almost identical.

Now, if a time-dependent solution goes through a configuration which does not depend strongly upon the initial conditions, the solution at all subsequent times may be taken as an approximation for any set of initial conditions.

Thus we may conclude with some confidence that the collapse of a bubble cavity is similar to the collapse of an impact cavity, and in particular that there is surface flow down the sides into the jet, so that the jet drops consist in large part of the interior surface of the bubble.

Blanchard (1963) found that jet drops would carry off surface films of "indicator oil" in amounts up to 200% of

the drop surface area. This indicates that the driving force which moved the oil into the fresh surface exposed by rupture was some force other than the spreading pressure of the oil itself, which would drop to zero as complete coverage was attained. Although the disruption of the jet is accompanied by a decrease in surface area, this is insufficient to compress the surface film by a factor of two. The presumption is that the additional oil is drawn into the forming jet by the flow of surface liquid.

#### THE RELATION BETWEEN JET DROP DIAMETER AND BUBBLE DIAMETER

Figure 2.3 shows the relationship found by Blanchard (1963). We need to extrapolate below his minimum size (at the point indicated by the break in the line); this is done by extending the linear portion of his curve. The analytic expression for this linear section is

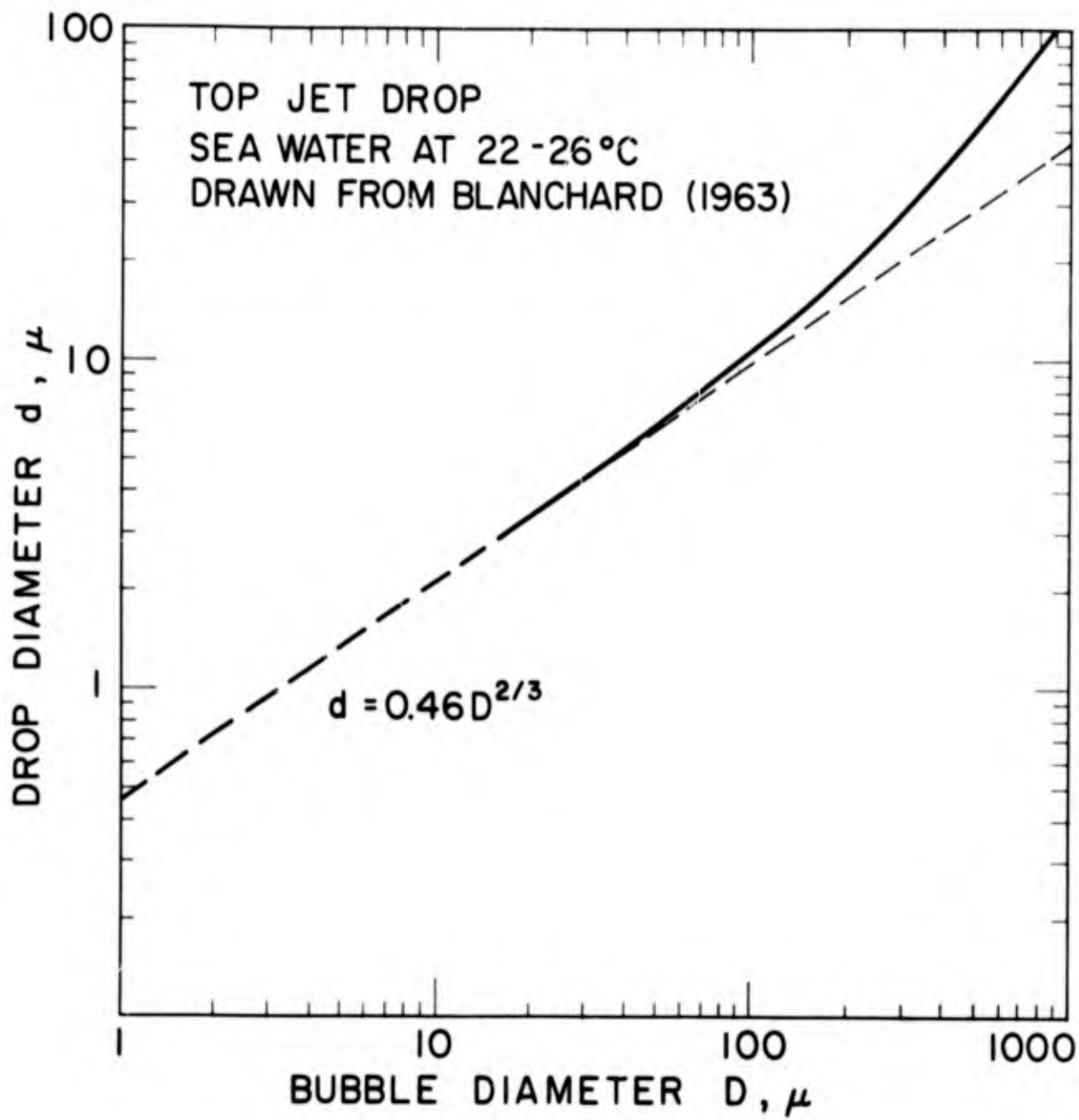
$$d = 0.46 D^{2/3}$$

where both the drop diameter  $d$  and the bubble diameter  $D$  are measured in microns. We will assume that this relation holds for drop sizes  $0.5 \leq d \leq 10$  microns.

#### THE SURFACE THICKNESS INCORPORATED INTO JET DROPS

We need to know what fraction  $\alpha$  of the bubble surface goes into a jet drop, and what the thickness  $dt$  of this "surface" may be. A mass balance between drop volume and bubble surface gives

Figure 2.3. Jet drop diameter vs. bubble diameter. The dashed line is an extrapolation from Blanchard's experimental curve.



$$(\pi/6) d^3 = \pi D^2 \alpha dt$$

Inserting the analytic expression assumed above gives

$$0.10\pi D^2/6 = \pi D^2 \alpha dt$$

or

$$\alpha dt = 1/60 \text{ micron.}$$

At this point, we can neither make any estimate of the separate values of  $\alpha$  and  $dt$ , nor predict how their relationship may vary with bubble size. Furthermore, the relation is based on a rather tenuous extrapolation, and at this point these numbers must be regarded as a guide and not as a mandate.

It is reasonable to suppose that as the bubble size changes, and the relative importance of gravity and surface tension changes, there will be concomitant changes in the flow pattern which affect  $\alpha$  and  $dt$ . For the size range of bubbles used in this work ( $D < 300 \mu$ ), such changes may be quite small, since surface forces are overwhelmingly dominant.

Reviewing what little is known, we find that Blanchard (1964) has found surface coverage (at zero surface pressure) up to 10 times the drop surface area, which indicates a highly compressed film. This can arise only from a value of  $\alpha > 1$ . From earlier work by the same author (1963), a tentative relation between  $\alpha$  and  $D$  may be derived:

$$\alpha = (D/2650)^{1.29} \quad 1000 \mu < D < 3000 \mu$$

There is no basis for extrapolating to  $D < 1$  mm with this form, which has  $\alpha = 1$  for a bubble of  $D = 2.65$  mm, and  $\alpha = 0.015$

for  $D=1$  mm. (Because of the well-known tendency for all experimental numbers to approach linearity when plotted on log-log paper, no particular significance beyond an order of magnitude estimate is intended to be drawn from this relationship.) Worthington & Cole's work (1898) suggests that the surface layer in motion is no more than 10% of the bubble diameter, and is probably much less than that. In any event, this requires  $dt \leq 10$  microns for a bubble of  $D = 100$  microns.

A momentum balance requires that the upward jet formation be accompanied by a similar jet directed downward in the bulk liquid. This can sometimes be observed at the edge of a small raft of bubbles, for occasionally a bubble in this situation will break and eject a jet horizontally, so that it remains entirely in the water. It is visible in the form of a pair of vortices, having dissipated its translational energy quickly. Simultaneously, the entire raft of bubbles is observed to move slightly in the opposite direction, showing that the reaction has been distributed to the whole assemblage.

If the velocity distribution in the flowing surface layer of the cavity increases linearly as it approaches the surface (starting from some assumed surface of no flow) it can be shown that only 0.3 of the total moving thickness can go into the upward jet. If, as is intuitively more likely, the flow is parabolic (being accelerated at the surface by surface tension, and viscously retarded in deeper layers),

the upward-directed fraction reduces to slightly over 0.2. Thus, in the case of a 100 micron bubble, we can expect a jet to be formed of nothing thicker than the 2-micron surface layer.

#### UNIFORMITY OF JET DROP FORMATION AT A CLEAN SURFACE

To indicate both the consistency of the jet drop formation mechanism and the ease with which the details of the process are modified by surface films, the author's one experience with unequivocally clean water will be described. This experiment shed some light on the criterion of bubble life as a measure of water purity, suggesting that it is a more stringent and far simpler test than surface tension measurements, when the surface tension approaches that of pure water.

In this experiment, an 8 ml polyethylene vial (previously cleaned in nitric acid, and kept in contact with "clean" water for some weeks) was pierced from below by a fine glass capillary through which bubbles would be blown. The open end of the vial, covered temporarily with a protective cap, was inside a continuous diffusion cloud chamber (Schaefer 1952). Condensation nuclei rained out for nearly an hour after the 10 X 10 X 20 cm chamber was turned on, and only when the air was swept free of particulate matter in this way was the vial uncovered, rinsed, and filled. All such manipulations were effected with flamed platinum wires, or through cleaned polyethylene tubes,

inserted into the chamber through a large hypodermic needle used as an entry port.

The filling solution was 0.5 M NaCl, using water from the still described below and reagent grade salt which had been kept at 500° C for some hours in a muffle furnace. It had been observed previously that the polyethylene filling tube, if pushed several cm below the surface of the liquid, would remove a monolayer of contamination from it upon withdrawal. Thus, final cleaning of the surface could be accomplished through the small diameter entrance port.

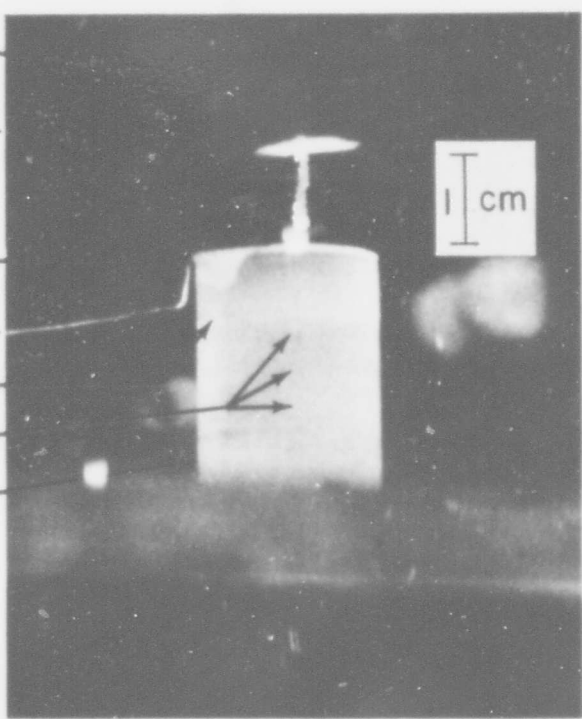
A heated collector located above the capillary tip served to catch and dry jet drops, 100 microns in diameter, from 1 mm bubbles blown at the rate of 4/sec. This collection was continued for 36 hours.

Midway in this process, a stalactite of salt 1 mm in diameter and 10 mm long had grown down from the collector toward the point of bubble rupture (Figure 2.4). In shape it was a rough-surfaced but uniform cylinder, and contained the dried residue of some  $5 \times 10^5$  jet drops. Surrounding its base was a faint halo of salt something less than 3 mm in diameter.

It should be noted that the surface of the solution was slightly concave because of hysteresis of contact angle on the polyethylene as evaporation and transport lowered the surface level. Thus, the central spot was not a stable position for bubbles, and if they persisted for any length of time, drift towards the perimeter would begin.

Figure 2.4. Salt stalactite formed by evaporation of  $10^6$  jet drops. (In the original photograph, three rising bubbles are visible in the micro-ocean.) This is the second (conical) stalactite mentioned in the text. The narrower cylindrical stalactite formed earlier is hidden behind the cone.

HEATED COLLECTOR  
HYPODERMIC NEEDLE  
ENTRY PORT  
SALT STALACTITE  
Pt GROUND WIRE  
SOLUTION LEVEL  
RISING BUBBLES  
8 ml VIAL



Evidently shutting off the gas flow to make the above inspection caused sufficient disturbance to the system to alter its surface behavior, for when it was next examined, a second stalactite had grown beside the first. This one arose from a point in the halo surrounding the first, and was in the shape of a slender but somewhat ragged cone, indicating a gradual increase with time in the dispersion of jet drop ejection direction.

The interpretation of this phenomenon is that it represents the displacement of the bubble by one bubble-diameter before rupture. (Some minor asymmetry of the capillary tip would account for the uniform direction of displacement.) This means that bubble life had risen sufficiently to allow the following bubble to reach the surface and move the surface bubble aside before it ruptured, and thus that surface life had increased to something on the order of 0.25 seconds.

The total weight of salt collected (25.0 mg) checks well with the bubble production rate, allowing two jet drops to reach the collector per bubble.

In conclusion, one can say that  $5 \times 10^5$  bubbles broke in a completely reproducible manner, with lifetimes much less than 0.25 second, and that an additional equal number were only slightly less reproducible after some small perturbation of the system. This remarkable uniformity suggests the possibility of developing a measure of surface contamination based upon bubble surface lifetime, or upon

jet drop behavior, which would be simpler, faster, more reliable, and more sensitive, than surface tension measurements.

The importance of cleanliness in this process is emphasized by the fact that up to the point at which the stalactite was observed, the experiment had been thought identical with several others that had preceded it, in which the collected sample was normally distributed over a 2-cm circular area. When radioactive tracers were added to this run, the same pattern of random deposition appeared.

This happened in spite of the extra care taken with the tracers. Being 10 microcuries each of K-42 and Na-24 as the chlorides, they were mixed with hot nitric acid-hydrogen peroxide and evaporated to dryness three times in the hope of destroying any organic material present. Nevertheless, by the time they were added to the micro-ocean, contamination had been added also, and the normal pattern of drop ejection returned.

## THE FILM CAP OF A BUBBLE

### AREA ESTIMATION

It is convenient to be able to estimate the total surface area which is available for drop formation in a population of bubbles of assorted sizes. Fortunately this is possible without any knowledge of the diameters except that they lie between 1 and 10 mm.

Toba (1959) has calculated the shape of bubbles resting at the surface; one of the values he tabulates is  $S$ , the surface area. Of several analytic representations which closely approximate his numerical data, the most convenient is

$$S = \pi(D - 0.08a)^3 / 6 \quad (\text{cgs units})$$

where  $D$  is the diameter of the equivalent spherical bubble and  $a$  is the capillary constant

$$a = (2\gamma / \Delta\rho g)^{1/2}$$

Since  $a = 0.38$  for water, the correction term to  $D$  is 300 microns, and for any bubble which is much larger than this, the surface area approximation becomes

$$S = \pi D^3 / 6 = V$$

Thus, if we know the gas flow in ml we can estimate the total surface area of the resulting film caps.

A parenthetical remark is in order here on the shape of bubbles below 1 mm in diameter. These are adequately approximated by the assumption of sphericity except for the film cap, which has a radius  $R$  of twice the bubble radius  $r$ . This is easily seen by considering the excess pressure

inside the bubble, which must be the same under the two-sided cap as inside the one-sided bubble. That is,

$$\Delta P = 2\gamma/r = 4\gamma/R$$

While Toba's values blend smoothly with this flattened cap, not all authors seem to have made this correction for the cap radius (e.g., Allan et al. 1961).

#### THE MECHANISM OF FILM CAP RUPTURE

Before inquiring how a film cap bubble breaks, we ask why it doesn't break. A pure liquid cannot foam or form metastable lamellae, and a persistent film cap is evidence of the presence of a second component. On a structured surface such as water there may be a short term stability conferred by the intrinsic double layer of the water surface, but its relaxation time is comparable to the rotational time of water molecules, and far too short to be observable in this context. The presence of an ionic double layer is sufficient to increase foam stability slightly, and truly permanent foams arise with surface active materials which form monolayers at each surface of the film.

Such a film thins rapidly to the equilibrium distance of double layer repulsion. If thinning continues, it is largely by evaporation, which on the open ocean amounts to 1 cm/day, or roughly 0.1 micron/sec. This is sufficient to ensure that any bubble on the ocean will break within a dozen seconds, if nothing interferes. The interferences that arise are simply the lower activity of the remaining

water in the film, and the increase in transport resistance across the monolayer on the outer surface.

There is general agreement that the film caps of ocean bubbles are 2 to 3  $\mu$  thick, and this is supported by the observation that interference colors are seldom if ever seen on bubbles in sea water. These colors begin at 1.5 microns, and this sets a lower limit on possible film thickness.

There are two well-developed theories of hole formation in thin films. Scheludko et al. (1963) consider failure by buckling of the film, which occurs at a film thickness near 0.03 micron, and is not applicable here. De Vries (1958) considers the formation of a hole in the film and shows that this requires an activation energy

$$\Delta E_{act.} = 0.73\gamma t^2 \text{ ergs}$$

(where  $\gamma$  is surface tension and  $t$  the film thickness) because the hole has at first a greater surface area than the unpierced film. The possible sources of energy are thermal fluctuations, acoustical and mechanical vibration, and variations in surface tension in the film itself. In toto, they may be considered to form a disturbance with a white noise spectrum of frequencies.

Once a hole has been formed, it expands with velocity

$$v = 2(\gamma g / \rho t)^{1/2}$$

(Rayleigh 1891) independent of hole diameter. This velocity exceeds the velocity of capillary waves in the film, so that the hole always grows into undisturbed film. A hole in a 2-micron film spreads at about 12 m/sec.

The material from the hole gathers into a toroidal rim (Facy 1951). This process has been photographed by Ranz (1959)--not, however, in a bubble, but in a horizontal film of large area punctured by an electric spark. In the absence of disturbance, the toroid would continue to grow until it reached the rim of the film cap, smoothly carrying with it the entire surface.

In the presence of noise, Rayleigh (1878,1892) showed that a cylindrical jet of diameter  $d$  would break up into drops in a configuration that minimized the total energy, surface and kinetic. The spacing between the drops is  $4.5d$ . In the case of the toroid rim, which is stabilized by the mesentery-like membrane of the film around its periphery, the wavelength should be longer, and indeed Ranz's photographs show that it lies somewhere between  $4.5$  and  $6.5$   $d$ . A complete dynamic analysis requires toroidal harmonics, and although these are known (Bateman 1962), the effort is hardly justified.

Hole expansion is too rapid to allow circumferential communication of a dominant wavelength around the torus, which is thus free to break up asynchronously, under the influence of local forces in the film. This is far too complex to attempt to follow, but we may approach the early stages and perhaps estimate the number and size of the initial drops that are produced.

Consider a general case in which the film thickness  $t$  is a minimum at the center and increases at a constant angle

0. We require a mass balance between the material removed from the hole and the material added to the rim. This gives

$$(b-a)^2(t+2(b-a)\theta/3) = 2ab(\pi a - 2(t+b\theta))$$

where  $b$  is the ring radius and  $a$  the generating radius, so that  $(b-a)$  is the radius of the hole.

If we assume that the initial breakup of the torus is uniform and occurs within a few microseconds after hole formation, or, which is the same thing, within a few 10's of microns of rim travel, we obtain a certain number  $n$  of drops of radius  $r$  from the torus. The circumference breaks up into pieces with a wavelength separating them of

$$\lambda' = 2\lambda a$$

where  $\lambda$  lies somewhere between 4.5 and 6.5. This results in

$$n = \pi b / \lambda a$$

and a maximum drop radius

$$r = (3\lambda/2)^{1/3} a$$

assuming that all of the material in the torus goes into the drops.

The relation between these quantities is shown in Figure 2.5, which plots  $r$  vs.  $b$  for a family of  $t$ 's in the region of interest, for the specific case  $\theta = 0$  and  $\lambda = 2\pi$ . Lines of equal  $n$  fan radially from the origin. As mentioned before, we cannot impose a circumferential wave on the torus to assure that it will break up into uniform drops.

However, as this breakup occurs, the surface area must pass through a local maximum, again representing an energy

of activation for the process. When the generating radius  $a$  is close to the film thickness  $t$ , this energy is high, and, without making this quantitative, we may suppose that the torus will not break up until  $a = 1.5t$ . It can be seen from Figure 2.5 that this line behaves exactly as do the  $n$ -lines, so that the net result is nearly the same as insisting that the torus break up into four drops.

#### COMPARISON WITH EXPERIMENTAL RESULTS

From counts obtained in a cloud chamber, which is insensitive to drop size, Blanchard (1963) tabulated the total number of film drops produced, as a function of bubble surface area. His data show a spread of two orders of magnitude, but it is the maximum production that is of interest in this context, and this number is plotted in Figure 2.6. This line may also be taken as Day's (1964) mean drop production value.

Also shown are the theoretical numbers predicted by Facy (1951) and the numbers obtained here for film thicknesses of 1 and 2  $\mu$ .

It will be seen that the observed number is much greater than the predicted number, and, in fact, that the predicted number increases as the square root of the hole diameter, whereas the observed number increases linearly. This is not totally unexpected, and may be attributed to two facts.

Figure 2.5. Radius and number of initial film drops. A section through the growing hole is shown in the lower right corner, together with the relevant quantities and the equations relating them. (The graph is drawn for  $\theta=0^\circ$ . Very slight changes are caused by assuming any reasonable angle for  $\theta$ .) For a given thickness  $t$ , the torus can break up into  $n$  drops of diameter  $d$  when the hole has reached a diameter of  $(b-a) \mu$ .

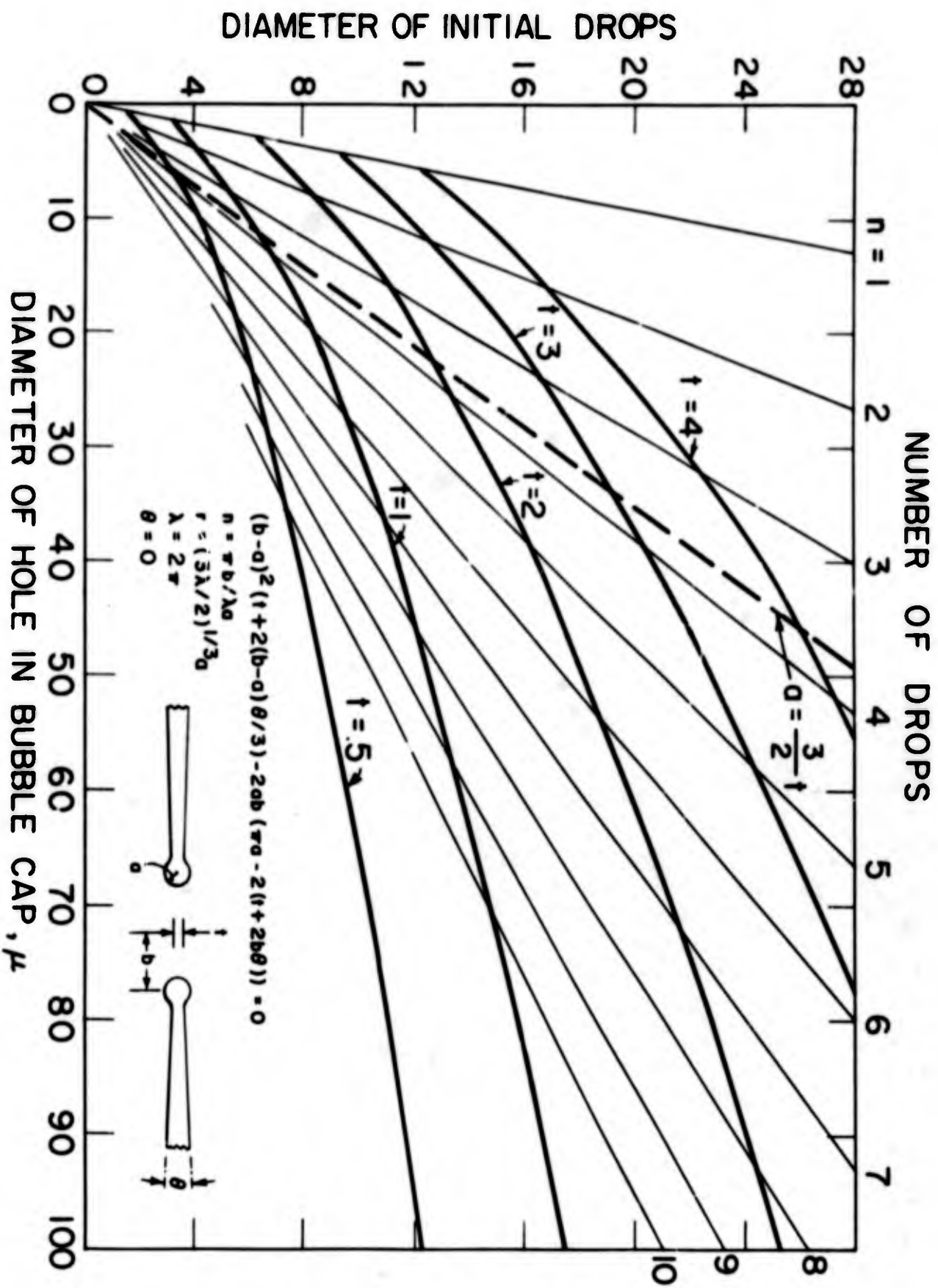
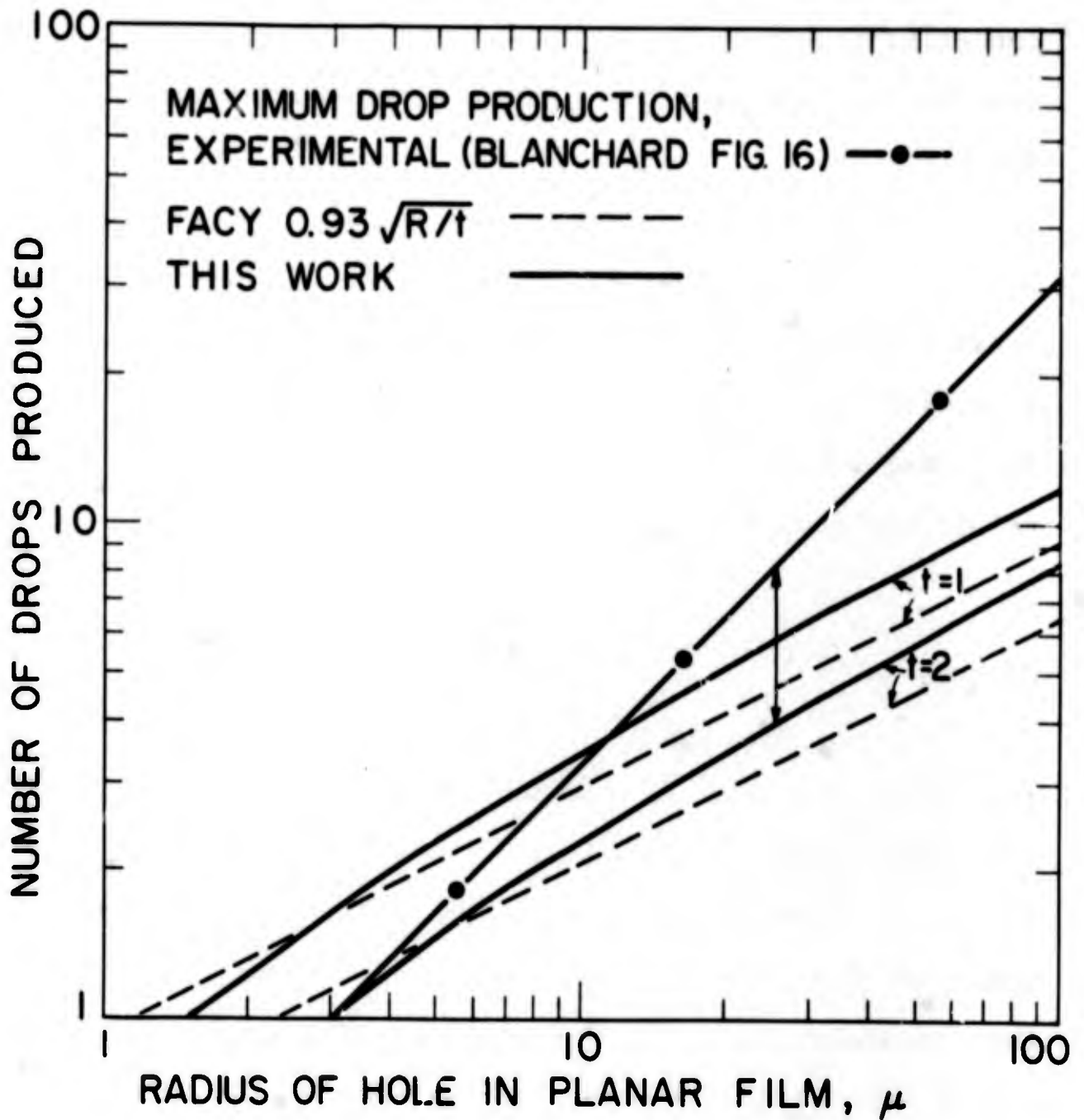


Figure 2.6 Film drop production. This plots  $\eta$  of Figure 2.5 vs.  $(b-a)$ , and compares the drop production with Blanchard's (and Day's) experimental values.



Firstly, the calculations consider only the major drops. All photographs taken of liquid threads breaking up into drops show the existence of one or more small drops for every large drop. Thus it can be claimed that the points connected by arrows in Figure 2.6 are in exact agreement, if one includes an extra small drop (which would be counted by the cloud chamber) for every large drop.

The second factor is the escaping air from the bubble. Shortly after the appearance of the hole, the excess pressure within the bubble will drive the air through the hole with sufficient force to begin blowing drops off of the expanding torus. Why this should result in a linear relationship with hole size is not clear.

#### DISCUSSION

The most important part of this is that we have taken the thinnest portion of the hubble cap, and turned it into a relatively small number of surprisingly large drops, which, in the experiments described later, will show up on the so-called 8-micron impactor stage, and will be seen to have the anomalously high phosphate enrichment. Further speculation as to the connection between bubble rupture and phosphate enrichment will be put off until the experimental results have been presented.

## FURTHER EXAMPLES OF DROP FORMATION

There are two additional occurrences of drop formation by bubbles which seem not to have been reported before, and which are interesting in their own right. Furthermore, since the parameters of interest can be varied over large ranges in these systems, they are well suited to investigations of the mechanics of bubbles.

Jet drops (and possibly film drops) are not limited to the air/water interface, but occur at the interface between any two immiscible liquids (subject to some restrictions upon viscosity and interfacial tension). A 1-mm drop of ether, rising through a water layer, stops at the interface, rests a moment, and then breaks, ejecting a jet drop of water about 2 mm into the ether layer. The drop appears to be slightly larger than comparable jet drops at the air/water interface.

Such systems offer advantages in testing theories of flow into the bubble cavity, since interfacial tension can be varied without the presence of surface-active material.

A two-dimensional analog of film drop formation is available within the structure of the thin film itself. When newly formed, such a film is not in gravitational equilibrium if it is possible for it to drain. Because drainage is fastest at the edges, where the excess material between the two surfaces can most quickly escape, a wide vertical film thins from the bottom up. That is, thin spots

form first at the bottom edge, but, since their surface density ( $\text{gm/cm}^2$ ) is lower than the surrounding thicker film, they rise like bubbles until they reach a zone of equal surface density.

When the film thickness drops to less than one-quarter of the wavelength of light, the film becomes non-reflective and virtually invisible, forming so-called "black spots". The boundary of a black spot is a discontinuity of thickness, so that there is a sharp visible "interface" surrounding it.

As a vertical film continues to thin, a black region accumulates at the top, separated from a bright straw-colored area below by a horizontal "interface". This discontinuity possesses many of the characteristics of a real interface, including a "surface tension" and the ability to propagate capillary waves.

Rising black spots behave exactly like bubbles, pausing at the interface to form film caps. These caps break at the thinnest point, and since the effective viscosity is so great, the resulting breakup into film drops proceeds at a leisurely rate and it can be seen that the retreating edge of the film beads up into a large drop which frequently, but not always, is shed to become a film drop before the rim contracts to the junction with the bulk liquid. This behavior is in complete agreement with the theory presented earlier.

It should be mentioned that in this high-viscosity situation the film caps themselves drain fastest at the bottom, so that rupture occurs not at the top, but near one end of the arch. This agrees well with Allan et al. (1961) who observed the same edge-thinning behavior in the film caps of three-dimensional bubbles in glycerine solutions.

**BLANK PAGE**

## CHAPTER III

## THE BAYLOR EFFECT

...You leave the mixture for an hour, and then bubble air through it. The blue stuff has combined with the gold to make a red compound. This is a surface active substance, and it all comes into the froth which you blow off the top. You dry the froth, add a little acid, and out comes the gold.

J. B. S. Haldane  
The Gold-Makers

## THE BAYLOR EFFECT

Baylor et al. (1962) and Sutcliffe et al. (1963) have described the following phenomenon: When bubbles are blown through sea water, the "inorganic" phosphate disappears. It is found (1) in the spray, (2) in the bulk solution as dissolved "organic" phosphate, and (3) in both solution and spray bound to particles of organic matter which have been created by the bubbling.

(The quotation marks indicate that the differentiation between organic and inorganic is that made by the oceanographers' standard molybdenum blue analysis (Ketchum et al. 1955), and that the exact forms are somewhat in doubt. It is clear, however, that the "organic" fraction must be autoclaved with sulfuric acid before it will give a visible reaction.)

It was this work which stimulated the investigation undertaken here--although the direction has changed somewhat since. The original questions addressed were two raised by Baylor: "What classes of organic compounds are responsible for binding phosphate?" and, "How does a bubble transform dissolved organic material into particles?" Though neither of these questions has been fully answered, each has left its imprint on the plan of the work. They greatly

Influenced the choice of organic additives in the experimental section of Chapter IV.

#### EARLY EXPERIMENTS

The first experiments performed were designed simply to verify the Baylor effect with a different analytical technique. This was done in the following manner:

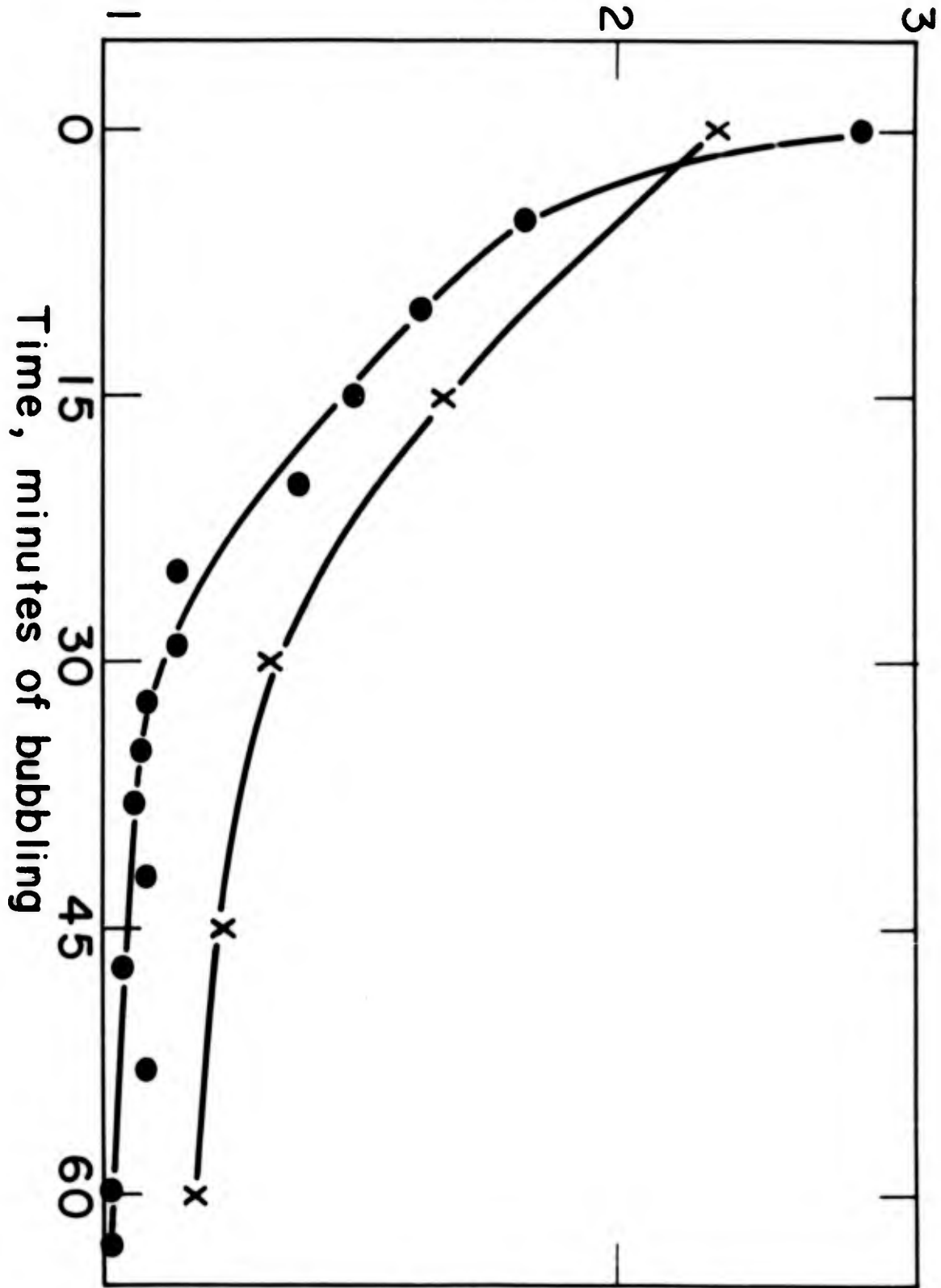
250 ml of sea water containing 10 microcuries of P-32 as  $H_3PO_4$  were vigorously bubbled, and all of the spray collected. The resulting distribution of P-32 after bubbling is compared with that of a similar experiment of Baylor's in Table 3-1.

Table 3-1. Distribution of Phosphate After Bubbling

	Sutcliffe et al. <u>(conc)aerosol</u> (conc)solution	MacIntyre <u>(counts/ml)aer.</u> (counts/ml)sol.
Original Sea Water	1.00	1.00
Residual Sea Water after bubbling	0.87	0.87
Spray	1.41	1.54
Particulate	1.08	0.88
Soluble	0.33	0.66

Figure 3.1. Time dependence of phosphate removal. All points are referred to the original composition of the sea water, and not to the concentration prevailing at the moment of drop formation.

$\frac{(P-32) \text{ aerosol}}{(P-32) \text{ sea water}}$



There is seen to be more than qualitative agreement between the two sets, in spite of widely different experimental conditions.

In other preliminary work it was noted (again in general agreement with Baylor) that P-32 transport into the spray decreased more or less exponentially with time. The results of two such experiments are shown in Figure 3.1.

The sample used in these experiments was 0.4 ml of spray, out of perhaps 0.5 ml which were collected in 5 minutes of violent bubbling. Thus, the ordinate may be read as time or as volume of spray. The bubbler was a glass frit, which led to a wide spectrum of bubble sizes, and the solution surface was covered with an assortment of bubbles, some breaking quickly, some forming stable film caps, with a thin head of foam around the periphery of the container.

#### EXTENT OF REACTION

It is evident that some agent is at work which can convert phosphate into particulate matter. The details are most easily observed in Experiment A of Sutcliffe et al., where the division between organic and inorganic products may be followed. Beginning with 100 parts of total phosphorus in Millipore-filtered sea water, and blowing bubbles through this, they arrive at the results shown in Table 3-2.

Table 3-2

## Transformation of Phosphate by Bubbles

Original Sea Water Dissolved-P		Spray Total-P	Spray Particulate-P
Organic	24	33	26
Inorganic	<u>76</u>	<u>02</u>	<u>01</u>
Total	100	35	27
		Residue Total-P	Spray Dissolved-P
		53	07
		<u>12</u>	<u>01</u>
		65	08

## SUMMARY

Input		Output	
		Unchanged	Altered
Organic Soluble	24	07	17
Inorganic Soluble	<u>76</u>	<u>14</u>	<u>62</u>
	100	21	79

Had the residual sea water been analyzed further, it too would doubtless have been found to consist largely of particulate organic phosphate. Even in the absence of such information about this largest reservoir in the system, we note that the state of at least 80% of the phosphate has been altered by bubbles. Not only has 70% of the original soluble organic phosphate been gathered into particles, but 80% of the ionic phosphate has been attached to organic material, at least some of which is particulate.

#### THE BUBBLE AS A MICELLE

Although normally one thinks of micelles as being submicroscopic in size and containing something less than 100 molecules, it is instructive to consider the bubble surface as though it were a giant micelle. The same driving forces are at work in both cases, and the free energy of each system is lowered by 750 cal/mole of  $-CH_2-$  groups which are removed from contact with water. The size and mobility of a bubble lower the effective critical micelle concentration (cmc) at which this energy decrease can be taken advantage of, so that bubbles will collect monolayers at concentrations below the normal cmc.

Colloid chemists use a number of terms to describe the various sorts of interactions between organic compounds in colloidal systems. One of these is "solubilization" (Klevens 1950), whereby aqueous solutions of surfactants at low concentrations dissolve water-insoluble compounds. A

closely related term is "comicellization" (Valkes & Epstein 1957), which is a solubilization below the cmc and one in which the insoluble component is incorporated at a greater than 1:1 ratio. An example of such comicellization is the solvation of tripolyphosphate by sodium decyl sulfate at a ratio of 4 phosphates per sulfate. The phenomenon of "interpenetration" in monomolecular films is analogous, and Goodrich (1957) has found that the free energy of mixing in two-dimensional films can be as much as -300 cal/mole for 1:1 mixtures of sodium hexadecyl sulfate and hexadecanol.

We may expect the bubble surface to display no less diversity of possible reactions than a micelle or a monolayer; thus we may anticipate a certain complexity to the organic material-phosphate-bubble system.

### PARTICULATE MATTER

#### AMOUNT FORMED

The total amount of particulates which can be produced by bubbling approximates the organic content of sea water. (This is particularly effective if the bubbles are formed by electrolysis of sea water.) The flocculent grey "snowflakes" are produced in large number and will alternately form rafts supported by small bubbles at the surface, or sink to form a sludge at the bottom. The total weight from 100 ml of sea water is on the order of 0.1  $\mu$ g.

## INORGANIC PARTICLES

Such snowflakes are not the only type of particle formed, and the picture is complicated by the occasional production of apparently inorganic particles. (These neither char in a flame, nor dissolve in 1 N HCl, ruling out the possibilities of organic material and also of carbonates, which might be expected to form after driving the CO<sub>2</sub> from CO<sub>2</sub> saturated sea water.)

The concept of "surface nucleation" or "two-dimensional nucleation" (Walton 1965) has, since the work of Frank (1959), been taken to mean growth at a screw dislocation or other crystal-surface imperfection (Nancolla & Purdie 1964). It is suggested here that there is an additional sort of two-dimensional nucleation on the surface of a bubble which arises because the local concentration sufficiently exceeds the solubility product to induce spontaneous nucleation. Since planar surfaces do not produce this effect (except through evaporation), nucleation itself may be aided by the peculiarities of flow patterns during rupture. Although Hunt & Jackson (1965) have reported nucleation arising from the collapse of bubbles, these last were cavitation bubbles in an undercooled pure liquid. The authors attribute their results to a lowering of the melting point of the solid because of the high pressure ( $10^5$  atm) reached during collapse. It may be that there is an analogous two-dimensional surface pressure during the collapse of a bubble which assists in nucleation.

These inorganic particles do not aggregate into flakes, but remain suspended to cause an opalescence. They can, however, be centrifuged into a grey-brown precipitate. Their relation to phosphate is not known, as their production appears to be an uncontrollable event peculiar to particular samples of sea water. Their mention serves chiefly to alert the reader to unresolved complexities in the process, and they will not be further considered here.

#### ORGANIC PARTICLES

The nature of the organic material of the flakes has not been determined, but they appear to contain the bulk of the organic material present. Baylor and Sutcliffe (1963) have shown that no other food source is necessary for brine shrimp, and Riley (1963) believes such "carbon-rich aggregated particles" to be of oceanic ecological significance.

Still, there is a relatively small number of candidates for the phosphate-binding components, so it seemed feasible to attempt to find a class of organics which, when added to artificial solutions, would duplicate the results obtained in sea water.

The requirements for such a material are (1) some known affinity for  $PO_4^{3-}$ , (2) some degree of surface activity, and (3) an oceanic concentration roughly approximating that of phosphate at  $10^{-6}$  M. The possibility that more than one substance is involved must be considered, for it may be that

the phosphate-binder is not itself surface active, but adheres to a monolayer of some other material.

Suspicion falls at once upon proteins, for the metaphosphate-protein reaction has been known since Berzelius (Briggs 1940, Drabikowski 1963). This reaction, which exhibits a sort of equilibrium constant involving the chain lengths of the reactants, has been used (Katchmann & Van Wazer 1954) to separate mixtures of proteins by selectively precipitating the high molecular weight fraction. Presumably the attraction between the metaphosphate and the reactive sites on the protein extends to single PO ions, even though there is insufficient bond formation to lead to crosslinking and precipitation. The locus of attraction on the protein has not been specified, and the phosphate may be N-bonded, O-bonded, or attached to a side chain.

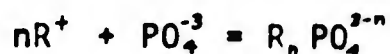
Glimcher & Crane (1964), studying the reaction of phosphate with collagen in vitro report several types of binding. They suggest that one form may be attachment to the sugars present. Similar bonding between the sulfate of sodium lauryl sulfate and the sucrose moiety of sucrose monolaurate has been observed by Ossipow et al. (1957), who also observed a negative interaction between the sucrose ester and lauroyl diethanolamine.

Sebba (1962) has categorized the process of adsorptive interaction between a charged surfactant and a dissolved ion as "ion flotation", and shown that it can be commercially

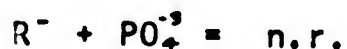
feasible to extract certain valuable metals from extremely dilute solutions by adding the correct "collector" and blowing bubbles. He reports no experiments with phosphate.

#### SURVEY OF POSSIBLE REACTIONS

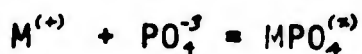
The simplest possible reaction between phosphate and a surfactant which may be reflected in bubble-surface composition is Sebba's ion flotation with a cationic surfactant  $R^+$ :



and a corollary lack of reaction with an anionic surfactant  $R^-$ :



Similar in principle, but perhaps distinguishable kinetically, is the reaction involving a preformed micelle or micelle-like structure  $M^{(n)}$  on the bubble:

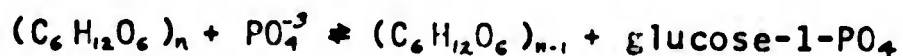


where the net charge is left undefined.

The metaphosphate reaction may take any of several forms. Perlmann (1955) has demonstrated the existence of orthophosphate crosslinks  $R-O-PO_2^- -O-R$  in pepsin and both pyrophosphate links  $R-O-PO_2^- -O-PO_2^- -O-R$  and phosphoamide links  $R-O-PO_2^- -NH-R'$  in  $\alpha$ -casein. Oncley (1959) suggests that  $R$  should be serine ( $-CH_2-OH$ ) or threonine ( $-CH(CH_3)-OH$ ), and  $R'$  arginine ( $-CH_2-CH_2-NH-CH(NH_2)=NH_3^+$ ) or lysine ( $-(CH_2)_4-NH_3^+$ ). In the special case of collagen,  $R$  would be hydroxylysine ( $-CH_2-CH(CH_2-N^*)-OH$ ) (where  $N^*$  is the peptide

bonded N), and hydroxyproline ( $-(\text{CH}_2)_2-\text{CH}(\text{OH})-\text{CH}_2-\text{NH}_3^+$ ), which latter is also an R' candidate. (These two residues are found only in collagen, and together make up one-third of the molecule.) Terminal linkages  $\text{R}-\text{O}-\text{PO}_3^-$  are known to occur naturally, but  $\text{R}'-\text{NH}-\text{PO}_3^-$  has not yet been found in biological systems.

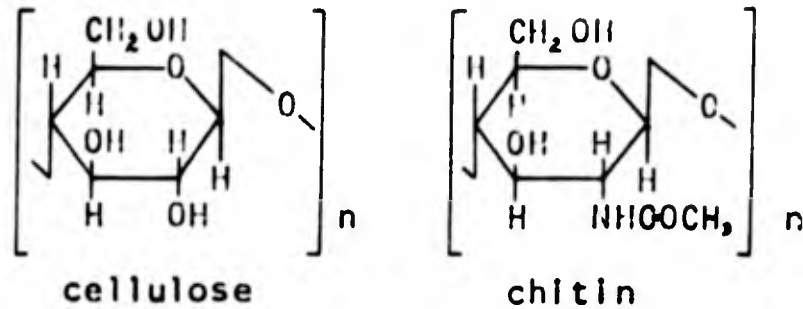
Esterification of sugars can occur on a wide spectrum of material likely to be found in sea water. Hassid et al. (1943) showed that there is an equilibrium between polysaccharide chains and phosphate mediated by the enzyme phosphorylase



which allows phosphorylase (known to be present in sea water) to behave as an amylase or as a polymerizing agent, depending upon the concentrations involved. Presumably, being a ternary reaction, this mechanism would be extremely rare in the ocean. Nevertheless, if an enzyme can lower the activation energy for the reaction, so might the bubble surface act to attach phosphate without necessarily splitting the glucoside linkage.

Polysaccharides are also known to form complexes with borate (Deuel & Neukom 1949) and with sulfate (Jirgensons 1962) without the necessity of enzymatic aid.

Of polysaccharides known to occur in sea water, cellulose and chitin (and their decomposition products)



are cited because they are among the most easily formulated. There is an endless variety of mucopolysaccharides, mucoproteins, and glycoproteins which offer similar reactive sites.

In addition to such inorganic-organic reactions, there exists the possibility of more complex reactions between monolayers and dissolved organic species (Arnold & Pak 1962).

#### BUBBLES AND THE MARINE PHOSPHATE CYCLE

The relevance of these artificial experiments to oceanological conditions may be questioned, since the bubbling rates used are higher than those generally found in the open ocean. However, North Atlantic storms at times entrain enough bubbles to make the water virtually opaque to sonar to a depth of 60 fathoms, and this occurs over large stretches of the ocean. Sutcliffe et al. (1963) discuss the less spectacular aspects of the interaction of phosphate with surface active material in sea slicks, and draw some interesting ecological conclusions.

In any event, it is difficult to assess the contribution of a portion of a cycle until it has been defined. Our

understanding of the marine phosphate cycle is still insufficient to permit its description in more detail than is given by Harvey (1960), who leaves it schematic and non-numerical. The important point is that there is but one "classical" route from phosphate ions to a form in which phosphate is accessible to zooplankton, and this is through the photosynthetic activity of phytoplankton.

We wish here to call attention to the existence of the second upward path, from inorganic ion to soluble organic phosphate to particulate organic to sea slicks, mediated by the surface of the rising bubble. The importance of this route derives from its three-fold opposition to prevailing trends.

Firstly, it is upward in a physical sense and opposes the constant gravitational settling, perhaps serving to keep the level of available phosphate higher in the euphotic zone than it would otherwise be.

Secondly, this path is upward in accessibility of phosphorus both to zooplankton and to higher forms such as surface-eating fish. It opposes the mineralizing agencies of bacteria on the surface of particles and the dephosphorylating enzymes present in sea water.

Thirdly, this path opposes the normal flow of entropy by acting as a concentrating agent and as a structure-builder.

Historically, this last may have been its most important contribution. From the ubiquity of the membrane

as a component of cellular organelles we may suspect that it arose early in acellular (or prebiochemical) evolution. The first self-reproducing chemical structures may well have been shielded by a similar membrane.

A bubble possesses three features not shared by a flat surface. The first is that small bubbles, convectively carried downward to regions of greater hydrostatic pressure, will go into solution, leaving their surfactant coat behind like a deflated balloon--or like the ghost of a red blood cell. In addition to forming proto-membranes, breaking bubbles offer the intriguing possibility of converting the mechanical energy of rupture into chemical bond formation in the surface film, which is rich in reactive sites and perhaps oriented in energetically favorable configurations by surface forces. Finally, when a bubble breaks and ejects a portion of its film into the atmosphere, it provides further scope for reactions induced by partial drying, radiation, and interaction with similar aerosol particles through aggregation.

Fox (1960) notes that phosphate exerts an activating effect upon protein biosynthesis, and Vegotsky & Fox (1959) have shown that the temperature necessary for polymerization of amino acids into polypeptides can be lowered from ca. 150°C to 70°C by the addition of a polyphosphoric acid. The demonstrated affinity of phosphate and organic material for the bubble surface strongly suggests that this combination may have played a crucial role in biogenesis.

(Note added in proof)

Miller (1963) calls attention to a problem in the necessary prebiological creation of organic phosphates, citing Gulick's (1955,1957) fears that the solubility of calcium phosphate in contemporary sea water (and thus the phosphate ion concentration) is too low for meaningful phosphate-organic reactions to occur. Gulick, seeing a continuing need for easily accessible phosphate in early biological evolution, would increase the dissolved inorganic phosphate by invoking the "hypophosphite hypothesis" --hypophosphite being stable in a Precambrian oxygen-free atmosphere, and much more soluble than phosphate.

Bubbles create organic phosphates from contemporary sea water with such efficiency that the fears of Miller and Gulick now appear exaggerated. Early self-reproducing systems were presumably too simple to use photosynthesis for energy, too primitive to prey on each other. That is, they were neither "plants" nor "animals", but more like heterotrophic fungi, requiring pre-formed high-energy food--not dissolved inorganic phosphate, but particulate organic phosphate. Bubble experiments in hypophosphite solutions would be of great interest in this connection.

Gulick, A., 1955: Phosphorus as a factor in the origin of life. *Amer Sci.* 43, 479-489.

Gulick, A., 1957: Phosphorus and the origin of life. *Ann. N.Y. Acad. Sci.* 69, 309-313.

Miller, S. L., 1963: "The origin of life", pp 845-865 In The Sea, Vol III, ed. M. N. Hill, Interscience, N.Y.

## CHAPTER IV

## EXPERIMENTAL RESULTS

Some thought them physical  
And some thought them chemic  
And some found the whole affair  
Slightly academic.

Frederick Winsor  
The Space Child's Mother Goose

## EXPERIMENTAL RESULTS

### THE BASIC EXPERIMENT

In the simplest terms, an experimental run consisted of adding 100 microcuries of P-32 as sodium phosphate and 100 microcuries of Na-22 as sodium chloride to 90 ml of water, blowing bubbles in the solution, catching the resulting spray by size classification in an aerosol impactor, and determining the P/Na ratio of the several drop size samples by means of beta- and gamma-counting.

### APPARATUS

An overall diagrammatic view of the equipment used to do this is shown in Figure 4.1. The entire working area is enclosed in a modified "Micro-Void" dust-free enclosure (1) as a first-stage protection against contamination. In this amber Plexiglas enclosure, a blower (9) takes 2 m<sup>3</sup>/min of air from the room and forces it through a 2.5-cm bed of activated charcoal (10), a Cambridge "Absolute" filter (11) which retains particles larger than 0.3 microns, and out through the access opening (12) at the front. Although tobacco smoke (0.5 micron) is completely stopped by the filter, not all of the large gaseous molecules responsible

for the odor of cigar smoke are retained by the activated charcoal, and it is presumed that some of the normal gaseous pollutants of an industrial atmosphere will also find their way through. When a cigar was moved throughout the normal working area, smoke would not remain within the enclosure, but was blown out without forming eddies. (This was carefully checked because the area of the opening had been increased fourfold by extending the height of the enclosure 15".) This outward current gives considerable insurance against adventitious contamination reaching the critical area.

The working volume (2) which encloses the "micro-ocean" (8) is supported on an instrument rack (3) inside the Micro-Void. The rack also supports minor electrical gear (4) required for generating gas bubbles (5) and powering heated jet drop collectors (6).

The working enclosure is shown in greater detail in Figure 4.2, in which it can be seen that it supports the aerosol impactor (7) in close proximity to the micro-ocean. An aspirator supplies the vacuum needed by the impactor (which draws in air filtered by the Micro-Void), and the flow rate is monitored by a vacuum gauge (13) and flowmeter (14). The enclosure also provides a nodal point for an oscillating horizontal capillary (15) which is bent into a J to dip into the micro-ocean. The loudspeaker driving unit which vibrates the capillary is shown at (17), while (16) is a magnetic stirrer for the micro-ocean.

Figure 4.1. Experimental apparatus. See text for details.

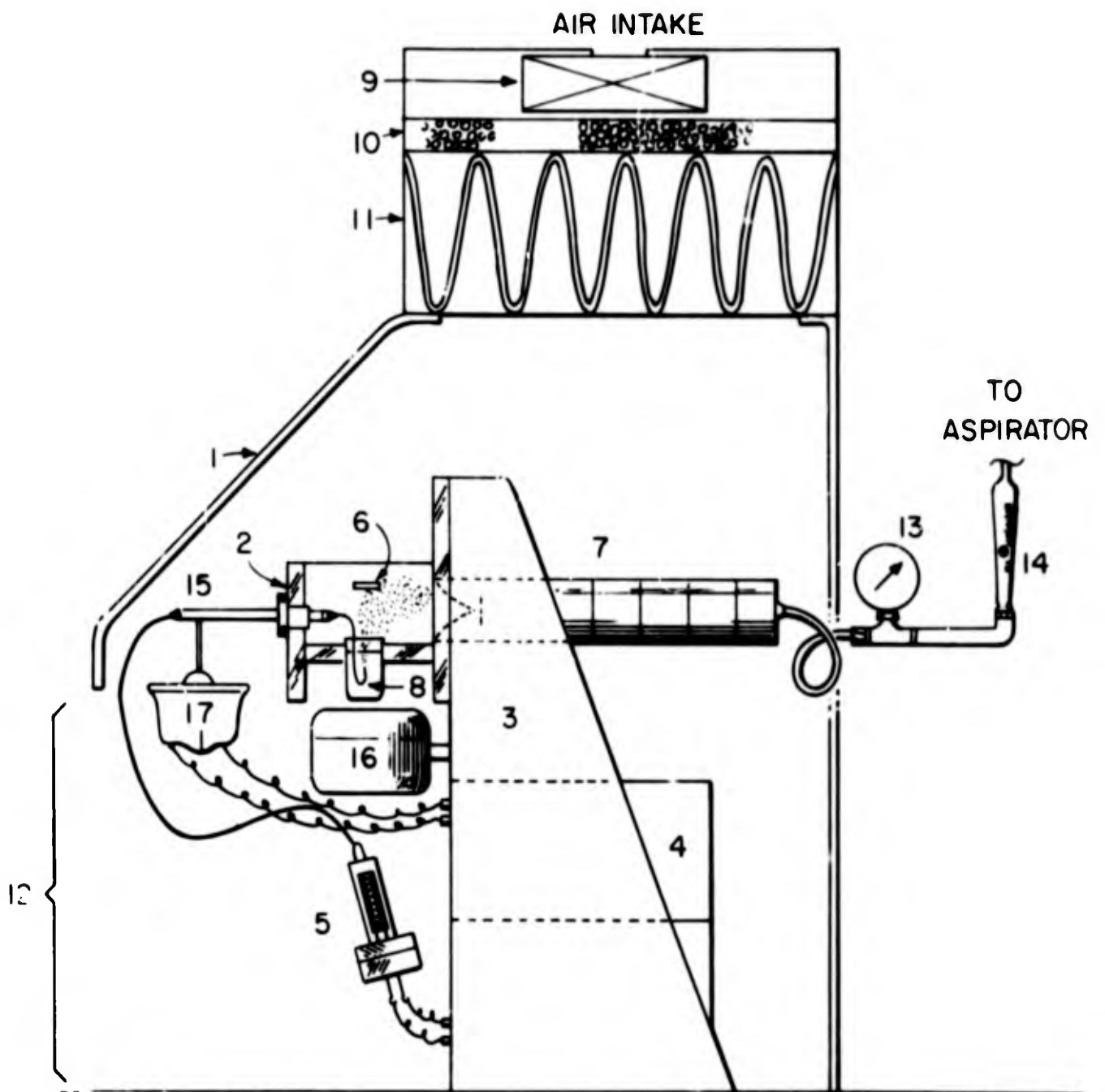
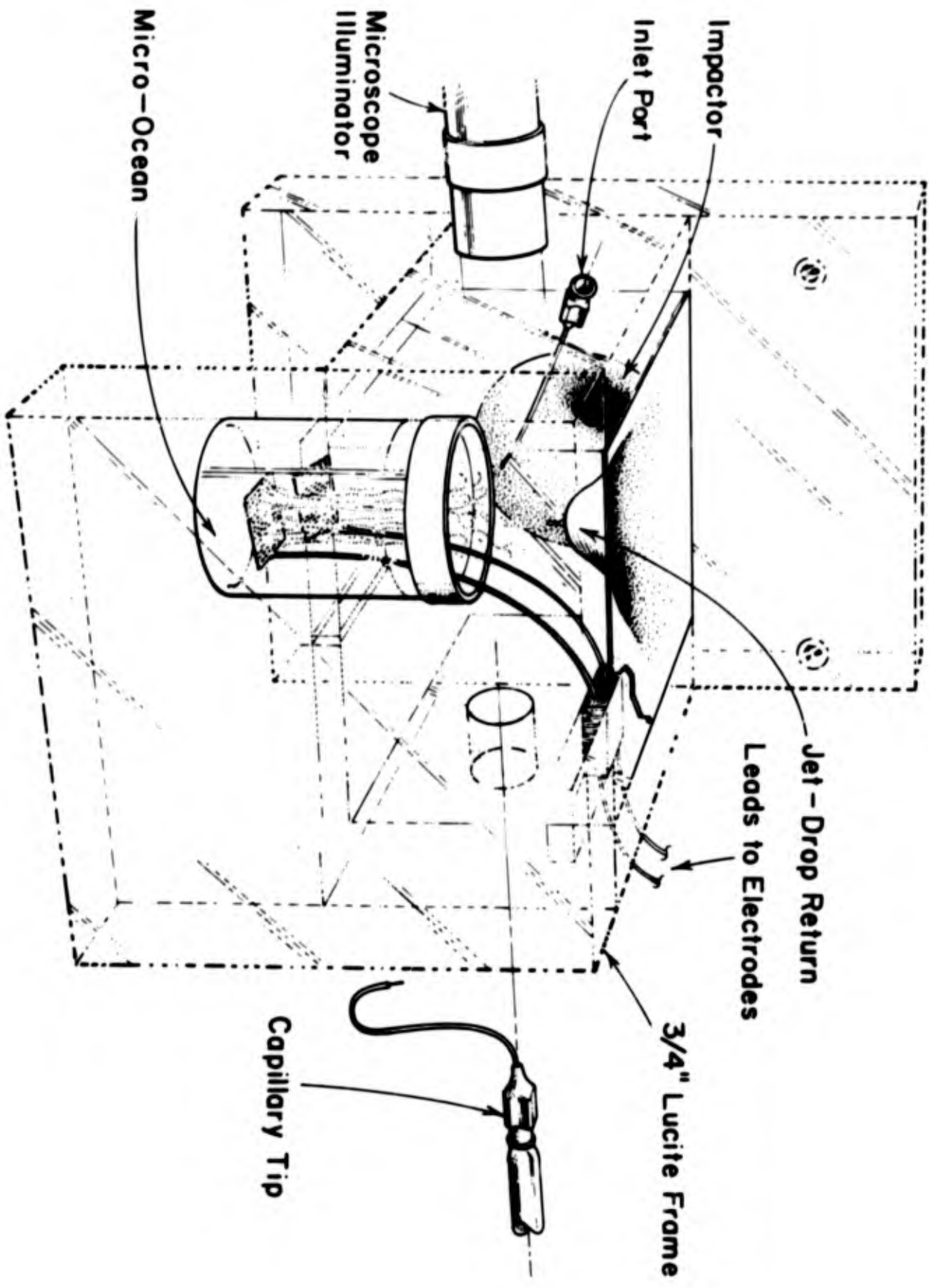


Figure 4.2. The "micro-ocean" and its enclosure. Jet drops over  $100\ \mu$  can be collected on a heated surface directly over the micro-ocean, inserted through the slot which is shown occupied by the electrode leads.



Micro-Ocean

Microscope Illuminator

Inlet Port

Impactor

Jet - Drop Return

Leads to Electrodes

3/4" Lucite Frame

Capillary Tip

Of crucial importance, if one wants to watch the movement of drops into the impactor entrance, is a microscope illuminator. Drops as small as one micron can be seen by forward scattering.

Above the micro-ocean is a curved surface which serves to catch large jet drops and return them to the container. This complex shape is easily made by stretching a piece of Parafilm over a thimble-shaped form--in this case, a polyethylene tubing protector. The Parafilm was replaced before every experiment, and was cleaned in hot nitric acid-hydrogen peroxide mixture before use, as was everything else that came in contact with the solution being studied.

The disposition of the platinum gauze electrodes used to produce bubbles by direct electrolysis can be seen, whereas the device which holds the oscillating capillary at a nodal point are not indicated. This was simply a brass ring holding three radial nylon screws which located the capillary. Although this construction introduced considerable damping, it was in general satisfactory.

#### SAMPLE COUNTING

The physical form of the sample obtained from the impactor is a small deposit (perhaps invisible) of dry salt adhering centrally to a 2.5-cm disc of 0.025-cm cellulose acetate. Upon removal from the impactor, the discs are immediately sprayed with "Krylon" lacquer, saturating the salt deposit and binding it firmly to the disc in a coating

which weighs 0.2 to 0.3 mg/cm<sup>2</sup>. (Both the total thickness and its variation are small compared to the 100 mg/cm<sup>2</sup> of the aluminum used as a beta-absorber.)

The tracers used are fully described in Table 4-1, where it will be seen that although P-32 is a pure beta-emitter, Na-22 produces both gammas and positrons. Furthermore, in practice, the gamma scintillation counter interprets bremsstrahlung of the high-energy P-32 betas as gammas, so that both nuclides in effect emit mixed radiation.

The gamma counter used was a Technical Measurement Corporation 400 channel pulse-height analyzer fed by a 5-cm well-type scintillator of NaI/Tl. Bremsstrahlung was reduced by 1.5 cm of aluminum, which also served to locate the sample disc accurately above the crystal. The question of whether to count the Na photopeak only (0.40 to 0.66 Mev) or the entire low energy spectrum (0.03 to 0.66 Mev) with its higher low-energy background contribution was answered by doing both until it became clear that the higher counting rate of the whole spectrum provided better statistics and a slightly lower error estimate.

Beta counting was done with a standard end-window proportional counter shielded by 100 mg/cm<sup>2</sup> of aluminum to absorb the Na-22 positrons. This counter sits above the gamma crystal, allowing simultaneous counts to be made.

---

 Table 4-1. Radiochemical data for nuclides used.
 

---

Nuclide	Half-Life	Energy Mev	Production Method	Specific Activity	Purity	Chemical Form
Na-22	2.58 y	0.54 1.28	Na-23(n,2n)Na-22	1 mc/gm	98+%	NaCl
P-32	14.3 d	1.71 no	S-32(n,p)P-32	Carrier free	99+%	Na PO

---

## RAW DATA

The raw data for a run comprised two sets, beta and gamma, each consisting of an even number (2 to 6) of repetitive five-minute counts of the seven impactor samples, a Na-22 and a P-32 standard, a duplicate pair from the bulk solution, a blank, and separate and combined counts of a "split standard", counted over a period of six to eight hours.

## DATA REDUCTION

The raw data is converted to useful numbers by computer, with the program given in Appendix B. Background is subtracted from the recorded beta and gamma counting rates to give corrected rates  $C_\beta$  and  $C_\gamma$ . These form a pair of simultaneous equations

$$Na_\beta + P_\beta = C_\beta$$

$$Na_\gamma + P_\gamma = C_\gamma$$

Counting standards provides the further relationships

$$Na_\gamma = a_N Na_\beta$$

$$P_\gamma = a_P P_\beta$$

where the  $a$ 's are absorption coefficients for the aluminum absorbers. Combining and solving in terms of beta counts per minute, we have

$$Na_\beta = (C_\gamma - a_P C_\beta) / (a_N - a_P)$$

$$P_\beta = -(C_\gamma - a_N C_\beta) / (a_N - a_P)$$

In practice,  $a_N = 30$ ,  $a_P = 0.1$ , so that, roughly speaking,

$$\begin{aligned} \text{Na}_\beta &\doteq C_\gamma / 30 & \text{or} & \text{Na}_\gamma &\doteq C_\gamma \\ \text{P}_\beta &\doteq C_\beta & \text{or} & \text{P}_\gamma &\doteq 0.1C_\beta \end{aligned}$$

Thus, as might be expected, the determination of Na-22 depends chiefly upon its 0.5 Mev gammas, while P-32 is seen by its 1.71 Mev betas.

In the process of solving these equations, the counting rates of the two isotopes are separately corrected back to zero time, including a correction for the decay of the sample during its collection. (Some runs required 48 hours to collect--an appreciable fraction of the 14.3-day half-life of P-32.)

The absorption coefficients needed in the simultaneous equations are computed for every run from the standards counted with the samples; a check of the over-all accuracy is obtained by counting the two halves (Na and P) of the "split standard", then counting the combination and subjecting it to the same data processing as the unknown samples. The errors found in this check are that the Na count is about 1% low, the P count 0.5% high. No reason is known for this variation, but since its effect is almost entirely removed in normalization, no serious effort was made to eliminate it.

Other checks upon the resolution of the method were those occasions when the P-half of the split standard was treated as though it were a mixed sample. For this presumably pure P-32 sample, the data reduction program reported 1 cpm of Na to 12000 cpm of P--a fact which gives

credence to the samples which show 1 cpm of Na to 1000 cpm of P.

Further data processing is limited to a determination of the various derived quantities discussed elsewhere, and to a determination of the standard deviation of all the numbers reported.

If the reader shares the author's mistrust of graphical data presented with no estimate of error, he will appreciate the standard deviation bars drawn at  $\pm 1$  sigma on the graphs herein, and may perhaps wonder at the large variability in their length.

These bars are a true estimate of the error of each individual point, and are not based upon an assumed error from counting statistics. They reflect background, absorption coefficients calculated from the standard counts, counter drift--in short, all errors in the counting process.

#### DESCRIPTION OF RUNS

This information is summarized in Table 4-2.

#### RUNS WITH NO SURFACTANT ADDED

In order to establish a base line for evaluation of the effects of surfactant additives, it is desirable to know the behavior of pure water. This goal has been approached but not reached, although efforts were made in a number of runs. With a few exceptions, these runs contained ca. 0.01 M  $K_2SO_4$  to provide sufficient conductivity for the generation of

oxyhydrogen bubbles by electrolysis. In the exceptions (Runs 3, 4, 8, 9, and 34), bubbles were blown only with capillary tips, and conductivity was not required. The water used in these particular runs was from the still described in Chapter V, considered the purest available.

Unfortunately, there is little consistency among these five runs save that 3-9 show almost no enrichment. Since all runs below 10 were preliminary in nature, (neither counting procedures nor data analysis had been optimized), these low enrichment values must be considered tentative.

#### INORGANIC SALTS PRESENT

The first runs of every suite were intended as blanks, with no surfactants added. Runs 10-15, 19, 20, and 24-27 fall in this category, containing  $K_2SO_4$ , trace amounts of  $Na_3PO_4$  and  $NaCl$ . Runs 12-14 were  $10^{-4}$  M in  $NaCl$ , while 13 and 14 were originally  $10^{-4}$  M in  $Na_2HPO_4$ . Run 24 tested the effect of phosphate concentration, with  $Na_3PO_4$  varying from  $10^{-10}$  to  $10^{-5}$  M. Run 26, at constant  $PO_4^{3-}$  but in all other respects identical to 24, tested the possible time-dependence of enrichment.

No typical behavior which can be attributed to the presence of inorganic salts was found.

## IONIC SURFACE ACTIVE AGENTS

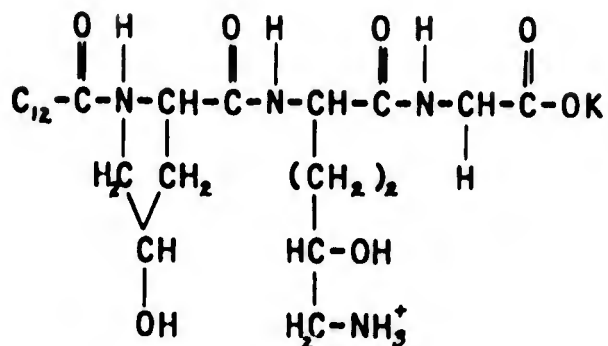
As pointed out in Chapter III, the presence of a charged surfactant should affect the adsorption of phosphate at the surface. Anionic sodium lauryl sulfate, "SLS", (Runs 16-18) and cationic cetyl trimethyl ammonium bromide, "CTAB", (Runs 21 and 22) were chosen as standard representatives to test this hypothesis. The concentration was  $10^{-6}$  M, for a 100-fold excess over the phosphate present.

## NON-IONIC SURFACTANTS

Several runs were designed to test the possibility of specific interactions between phosphate and sugars (Run 35), and the metaphosphate-protein reaction (Runs 28-31). Again, the concentrations used were  $10^{-6}$  M.

### "Maypon"

The material used to investigate the metaphosphate reaction is known as Maypon 4C, and was furnished by the Stepan Chemical Company. It is not a well-characterized compound, being the reaction product of coco-acid chloride with hydrolyzed collagen, and the resulting material contains 2 to 5 amino acid residues attached by a peptide bond to a long hydrocarbon chain which confers surface activity. Apparently the only analysis is that of Naudet & Desnuelle (1948), who report 130 parts protein to 100 parts acid. If the acid is lauric, the effective molecular weight is 460, and the generalized structure of Maypon is



with the understanding that the amino acid sequence is random among the constituents of collagen.

In spite of its uncertain composition, the material has two advantages. It allows either N-binding or O-binding of phosphate (both of which occur in nature), while possessing less foam-stabilizing tendency than true proteins at the same concentration. It is also much more surface-active than protein, and more easily collected by bubbles.

### "STRactan"

This material, furnished by Stein, Hall & Co., is a poly(arabinogalactan) obtained from the gum of larch trees, having the approximate composition



In terms of possible phosphate binding sites, this is similar to agar, carrageenin (the polysaccharide of Irish Moss, Chondus crispus), and algin (from kelp); and to cellulose, chitin, starches and glycogens, all of which occur naturally in sea water. It was chosen because of its low viscosity, good electrolyte compatibility, high gelation concentration, and high surface activity.

EXPERIMENTAL RESULTS

## NOMENCLATURE AND DERIVATIONS

The basic data obtained in these runs are

$$N_{\alpha} = \text{cpm Na-22 per impactor stage } \alpha$$

$$P_{\alpha} = \text{cpm P-32} \quad "$$

$$N_{\omega} = \text{cpm Na-22 per 25 microliters of bulk solution}$$

$$P_{\omega} = \text{cpm P-32} \quad "$$

From these are obtained the ion ratios  $R_{\alpha}$  and the fractionation ratios  $F_{\alpha}$  for each stage  $\alpha$ :

$$R_{\alpha} = P_{\alpha} / N_{\alpha}$$

$$R_{\omega} = P_{\omega} / N_{\omega}$$

$$F_{\alpha} = R_{\alpha} / R_{\omega}$$

This is the point at which atmospheric chemistry must stop, and most atmospheric data are presented in one or the other of these forms. Here, however, additional derived quantities may be obtained from the data, which are:

$$V_{\alpha} = (N_{\alpha} / N_{\omega}) 25 = \text{total volume of aerosol collected per stage, microliters}$$

$$\bar{d}_{v\alpha} = \text{the volume-average diameter of the drops collected on stage } \alpha$$

$$\bar{d}_{s\alpha} = \text{the surface-average diameter of the drops collected on stage } \alpha$$

(See Appendix A for the derivation of these.)

$$n_{\alpha} = V_{\alpha} / (\pi \bar{d}_{v\alpha}^3 / 6) = \text{the number of particles of diameter } \bar{d}_v \text{ collected on stage } \alpha$$

$$A_{\alpha} = n_{\alpha} \pi \bar{d}_{s\alpha}^2 = \text{the total surface area of drops of}$$

diameter  $\bar{d}$ , collected on stage  $\alpha$ ,  $\text{cm}^2$ .

We postpone the definition of further quantities until after discussion of the sodium results. Since the interpretation of the phosphate results depends to some extent upon the interpretation of the sodium results, we begin with the analysis of the latter.

## SODIUM RESULTS

The assumption is made (and justified below) that the Na-count of a given sample accurately represents the original water content, and that there is no change in concentration during whatever processes are operative in drop formation.

The information contained in a particular Na-count is thus the total volume of the liquid collected upon a given impactor slide.

Implicit in this assumption is another, which holds that there is no appreciable loss or gain of water by the drop between its genesis and its capture. Early experiments used dry nitrogen instead of air as the gas which swept the working volume into the impactor, and attempts to humidify the nitrogen seemed to cause more problems than they solved. With completely dry gas and a sufficiently high drop production rate, one finds that liquid has dripped off every collector slide in the impactor, indicating rapid humidification of the gas before reaching the first stage. Ultimately the drop production rate was adjusted to provide

deposits which (if one were quick about disassembling the impactor after a run) would be seen to dry as one watched. (The only truly satisfactory approach would be to monitor the humidity of each stage of the impactor to determine evaporation loss as a function of transit time, which would be a major undertaking.)

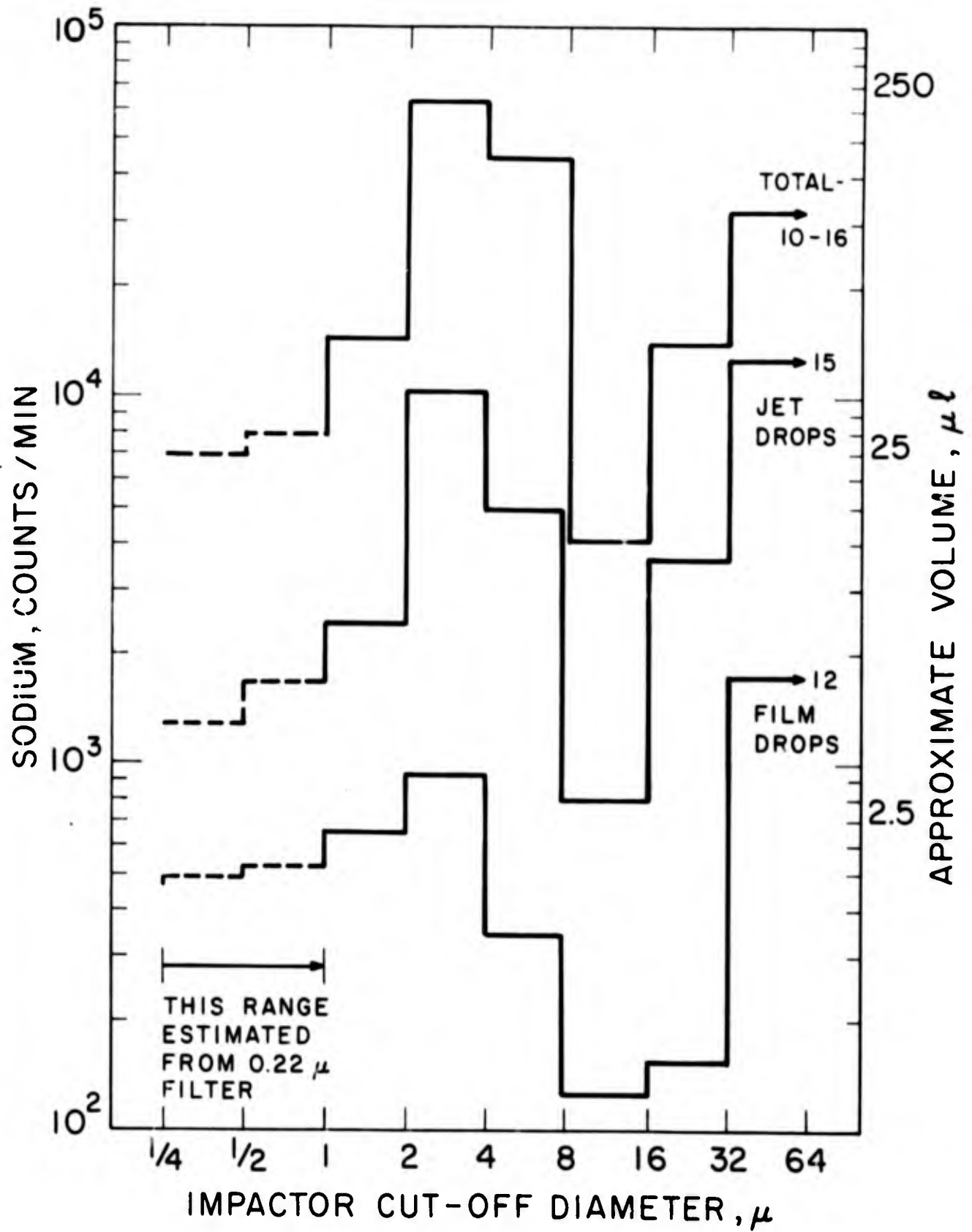
The volume distribution curve, subject to the above assumptions, from both jet drop and film drop runs is shown in Figure 4.3. Also shown is a summation of several runs of both types, which accentuates the uniformity of the volume distribution curve in spite of the drop production differences.

It should be noted that the filter-stage of the impactor (the isolated point at 1/4 micron) has been divided into two portions which are smoothed into the tail of the curve.

#### PARTICLE NUMBER

If the size range collected upon a given slide is known, the volume-average drop diameter  $\bar{d}_v$  can be obtained (Appendix A) and thence the number of drops of this diameter required to fill the observed volume can be computed. (Since  $\bar{d}_v$  is a function of the drop size distribution, which changes somewhat with every run, these average diameters are computed for every case. The range of  $\bar{d}_v$  found on each collector is indicated by the width of the points in Figure 4.6)

Figure 4.3. Volume of aerosol collected,  $V_{\alpha}$ . Total volume per stage above the 50% cutoff diameter.



The number so obtained is the particle number,  $n_x$ , which is plotted (as  $\log n$ ) vs  $\log \bar{d}_v$  in Figure 4.4.

The values are normalized to remove the effects of variable collection time. Furthermore, both jet-drop and film-drop runs are plotted together, although in total numbers per run there are one or two orders of magnitude more jet drops collected. This normalization emphasizes the remarkable similarity of size distribution between the two types of drops, even though the mechanisms which generate them are presumably quite different.

Both end points of the volume curves are uncertain. At the large end, the 32-micron stage will collect all particles over 32 microns. Occasionally very large drops, too heavy to remain airborne, are ejected obliquely toward the impactor entrance. A few of these will greatly influence the apparent particle number on the 32- $\mu$  slide, and this effect is undoubtedly the cause of some of the high values for this end of the curve.

The small-particle end of the impactor is an 0.45 micron membrane filter which catches everything smaller than 1 micron because of the high electric field strength at the corners of the pores. (A backup filter of 0.10 micron pore size was never found to have appreciable activity on it, and was abandoned since it served only to reduce the flow rate.)

Thus, the membrane filter stage is a cumulative stage, and there is little justification for treating it as though it were representative of the same two-fold interval which

characterizes the other stages of the impactor. On the other hand, it is convenient to do this, and can be partially justified in this way:

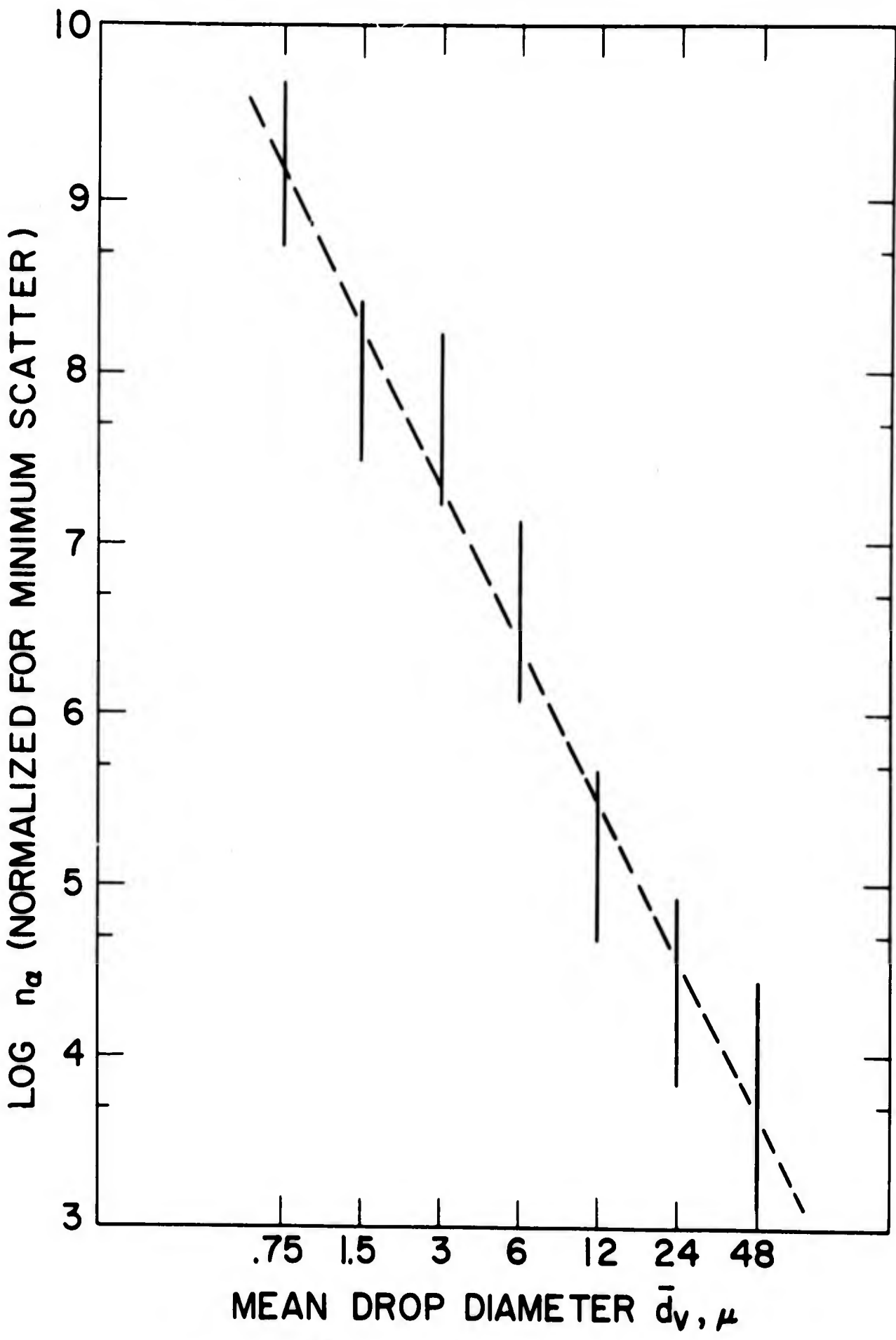
The volume calculated from the membrane filter can be attributed to two or more size classes, as was done in Figure 4.3. It may be assumed to comprise the total of the 1/2 to 1 micron range, plus the 1/4 to 1/2, plus the 1/8 to 1/4, etc. The only available criterion is the smoothness of fit to the tail of the volume curve. The particle numbers calculated from the smoothed curve have little effect upon the shape or slope of the particle number curve, and since the smoothing involves subjective judgement while producing little effect, it seems better to treat this datum uniformly with the others, remembering always that it is suspect.

#### 8-MICRON MINIMUM

There is in these curves a pronounced minimum at 8 microns which deserves comment. Since, as will be seen, this corresponds to the phosphate enrichment maximum, an apparent lack of sodium raises important questions of the possibility of sodium depletion rather than phosphate enrichment being responsible for the observed ion ratios.

A microscopic examination of the collecting slides verified the volume minimum at the point of collection, and since the minimum persists when flow rate through the impactor is changed to cause this size fraction to impact on an adjacent slide, the minimum cannot be an artifact of the

Figure 4.4. Particle number distribution from breaking bubbles. Jet and film drop runs are shown, normalized to remove inequalities in collection time. Both types of drops fit the same curve.



collector.

#### THE CONSTANCY OF THE SODIUM/WATER RATIO

There is a fundamental difference between positive and negative surface adsorption which arises from the absolute amounts of material which are available for transfer from bulk phase to surface phase. Negative adsorption can only remove material from the 10 Å surface. Considering a one-micron cube at the surface of a solution which is  $1/6 \times 10^{-5}$  M in a certain ion, with 1000 ions per cubic micron, complete negative surface adsorption will reject all--i.e., one--ion from the 10 Å surface. Even if this ion is removed completely from the cube and returned to the interior of the solution, the concentration change in the cube has changed only by 1 part in 1000.

Positive adsorption is not limited to removing what is there at low concentration, but can proceed until the surface is covered, the bulk solution depleted, or some lesser demand of equilibrium is met. As a counter example to the complete negative adsorption, consider the formation of a monolayer from the same  $1/6 \times 10^{-5}$  M solution--a not-uncommon occurrence in practice. At  $10^{14}$  molecules per  $\text{cm}^2$ , we have added  $10^6$  per square micron, which is a 1000-fold enrichment over the original composition averaged into the volume of the cube.

Since the effects of incomplete positive adsorption can easily be  $10^6$  times as great as the effect of incomplete

negative adsorption, it will be assumed that whatever negative adsorption sodium ions undergo may be safely neglected, at least in the real ocean, and no significant errors of interpretation will arise from considering that the sodium/water ratio is constant until the drop is airborne and evaporation begins.

With this in mind we return to interpret the particle number plots.

#### HIGH-WIND AEROSOL DISTRIBUTIONS IN NATURE

Since natural marine aerosols arise from the same basic mechanism of bubbles, it is natural to compare the distribution observed here with the particle size spectra found over the ocean. Those most suitable for our purpose are some presented by Eriksson (1959) from the Hawaiian data of Woodcock (1953). In essence, these plot particle number against the square root of particle radius as a function of Beaufort wind force. There is a break in the lines at approximately 4 microns, indicating that heavy particles do not remain airborne in light winds. Above Beaufort Force 3, the particle number lines turn upward, indicating a larger number of heavy particles as the wind picks up. This behavior is shown in Figure 4.5, taken from Eriksson.

In Figure 4.6 the particle numbers from this investigation are plotted in the same coordinates, and it is seen that while the break occurs at a different diameter (which may be partly accounted for by the different

Figure 4.5. Oceanic aerosol distribution as a function of Beaufort wind force. Note the effect of high wind in keeping large drops airborne.

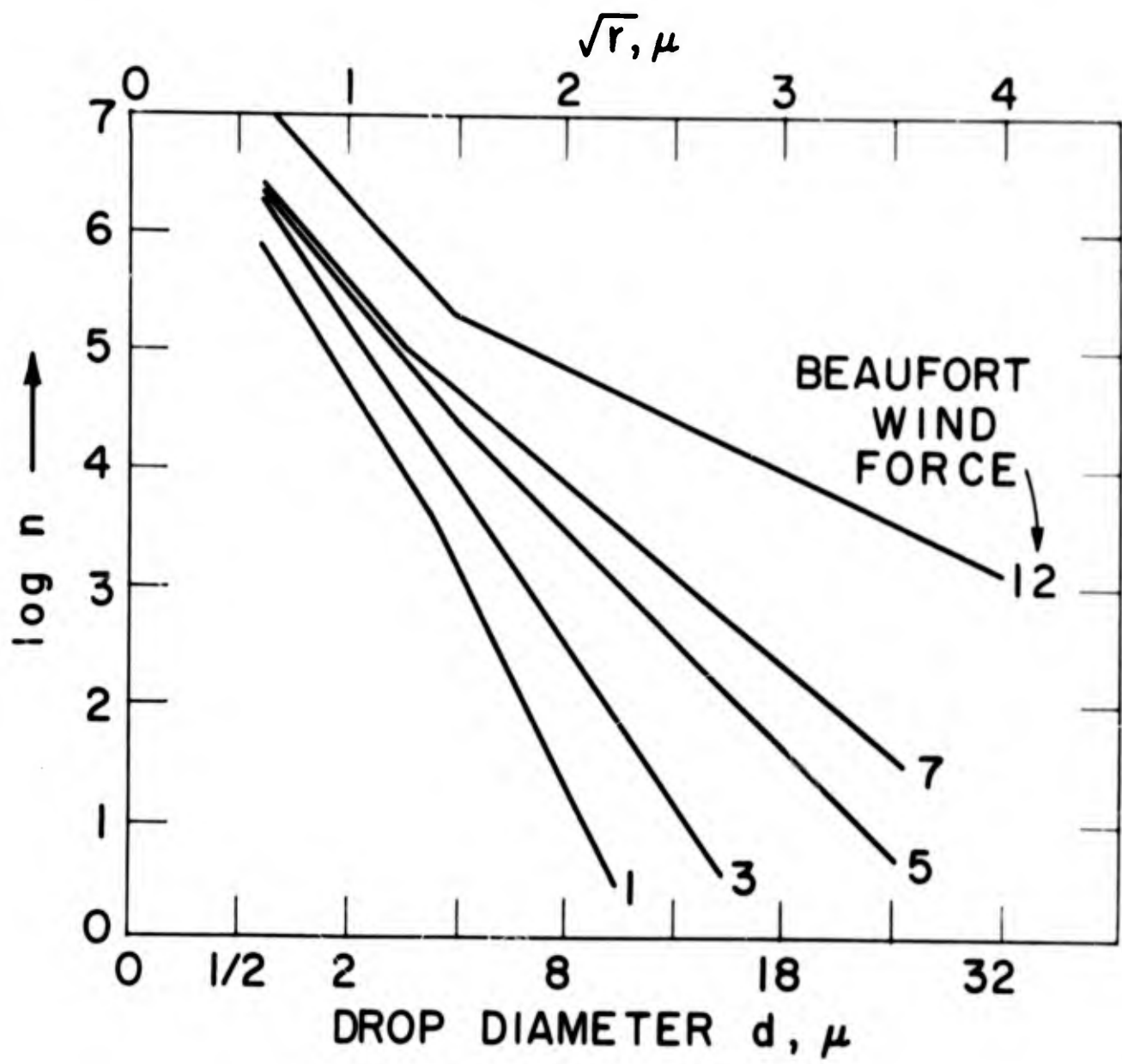
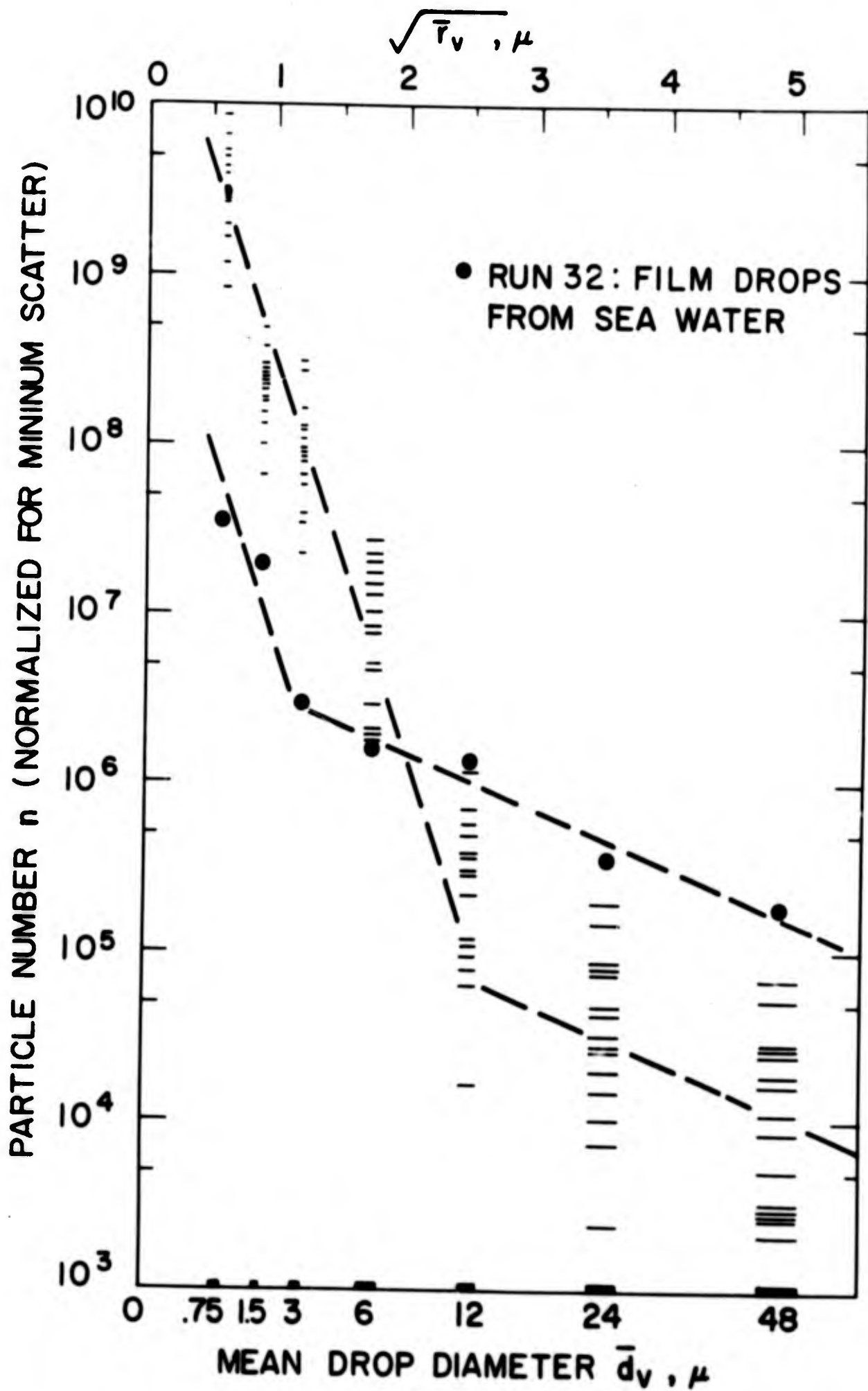


Figure 4.6. Laboratory aerosol distribution plotted against square root of drop radius. Note the similarity to Figure 4.5.



humidities prevailing during the two collections), there is a strong correspondence between the marine distribution and the laboratory distribution. The slope of the small-diameter steep portion of the curve is in good agreement, suggesting that bubbles break in much the same way in both the laboratory and on the ocean.

## PHOSPHATE RESULTS

As can be seen from Figure 4.7, which plots phosphate content  $P_\alpha$  vs. drop diameter  $d$ , there is little correlation between the absolute amount of phosphate collected and the drop size. The aerosol fractionation ratio  $F_\alpha$  is at once more regular and more meaningful, and can be reconstructed simply from subsequent graphs of  $E$  ( $=F-1$ ) whose interpretation requires further quantities defined below.

## ADDITIONAL NOMENCLATURE

We first define the "excess phosphate"  $P_{x\alpha}$  as the total amount (in cpm) on a given collection slide minus the product of the bulk solution concentration ( $=P^0=P_\omega/25$ ) and the volume collected on the slide. Thus

$$P_{x\alpha} = P_\alpha - P^0 V_\alpha = P_\alpha - N_\alpha R_\omega .$$

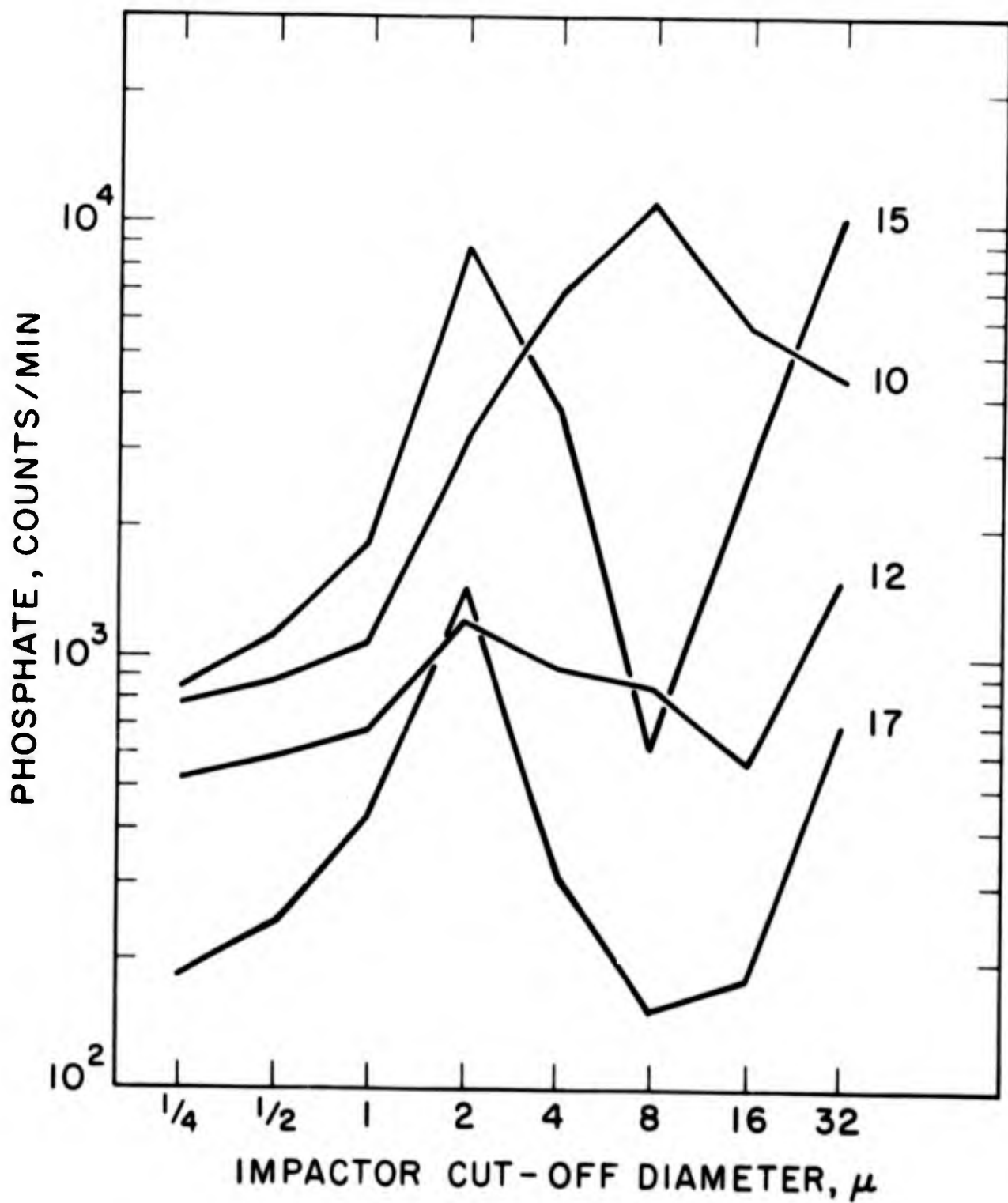
We next define a "drop-surface excess phosphate"  $\Gamma_s$  as

$$\Gamma_s = P_{x\alpha} / A_\alpha$$

In which we attribute all of the phosphate discrepancy to the surface of area  $A_\alpha$ . Though the name is formidable, this definition is the usual thermodynamic definition of the surface excess (Gibbs 1878, Lewis et al. 1961).

We will find it convenient to consider a different sort of excess called the "drop-volume excess phosphate"  $\Gamma_v$ , defined by

Figure 4.7. Phosphate content of aerosol,  $P_a$ . Unlike the Na data, there is no regularity to the amount of phosphate collected.



$$\Gamma_v = P_{\alpha} / V_{\alpha} = (P_{\alpha} - P^{\circ} V_{\alpha}) / V_{\alpha} = P^{\circ} (E_{\alpha} - 1) = P^{\circ} E_{\alpha}$$

where  $E_{\alpha}$ , called simply the "enrichment", may be thought of as a "normalized excess", being the added phosphate per phosphate expected from the bulk solution value. (i.e.: A value of  $E=2$  means that there are 3 phosphate counts in the volume where 1 was expected.)

All these quantities are defined in terms of counts per minute, which introduces no conversion constants. Direct measurement of concentration is difficult because of the tenuous relation between the high activity and the small volume of the tracers as used, and the simplest approach requires a knowledge of the decay constant  $\lambda$  of P-32

$$\lambda = \ln 2 / t_{1/2} = 3.366 \times 10^{-5} / \text{minute},$$

and the counter efficiency  $\theta$ , which is on the order of 0.05. From these we have the bulk concentration of P-32 in ions/ml

$$c_{\omega} = 10^3 P_{\omega} / 25\theta = 1.19 \times 10^6 P_{\omega} / \theta \pm 2.5 \times 10^7 P_{\omega}$$

and in moles per liter

$$C_{\omega} = 10^3 c_{\omega} / N = 1.97 \times 10^{-15} P_{\omega} / \theta \pm 4 \times 10^{-14} P_{\omega}$$

where  $N$  is Avogadro's number. From these we obtain a drop-volume excess phosphate  $\Gamma_c$  in terms of concentration

$$\Gamma_c = c_{\omega} E_{\alpha} \pm 6 \times 10^6 \Gamma_v$$

which may be seen to be the number of "unexpected" phosphate ions present in the volume considered.

#### EXCESS PHOSPHATE DATA FROM JET DROP RUNS

The first and most logical assumption to test is that the observed enrichment of phosphate in drops arises from a

surface excess which is expected not to vary with drop diameter. But  $\Gamma_s$ , plotted vs.  $\log d$ , is not constant, but increases linearly with  $d$ . This can be seen from Figure 4.8, which presents the results for the jet drop runs.

The conclusion which must be drawn from these data is that the enrichment--wherever it may come from--does not arise from a surface effect which is related to the drops per se.

The slope of  $\Gamma_s$  vs.  $\log d$  indicates that the drop-volume excess  $\Gamma_v$  (or, equivalently,  $E$ ) is constant with respect to  $d$ . This is shown in Figure 4.9, where, for reasons which will become clearer further on,  $E$  has been split into two components. One of these, here called the "linear enrichment"  $\bar{E}$ , is nearly constant for all drop sizes in a given run, and always present, while the second is a log-normal peak centered about a drop diameter  $d=15 \mu$ . It will be referred to as the "peak enrichment",  $\hat{E}$ , and it may be absent.

Figure 4.9 emphasizes the linearity of  $\bar{E}$  by showing the experimental values minus an estimated peak enrichment  $\hat{E}$  for certain runs. Thus, the observed data for Runs 11, 16, and 19 are the sums of the two curves shown.

Support for this arbitrary division of the enrichment into two components comes from the film drop runs.

Figure 4.8. Drop-surface excess phosphate. Experimental numbers are in  $\text{cpm}/\text{cm}^2$  at left. Estimated surface excess, in  $\text{ions}/\text{cm}^2$ , is shown at right. These values are based upon an assumption of carrier-free P-32, and an estimate of detector efficiency, and represent lower limits. The dotted line is that expected if the excess is proportional to the drop volume, not to the surface.

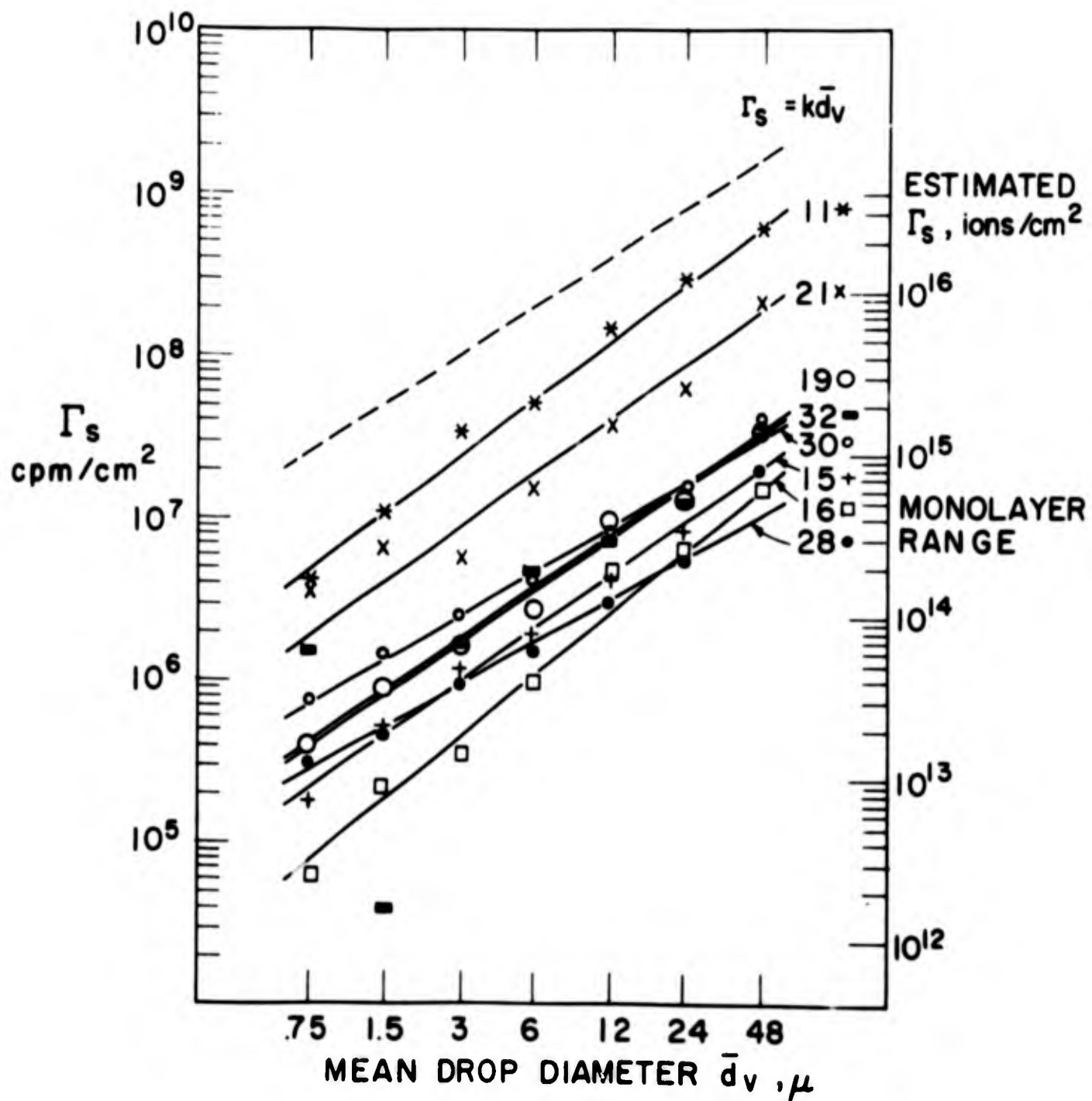
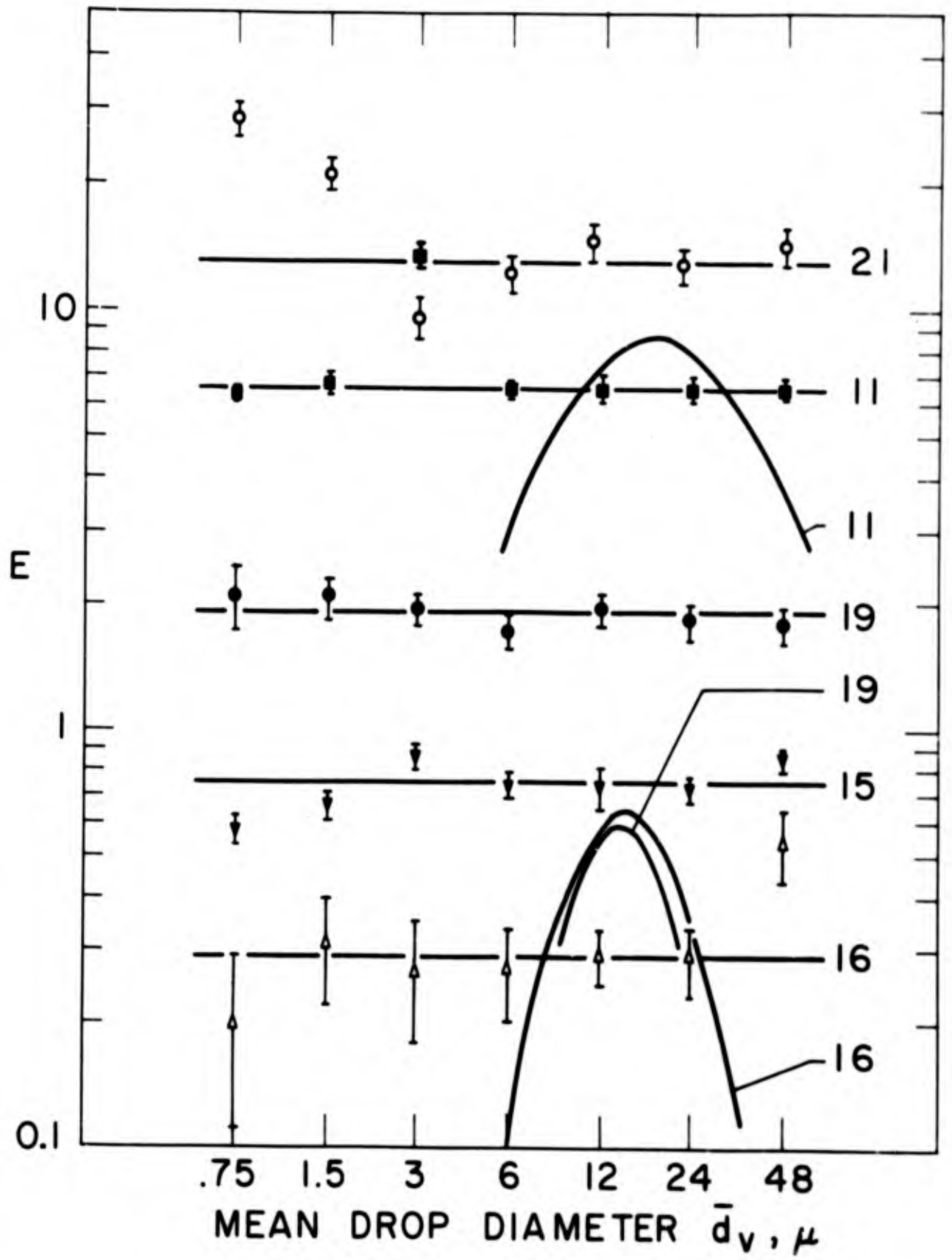


Figure 4.9. Jet drop runs. The data are presented graphically to emphasize the relative importance of the  $\pm\sigma$  bars. The "parabolas" of  $\dot{E}$  are in fact log-normal curves. Where two curves are shown for a single run, the observed data can be reconstructed by summing the two curves.



## PEAK ENRICHMENT $\hat{E}$ FROM FILM DROP RUNS

Figures 4.10 through 4.14 give the results for film drop runs, and are to be compared with Figure 4.9 (jet drop runs). The most obvious difference is the unequivocal dominance of  $\hat{E}$ , which justifies its subtraction from the jet drop runs even though it was not obvious in them.

The data points are shown as observed, and  $\hat{E}$  has been drawn by subtracting a linear  $\bar{E}$  determined from the small-diameter end of the curve. (In some cases other criteria were used, including (Run 31) the circular one of choosing an  $\bar{E}$  which made  $\hat{E}$  log-normal.) In all cases, if  $\bar{E}$  and  $\hat{E}$  are summed, the result will be seen to lie within experimental error.

The Maypon suite is shown in Figure 4.12, with the exception of Run 30, which nearly overlaps 28. Run 27 is the reference run and contains no Maypon.

Two independent sea water runs (from the same 5-liter sample) are shown in Figure 4.13. The small-diameter end of Run 32 (a vibrating capillary run) suffered from small sample size and also from fluctuations in radioactive background, making the standard deviation of these counts excessive.

Figure 4.14 shows a blank run 34 in which the drops with  $d \geq 16 \mu$  were combined, as were drops with  $d \leq 4 \mu$ . The remaining sample at  $8 \mu$  contained less than 1 cpm of Na in the presence of nearly 1000 cpm of  $PO_4^{3-}$  (as did the same sample in Run 35, containing STRactan). Thus these two

points are subject to considerable uncertainty, which is compounded with the background fluctuations mentioned above. Although they show no error bars, they are perhaps the most unreliable data of all. The dashed lines indicate averages over size classes, and Run 35 has been averaged for direct comparison with 34.

Figure 4.10. Film drop runs.  $\dot{\epsilon}$  now predominates.

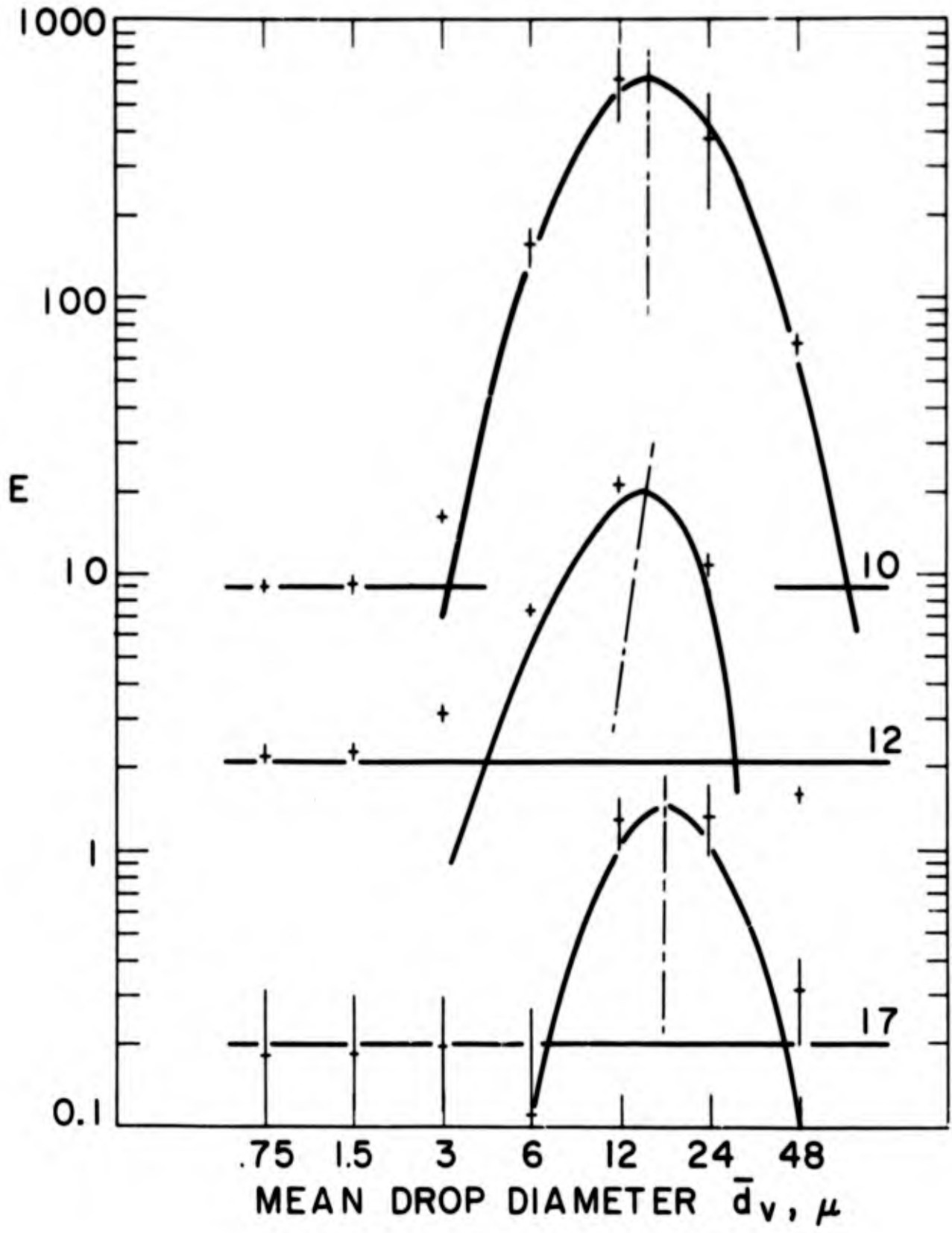


Figure 4.11. Film drop runs.  $\hat{\epsilon}$  must sometimes be skewed to fit the data.

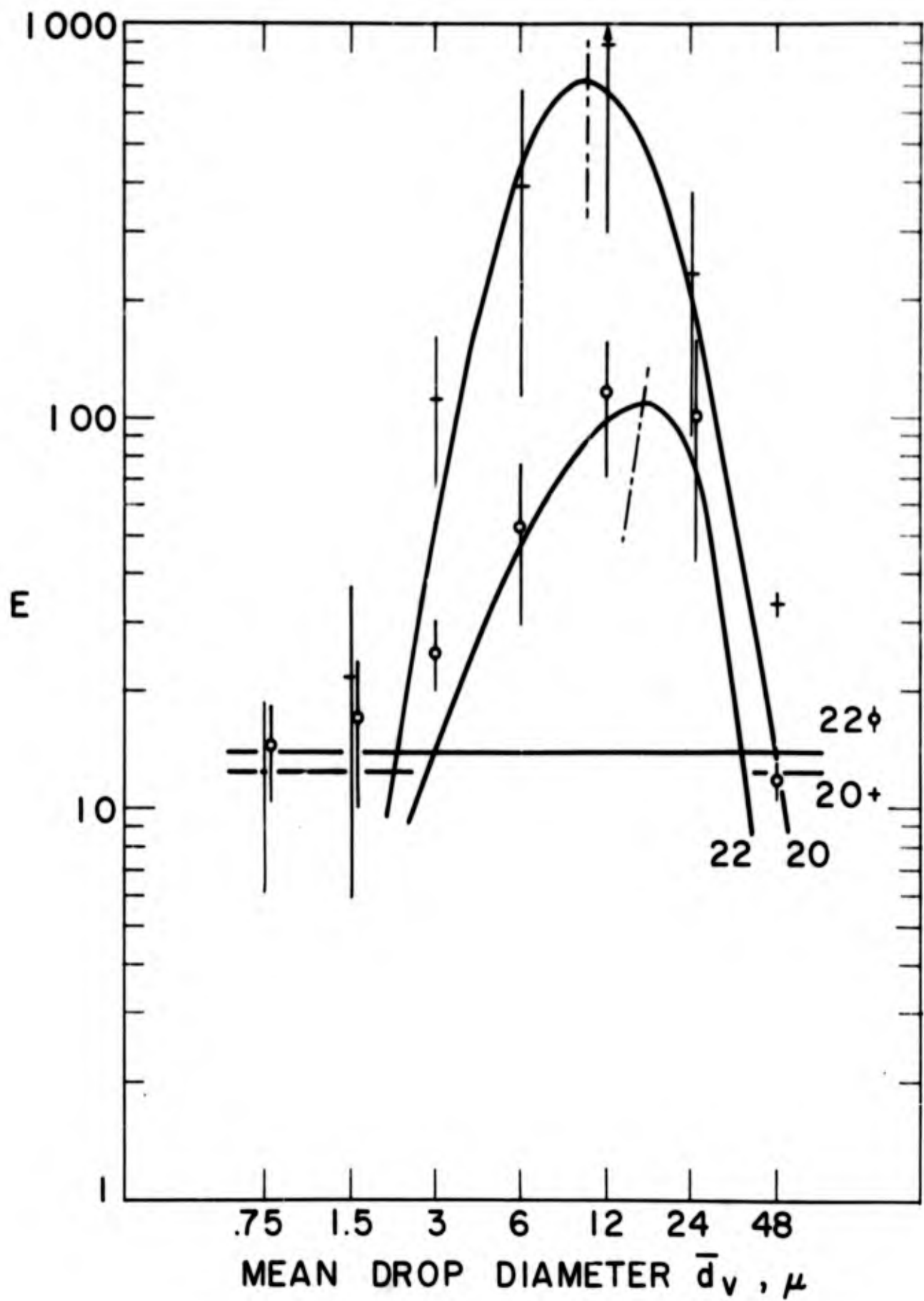


Figure 4.12. Maypon runs.

27: Base run. Vibrating capillary. Mixed jet and film drops.

28:  $10^{-6}$  Maypon added. Electrolytic bubbles, jet drops. Large volume of sample.

30: Not shown. Similar to 28. Small volume.

31: Large bubbles, film drops.

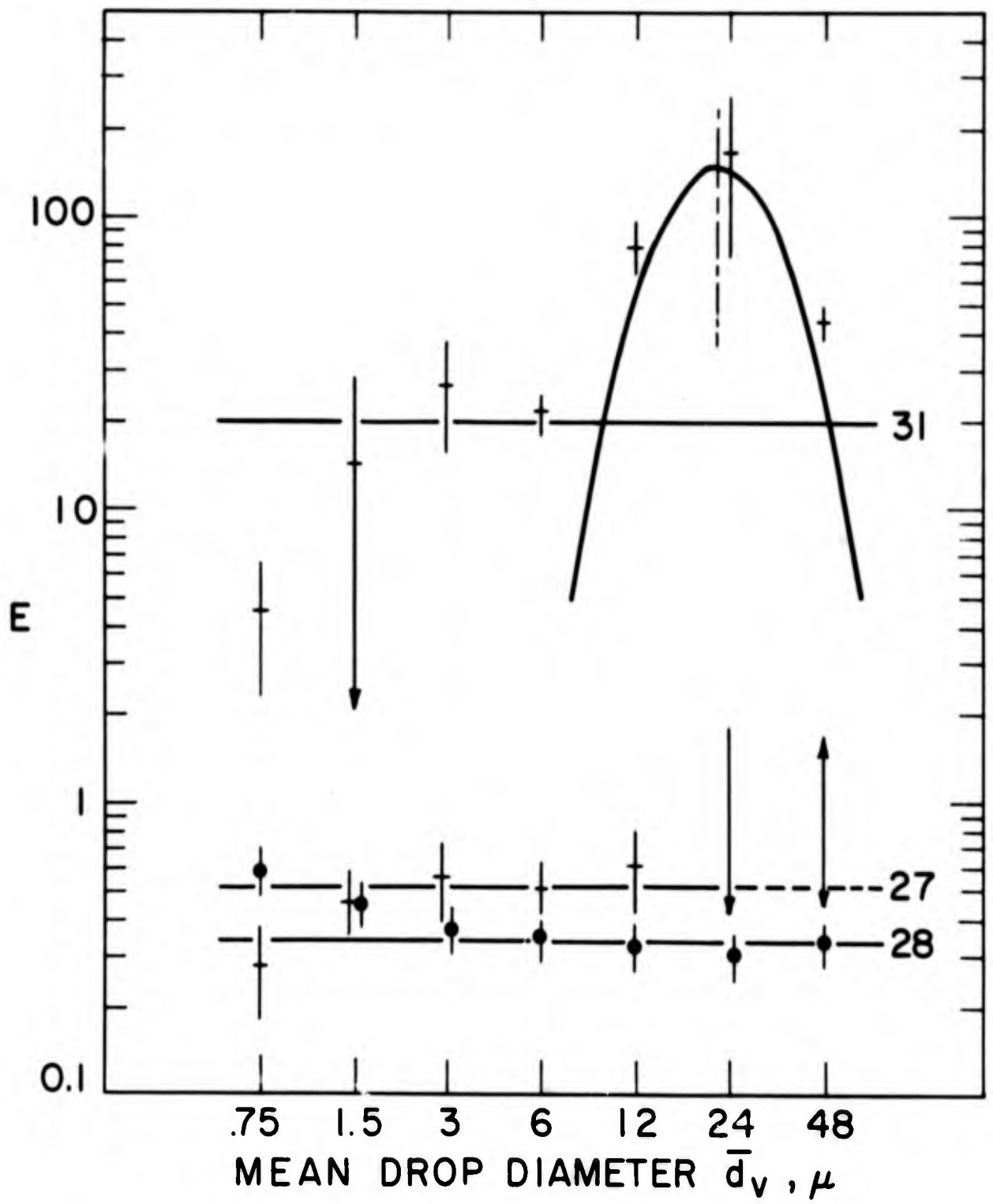


Figure 4.13. Sea water runs. Note that the  $\hat{E}$  maximum has shifted towards small drops in both of these runs.

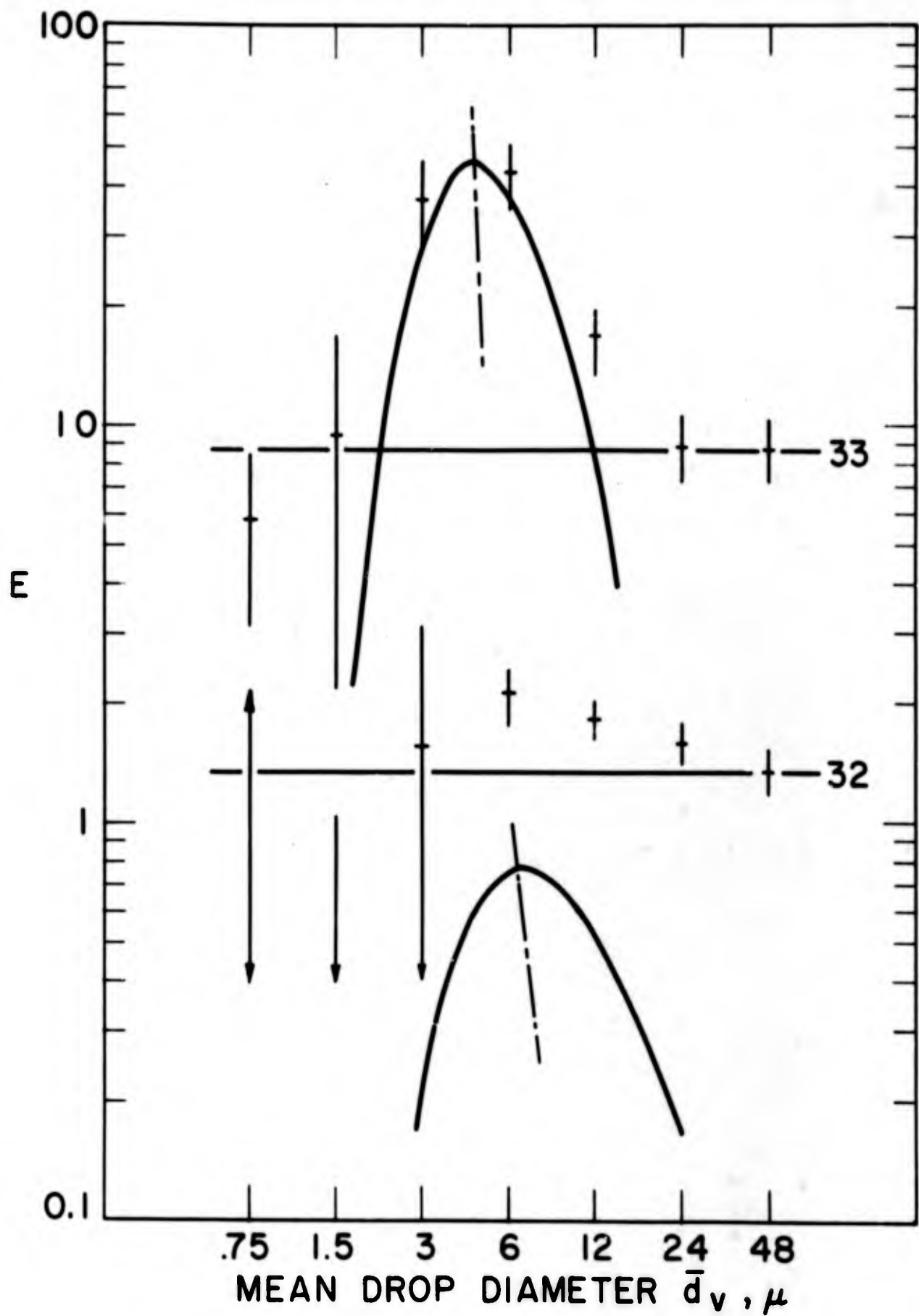
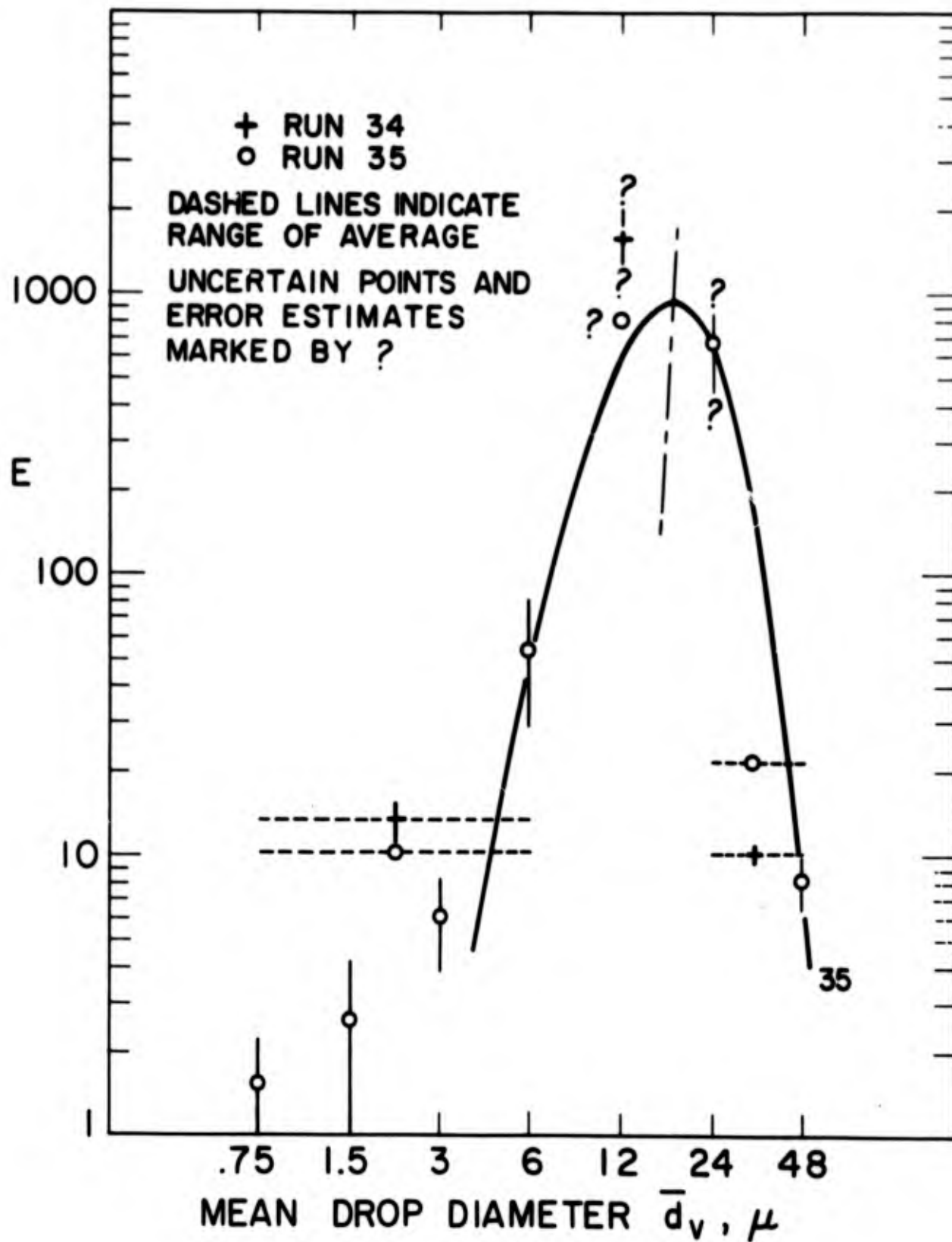


Figure 4.14. STRactan runs.

34: Base run, no intentional additive.

35:  $10^{-6}$  M STRactan added.

There is no significant difference between the runs, and no satisfactory explanation for the high  $\bar{E}$  in the base run.



## DISCUSSION

INTERPRETATION OF RUNS

Table 4-2 summarizes much of this information.

The sequence of runs 10-12, with no intentional organic additive, shows a decrease in both  $\bar{E}$  and  $\hat{E}$  with time, which may indicate that some trace substance present in the input water is being depleted by removal. This is an interpretation which is not contradicted by any subsequent evidence.

The pair 13-14 (not shown graphically) were run from the same micro-ocean as 10-12, with the addition of  $10^{-4}$  M  $\text{Na}_2\text{HPO}_4$ , in an attempt to investigate the effect of non-trace amounts of  $\text{PO}_4^{3-}$ . Unexpectedly, the acid phosphate attacked a stainless steel hypodermic needle in the solution, yielding a flocculent green precipitate of large surface area. This precipitate did not greatly lower the P-32 activity of the solution, but it completely suppressed any enrichment. ( $\bar{E}$  for the two runs averaged only 0.02, and  $\hat{E}$  was absent.) This finding is consistent with the removal of organic material by adsorption onto the large surface of the floc.

Runs 15, 19, and 20 duplicated 10-12, but with variable  $E$ 's. If this reflects uncontrollable differences in the input water composition, the enrichment is an extraordinarily sensitive indicator of trace materials!

Runs 16-18 contained sodium lauryl sulfate, 21-22 contained cetyl trimethyl ammonium bromide, and the

Table 4-2. Summary of runs.

Run Number	Bubble type	Drop type	Water source	K <sub>2</sub> SO <sub>4</sub> added	Na <sup>+</sup> > 10 <sup>-4</sup> M	PO <sub>4</sub> <sup>3-</sup> > 10 <sup>-4</sup> M	Surfactant added	Linear enrichment E	Peak enrichment E occurring at	Diameter, μ	Width of peak, σ units	Fractionation F <sub>z</sub> for entire run	Notes
3	C	?	St	-	-	-	-	1.0	---none---	---	---	---	(1)
4	C	?	St	-	-	-	-	1.0	---none---	---	---	---	(1)
8	C	?	St	-	-	-	-	---	0.5 at 32	---	---	---	(1)
9	C	?	St	-	-	-	-	---	0.2 at 16	---	---	---	(1)
10	F	F	L	x	-	-	-	9.0	630 at 15	.8	.8	56.0	
11	E	M	L	x	-	-	-	6.5	8.6 at 18	1.1	1.1	12.6	
12	F	F	L	x	x	-	-	2.1	20 at 15	.7	.7	4.29	
13	E	J	L	x	x	x	-	0.1	---none---	---	---	1.11	(2)
14	E	J	L	x	x	x	-	---	---none---	---	---	(0.93)	(2)
15	E	J	L	x	-	-	-	0.75	---none---	---	---	1.79	
16	E	M	L	x	-	-	SLS	0.29	0.64 at 14	.7	.7	1.36	
17	F	F	L	x	-	-	SLS	0.2	1.45 at 17	.7	.7	1.26	
18	F	F	L	x	-	-	SLS	---	---none---	---	---	(0.94)	(3)
19	E	J	L	x	-	-	-	1.9	0.6 at 14	.6	.6	2.89	
20	F	F	L	x	-	-	-	12.5	720 at 10	.8	.8	97.6	
21	E	J	L	x	-	-	CTAB	12.0	---none---	---	---	13.1	
22	F	F	L	x	-	-	CTAB	14.5	110 at 15	.9	.9	25.6	
24	E	F	L	x	x	x	-	---	-----	---	---	---	(4)
26	E	F	L	x	-	-	-	---	-----	---	---	---	(5)
27	V	M	L	x	-	-	-	0.52	---none---	---	---	1.50	
28	E	J	L	x	-	-	Maypon	0.38	---none---	---	---	1.34	1.2ml
30	E	J	L	x	-	-	Maypon	0.95	---none---	---	---	2.05	24μl
31	F	M	L	x	-	-	Maypon	20	150 at 22	.6	.6	47.4	
32	V	F	Sea	-	x	x	-	1.3	0.78 at 6.5	.9	.9	2.62	
33	E	M	Sea	-	x	x	-	8.8	46 at 4.5	.7	.7	15.6	
34	V	F	St	-	-	-	-	-?-	940 at 16	-?-	-?-	18.7	
35	V	F	St	-	-	-	STRactan	1.5	940 at 16	.5	.5	18.7	

Abbreviations: C=Capillary, E=Electrolytic, F=Film caps/Film drops, J=Jet, L=Barnstead still, M=Mixed, St=Special still (Chap. V), V=Vibrating capillary.

Notes: (1) Preliminary runs, not discussed in the text.  
 (2) Acid phosphate reacted with hypodermic needle.  
 (3) Bubbles exploded early.  
 (4) PO<sub>4</sub><sup>3-</sup> dependence test. (3 hour run.)  
 (5) Time dependence test. No change in E over 3 hrs.

tentative interpretation is that the enrichment is affected in the expected direction by charged material at the surface. Thus, negative SLS depressed, and positive CTAB increased, the enrichment. The data are too sparse to allow the serious treatment of electrostatic interaction at the interface which would be required to substantiate the interpretation.

#### MAYPON RUNS (28-31)

These are shown in Figure 4.12. Run 28 is noteworthy in that the total volume collected was 1.2 ml, or 1.3% of the micro-ocean volume. (It shows a slightly lower total fractionation ratio  $F_z$  for the entire run (1.34) than does the subsequent run 30 ( $F = 2.05$ ), identical except that it collected only 24  $\mu$ l.) This shows that enrichment is an equilibrium process which regenerates a surface excess and persists until the solution is depleted.

Run 31 (film drops) shows a high peak enrichment, and is to be compared to the base run 27, before the addition of Maypon. Direct comparison is risky, because the bubbles of Run 27 were generated by a vibrating capillary, and were of a size to produce both jet and film drops. (It should be noted that the jet drop component of this run is not significantly different from jet drops produced by electrolytic bubbles. It may be concluded that no visible artifacts are caused by electrolysis.)

Later runs (32,34,35) using the vibrating capillary showed high  $\hat{E}$ 's, characteristic of film drops, and it may be assumed that there were film drops present in run 27. This is significant, because 27 is the only film drop run not to show a high peak enrichment. Thus Maypon is the only substance investigated which has affected the enrichment. This may be taken as evidence supporting the metaphosphate protein interaction as a cause of phosphate enrichment.

#### SEA WATER RUNS (32, 33)

The sea water runs (Figure 4.13) are remarkable chiefly for the fact that the  $\hat{E}$  maximum has shifted down to 5  $\mu$ . (Note that this same shift occurred in Run 32 in the drop-production spectrum of Figure 4.6.)

The important difference between distilled water and sea water is probably not the ionic strength (which has no obvious influence upon  $\hat{E}$ ), but the organic content, which can affect  $\hat{E}$  either directly by chemical action or indirectly by lowering the surface tension.

The peak shift is not a chemical but a physical phenomenon, which suggests that the physical cause is the more probable. We will return to this point in the discussion of the origin of  $\hat{E}$ .

Unfortunately, the surface tension of the sea water was not measured, so that no direct evidence is available.

**STRACTAN RUNS (34,35)**

Under the pressure of time, the base run 34 (Figure 4.14) was made with only three stages of the aerosol impactor. A typical sample was collected only at the point of the expected  $\hat{E}$  maximum. With a short collection time, pooling size-classes in this way produced a normal-sized sample at each end of the drop size range but an inadequately small sample at  $8 \mu$ , which perversely had the largest (ca. 2000) and most unreliable  $\hat{E}$  yet observed. This is particularly awkward because the water used in this run came from the special still (Chapter V) which was newly in operation after repairs necessitated by moving to new quarters. The water should have contained less organic material than any run since 9, but this does not seem to have been the case.

In any event, the STRactan run 35 behaves in exactly the same way as the base run, allowing one to conclude, with equal probability, that polysaccharides have no effect upon the enrichment, or that the micro-ocean was so contaminated by unknowns that the trace amount of STRactan added was insignificant by comparison.

**SUMMARY**

As a first step in explaining phosphate enrichment, we summarize these observations into some tentative effects. Beginning with a surmise, and proceeding in order of decreasing certainty, these are:

- (1) Protein-like substances appear to increase both  $\bar{E}$  and  $\hat{E}$ ;
- (2) The drop size of maximum  $\hat{E}$  may be affected by surface tension;
- (3)  $\bar{E}$  may be influenced in the expected direction by charged surfactants;
- (4) Polysaccharides apparently do not interact with phosphate.

#### INTERPRETATION OF $\bar{E}$

Far more is known about surface thermodynamics than about the details of flow in a breaking bubble, and Occam's razor suggests that the concept of surface adsorption should not be abandoned just yet. We have only to move the surface in question off the drop and back to the interior of the bubble.

It is clear that the surface of the bubble is in thermodynamic equilibrium (or nearly so, if sorption kinetics are slow) with the bulk liquid. The bubble surface has a composition which differs from the bulk liquid.

All that is required at this point is a McBain microtome (McBain & Humphreys 1932) with which to slice a thin layer from the inside of the bubble--and we have one.

There is in the mechanism of jet formation of Chapter II a tool which will do just this, removing the surface, and only the surface from the interior of the bubble cavity.

This will create a drop in which the drop-surface excess  $\Gamma_s$  is meaningless because the drop itself does not have the composition of the bulk solution.

#### THE DROP-VOLUME EXCESS PHOSPHATE

$\Gamma_c$ , on the other hand, will provide a measure of the thickness  $dt$  of the surface skimmed from the inside of the bubble. If we write  $P_x$  and  $\Gamma_c$  in terms of the surface area  $s$  which goes into a single drop, the surface excess in the bulk solution  $\Gamma_i$ , and the particle number  $n$ , we have

$$P_x = ns\Gamma_i$$

$$\Gamma_c = (2.5 \times 10^7) P_x / V_x = ns\Gamma_i / nsdt = \Gamma_i / dt$$

and since

$$\Gamma_i = -(\partial\gamma / \partial \ln a) / RT$$

is an observable quantity ( $\gamma$  being the surface tension and  $a$  the activity), we now have in principle a direct measure of  $dt$ .

$\Gamma_i$  has not been determined for any of the solutions studied here for the simple reason that the concentrations were so low that the surface tension was indistinguishable from that of pure water (by capillary rise and maximum bubble pressure methods).

Making a very rough order-of-plausibility guess, we can satisfy the relation between surface excess and drop-volume excess with

$$(2.5 \times 10^7) P_x E_x = (2.5 \times 10^7) (2 \times 10^{-3})^5 = (2.5 \times 10^{11}) = \Gamma_c$$

$$\Gamma_c = \Gamma_i / dt = (2.5 \times 10^7) / 10^{-4}$$

where we have taken  $dt = 1$  micron in anticipation of the film drop results, and a median value of  $\Gamma_c$  from the data. This value of  $\Gamma_i = 2.5 \times 10^7$  is comfortably low, since complete coverage is  $10^{14}$  ions/cm<sup>2</sup>, and is achieved with typical surfactants at a concentration near  $10^{-3}$  M.

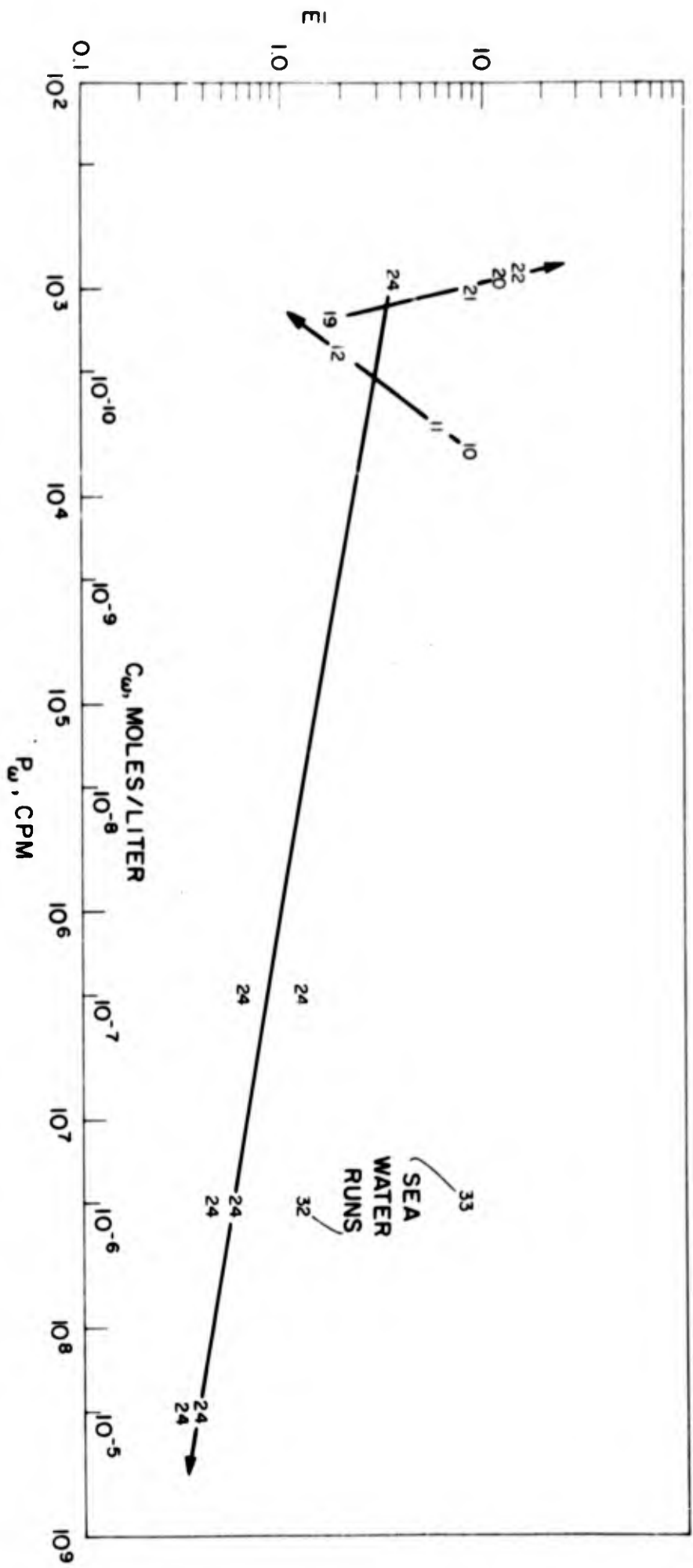
We have related  $\bar{E}$  to a universal property of solutions: a surface with a different composition than the underlying liquid. If, however,  $\bar{E}$  were a purely inorganic effect, we would expect to find a consistent relationship between the solution concentration and  $\bar{E}$ .

#### THE CONCENTRATION DEPENDENCE OF THE LINEAR ENRICHMENT $\bar{E}$

Figure 4.15 plots the linear enrichment  $\bar{E}$  against the phosphate concentration  $P_w$ . Run 24, to which  $PO_4^{3-}$  was added, is shown, as are two suites of runs, in each of which the same micro-ocean was used throughout the suite, with additions of surfactants of various sorts between runs. Decrease of phosphate occurs due to removal into the aerosol phase, and (if the tracer is effectively carrier-free) by decay of P-32. It can be seen that there is no agreement between the various suites, and that the trends observed do not depend upon the phosphate concentration, but upon some variable or constituent which was not well controlled.

The relatively high enrichment shown by the sea water runs should be noted, although it would be premature to conclude that all sea water samples would show high

Figure 4.15. Concentration dependence of the linear enrichment. No significant dependence is demonstrated.



phosphate enrichment.

#### THE 15-MICRON $\bar{E}$ MAXIMUM

This is the most exciting and least understood feature of this work. The evidence suggests that the peak is associated with film drops only, and appears in the jet-drop runs only accidentally. Since the bubbling process converts soluble phosphate into particulate phosphate in sea water, the reproducibility at 15  $\mu$  might be caused by 15- $\mu$  particles, or by 15- $\mu$  drops bearing smaller particles, but it is hard to see what sort would be formed in each of the solutions studied. The "15- $\mu$ " peak occurs at 5  $\mu$  in the two sea water runs, indicating that the details of the peak enrichment can be modified by unknown factors.

It has been shown that a 2- $\mu$  film cap will initially break into a small number of 15- $\mu$  drops. This fact offers a mechanism for converting the thinnest portion of the bubble apex into the enriched drops.

Attempts were made to show that a two-sided 2- $\mu$  film could have its surfaces interact with each other to enhance phosphate enrichment. These failed because of the short range of surface forces. Thus, sodium exclusion might be nearly complete in a 20  $\text{\AA}$  film, but it would require a 1000-fold increase in the range of intermolecular potentials to drive the sodium from a 2- $\mu$  film. Appealing as this hypothesis of synergistic surface interaction may be, it does not seem able to work in the range required.

If thickness per se is not sufficient, other possible mechanisms include: (1) electrostatic effects, drawing negative phosphate ions to the bubble apex. There are two objections to this. First, both the solution and a platinum wire 3 cm above it were grounded, so that there should be but little field available. Second, film drops in general carry a small charge which averages to zero, and there is no evidence to suggest that these drops carried any particular excess of charge. (2) Steep temperature gradients produced in the 2- $\mu$  film by radiation and evaporation might cause chemical redistribution (Soret effect)--but presumably it would be in a direction perpendicular to the film surface, which would not be reflected in the drop composition.

(3) If the phosphate responsible for the peak is associated with regions of low density (e.g., by attachment to an organic molecule) it might literally float to the bubble apex. This requires time, since the small gravitational force must move the molecule against viscous forces. One interpretation of the absence of enrichment in Run 18, in which film caps were broken shortly after formation (by explosion of the oxyhydrogen), is that there simply had not been time for phosphate to collect in this manner.

One might suggest that the same material is responsible for both the peak and linear enrichment, but that the peak arises from a local concentration of material at the point of bubble rupture. This "point", as can be seen from from

Figure 2.5, will be about  $35 \mu$  in diameter, and its concentration of phosphate roughly 100 times that of the normal surface. Thus it must represent the accumulation from the interior of a 1 mm bubble--or from a similarly small area of the large film cap.

To ensure rupture at the point of phosphate concentration, it seems necessary to postulate a concomitant weakening of the film at this point, perhaps caused by a surface tension lowering. (Knelman et al. (1954) have photographed a film cap rupturing by the formation of a secondary bubble protruding from just such a weakened area.)

The analysis of film cap rupture of Chapter II supposed minimization of surface area to be a prime consideration in the breakup of the torus, which led to a small number of large drops. If the surface tension is low, so that small drops no longer carry the energy penalty, the preferred mode of disintegration may be into more numerous small drops, thus accounting for the peak shift in sea water.

There is agreement (within an order of magnitude) between the number of initial drops produced (i.e.: estimated number of film caps broken  $\times 4$ ) and the number of drops collected which show the maximum  $\hat{E}$ . This lends credibility to the connection between  $\hat{E}$  and the point of rupture.

CORRELATION BETWEEN  $\bar{E}$  AND  $\hat{E}$ 

Figure 4.16 plots  $\bar{E}$  and  $\hat{E}$  for all runs, including those for which  $\hat{E}$  was not observed. When both are present, the two types of enrichment are seen to be coupled. The relation between them can be empirically expressed by

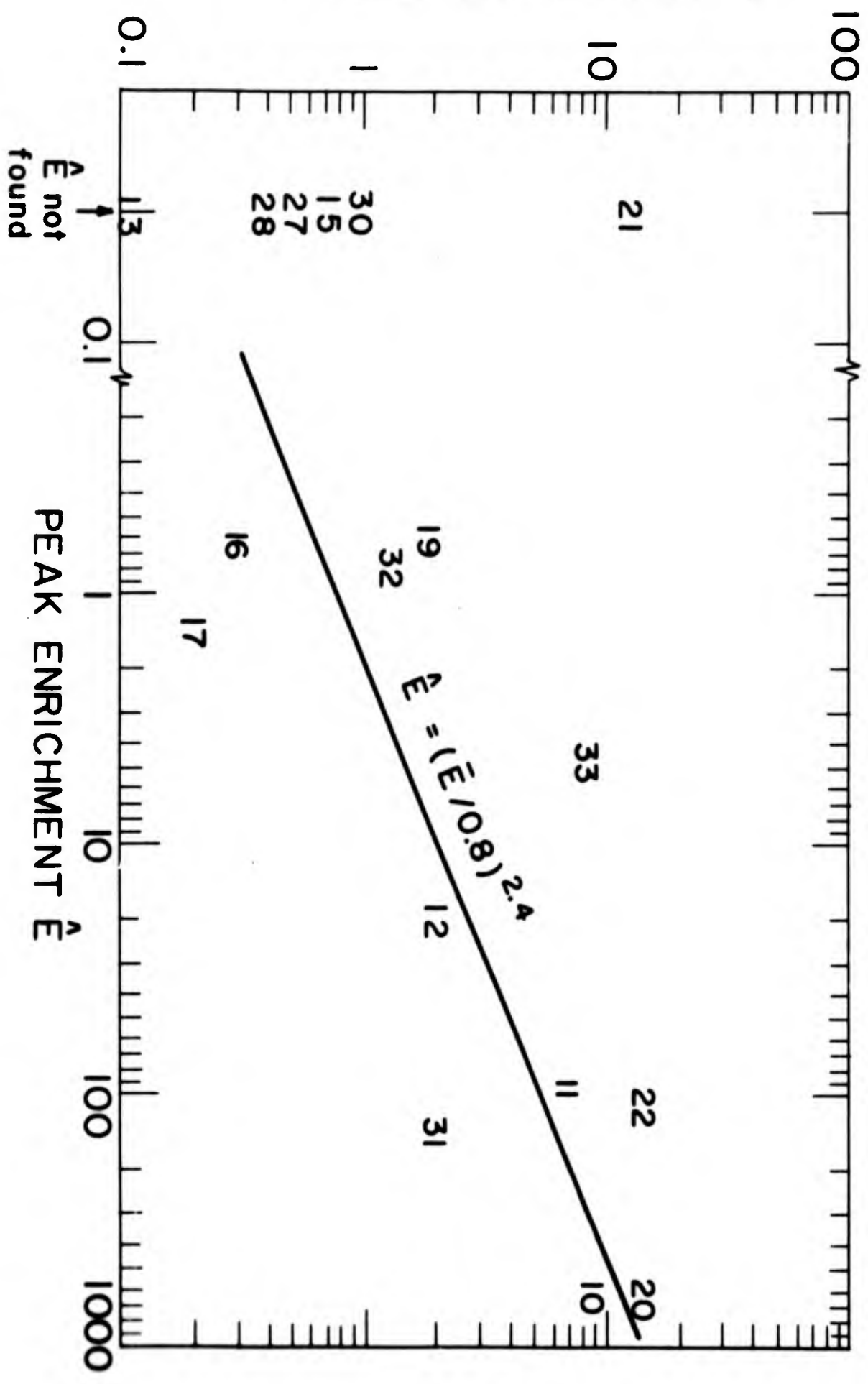
$$\log \hat{E} = 2.4 \log(\bar{E}/0.8)$$

with a correlation of 0.6. (Only slightly poorer fit is given by  $\hat{E} = \bar{E}^2$ .) In view of the experimental uncertainties and subjective evaluation by which  $\bar{E}$  and  $\hat{E}$  were separated on each run, this correlation is sufficiently high to represent a real effect.

This supports the interpretation that there is but a single chemical mechanism responsible for the two modes of enrichment, with two physical processes corresponding to the two mechanisms of drop formation. This is far more acceptable than invoking two distinct surface-chemical mechanisms, particularly given the variety of surfactants which had no effect upon the existence or size of the peak enrichment.

Figure 4.16. Correlation between  $\bar{E}$  and  $\hat{E}$ . When  $\hat{E}$  is present, its magnitude depends upon  $\bar{E}$ .

# LINEAR ENRICHMENT $\bar{E}$



## ERROR ANALYSIS

It seems advisable to conclude the discussion by noting the possible sources of error which have been considered and corrected for in these experiments, particularly as the data have seemed controversial to some people.

To begin at the easiest point of attack, we return to the solution of the simultaneous equations which separate the Na counts from the P counts. All of the numbers which went into the solution came from measurements of radioactivity, with its well-known statistical fluctuations, and it became evident early in the experiments that a measure of the reliability of a given number was urgently needed if one hoped to interpret the data. The utility of knowing the error limits of individual points rises rapidly when points are few and unconnected by theory.

Since multiple counts were taken, the standard deviation of each sample could be obtained. From these, it is possible to express the standard deviation of, say, the Na beta count in the following form:

$$\sigma(\text{Na}_\beta) = \left\{ [\sigma^2(C_\beta)(\text{Na}_\beta)^2 + \sigma^2(a_N)(C_\beta)^2 + \sigma^2(C_\gamma)] / (a_N - a_P)^2 + [\sigma^2(a_P) + \sigma^2(a_N)] [(C_\gamma - a_P C_\beta) / (a_N - a_P)^2] \right\}^{1/2}$$

where  $\sigma^2(x)$  is the variance of  $x$ , the  $a$ 's are the absorption coefficients, and the  $C$ 's are counting rates.

Further treatment of the data results in similar expressions for the error. Not only are these time-consuming to evaluate by hand, but they are also

sufficiently complicated to be troublesome to program.

Feeling that this was the sort of drudgery at which the computer excels, the author (MacIntyre 1965) wrote an extension to the MAD programming language which automatically computes these error terms (Appendix C). Known as "FUZZ", this feature will follow the propagation of error through any arithmetic processing and through special functions as needed, requiring only that it be given the standard deviation of the input data. FUZZ provided an error estimate for every number obtained in this study, except for the early runs which were processed by hand.

Although this accounts for the vagaries of counting statistics, it tells nothing of systematic or procedural errors, to which we now proceed.

#### COUNTING ERRORS

Assuming that all major sources of error in counting have been corrected (e.g.: see the section on Counting Eccentric Samples), we may look for minor errors in counting. However, these were largely guarded against by the fact that standards and a known sample were counted concurrently with each set of samples. Furthermore, normalization removes many possible errors of this type. In particular, the count-ratios are very insensitive to apparently large errors which were, on occasion, introduced by mispunching data cards. Absolute changes of 10% in the beta activity (of all counts) in a given run produced only

0.1% changes in the reported fractionation ratios  $F$  of the several samples.

Systematic errors include dead-time corrections for the detectors, and errors arising from simultaneous events being seen as single events. These are unimportant at low counting rates, but an occasional sample would show exceedingly high activity requiring correction. An estimate of dead time (20 microseconds) based on previous experience was used for the beta counter. The gamma spectrometer corrected for its own electronic dead time, and summation events were effectively removed by rejecting the spectrum immediately above the 0.5 Mev photopeak of Na-22.

Simultaneous events in the beta counter were more troublesome, and samples with activities over 100,000 cpm invariably showed variances up to 500 times the value expected for counting statistics. The effect is an underestimation of the amount of activity present, and the bias introduced by ignoring this condition on the few samples in which it was evident can only make the reported enrichment of phosphate lower than it was in actuality.

Errors can arise if the samples do not have the same geometry. It was considered that the difference in diameter of the aerosol deposits (which range from 1 to 10 mm) could be ignored, since the deposits were all concentric. To bring the reference sample (25 microliters) of the micro-ocean into similar geometry, it was found necessary to punch a small depression (with a ball bearing on a lead

brick) in the plastic disc. The standards were treated in the same manner.

#### SYSTEMATIC ERRORS

The drop samples and the reference micro-ocean sample are collected differently. This permits a systematic error which will affect all members of one run equally, but may be variable between runs. The micro-ocean sample was transferred by pipet, and trouble was experienced with adsorption of phosphate activity onto the glass, causing variable losses sometimes approaching 50%. This was eventually minimized (but not entirely cured) by conditioning the pipet with  $\text{Na}_3\text{PO}_4$  before each use, filling all the exchangeable sites with inactive  $\text{PO}_4^{3-}$ . This reduces loss of active  $\text{PO}_4^{3-}$  to exchanges between the glass surface and solution.

That gross errors have been avoided is indicated by consistencies within the several suites, each of which tends to maintain its approximate E as though this were a function of the input water. However, it may not be wise to draw conclusions about small changes in E among the runs in a suite, since these will be affected by any transfer losses.

## CONCLUSIONS

The existence of two types of phosphate enrichment corresponding to the two types of drops produced by breaking bubbles seems well established.

JET-DROP ENRICHMENT  $\bar{E}$ 

The jet-drop enrichment  $\bar{E}$  is largely independent of drop size, is universally present, and in magnitude lies between 1 and 10. It arises from a thermodynamic surface excess--not, however, of phosphate, but of a phosphate-binding organic material. The evidence favors proteinaceous compounds and suggests that polysaccharides are not responsible.

The surface involved is the interior of the bubble. During jet formation, this interior flows down the cavity wall to meet at the center, and a fraction  $\alpha$  is incorporated in the jet drops. The thickness  $dt$  of the layer carried off is

$$\alpha dt \approx 1/60 \mu$$

Since  $\alpha$  is typically greater than 0.01,  $dt$  may be quite thin. It is at least two orders of magnitude thinner than the surface microtome can achieve by surface skimming, and opens the possibility of direct chemical investigation of surface excesses down to  $\Gamma_i = 10^6$  ions/cm<sup>2</sup>, through the relation

$$\bar{E} = \Gamma_i / c_i dt$$

where  $c_i$  is the bulk solution concentration.

This specificity of surface removal by breaking bubbles can be invoked to explain most of the observed anomalies in the ion ratios of the marine atmosphere, for it insists that all drops small enough to remain airborne have come from the (molecular) surface of the sea, and will not have the composition of bulk sea water.

#### FILM-DROP ENRICHMENT $\hat{E}$

The film-drop enrichment  $\hat{E}$  is strongly drop-size dependent, being log-normally peaked at  $15 \mu$ , with a standard deviation about the geometric mean of  $\log 1.75$ . It appears only from film caps which have had a lifetime measured in seconds. In magnitude it lies between 1 and 1000, and when present is empirically related to  $\bar{E}$  by

$$\log \hat{E} = 2.4 \log(\bar{E}/0.8)$$

(approximately  $\hat{E} = \bar{E}^2$ ) with a correlation coefficient of 0.6. This correlation is considered high enough to be evidence that there is but a single chemical mechanism involved in both types of enrichment.

The physical mechanism suggested for  $\hat{E}$  is that it arises from a local concentration of the phosphate-binding material. The nature and cause of such a concentration are not known. It may be related to the known particle-forming ability of bubbles. Perhaps surface orientation or surface hydrolysis is sufficient to enable "dissolved" protein to

dehydrate, forming a "solid" layer at the surface. Or it may be that a region of slightly lower surface tension is formed by gravitational drift of light material to the bubble apex.

In either case, the result must be that the bubble is weakened at the point of concentration (which need be no larger than  $35 \mu$  in diameter). When rupture occurs, the phosphate-enriched material is found to be upon the small number of relatively large ( $15 \mu$ ) drops formed by the initial disintegration of the thickened rim of the expanding hole in the film cap.

#### ENRICHMENT OF OTHER MARINE IONS

While there is no evidence for purely inorganic ion enrichment, the phenomena described are by no means limited to phosphate. Any polyvalent ion in sea water, regardless of charge, should find some surface active material with which to associate, leading to an aerosol enrichment with respect to sodium.

The case for univalent ions is not so clear, except for those which are biologically enriched in the organic detritus which is also ejected by bubbles.

Specifically, one should expect to find enrichment of sulfate, iodine, organic nitrogen, calcium, magnesium, and potassium from one or the other of the above mechanisms. The question of the chlorine/sodium ratio remains open.

CHAPTER V

SUPPORTING WORK

As unstable as a water bubble

The Panchatantra

ON HIGH-PRECISION COUNTING OF  
ECCENTRIC RADIOACTIVE SAMPLES

There are two widely held beliefs about the precision obtainable by beta counting. The naive hope is that  $\sigma = \sqrt{N}$  is the standard deviation which one can achieve. The jaundiced view, generally held by those who began with the first, is that one is lucky to be able to count within 1%, and that high precision work should not be expected from beta counting.

Early in this work, the naive view was taken, in the expectation of seeing 0.1% differences in fractionation ratios. Although all the recommended precautions were heeded, the counting precision attainable was far below the theoretical maximum. Eventually the errors were traced to eccentric samples rotating at random (by virtue of the sample changing mechanism) under a counter with a non-uniform response.

This problem appeared worthy of attention for three reasons: (1) non-uniformity is a characteristic common to all counters, (2) one cannot guarantee centrally symmetric samples in many cases, and (3) contrary to the statistical problems in counting, the error introduced by this imperfection becomes increasingly important with higher

sample activity. This section reports some theoretical and practical considerations on achieving high precision when counting eccentric sources.

It is not always possible to prepare solid-source beta-emitters in such a manner that the center of sample activity is located reproducibly beneath the center of a counter window. Examples include biological thin sections with localized activity, atmospheric filters with active particulate matter, and other samples whose deposition upon the planchet is not strictly controllable. This unavoidable eccentricity can result in highly erratic repetitive counts with a variation far exceeding counting statistics. Questions then arise as to what confidence one can put in such counts, and whether it is wiser to choose the average value of the counts, or perhaps their maximum value. Will additional knowledge of a particular counter be of assistance in making decisions?

The problem is perhaps commoner than realized, for it appears that no commercial window counter has a uniform response across its face. As an example of the subtlety of the problem, the reader is invited to examine Figure 5.1 by covering all portions except the 60 consecutive counts from 31 to 91. Although it is easy to continue the shaded trend line through this region, disclosing a real fluctuation of some 4%, there seems little justification for so doing until one has seen the ends of the curve. (When this data was first plotted, the trend was not noticed until the upswing

Figure 5.1. Eccentric sample free to rotate. Counts obtained with automatic sample changer using circular planchets. The shaded line marks a trend, and can be continued through the random-appearing central portion.

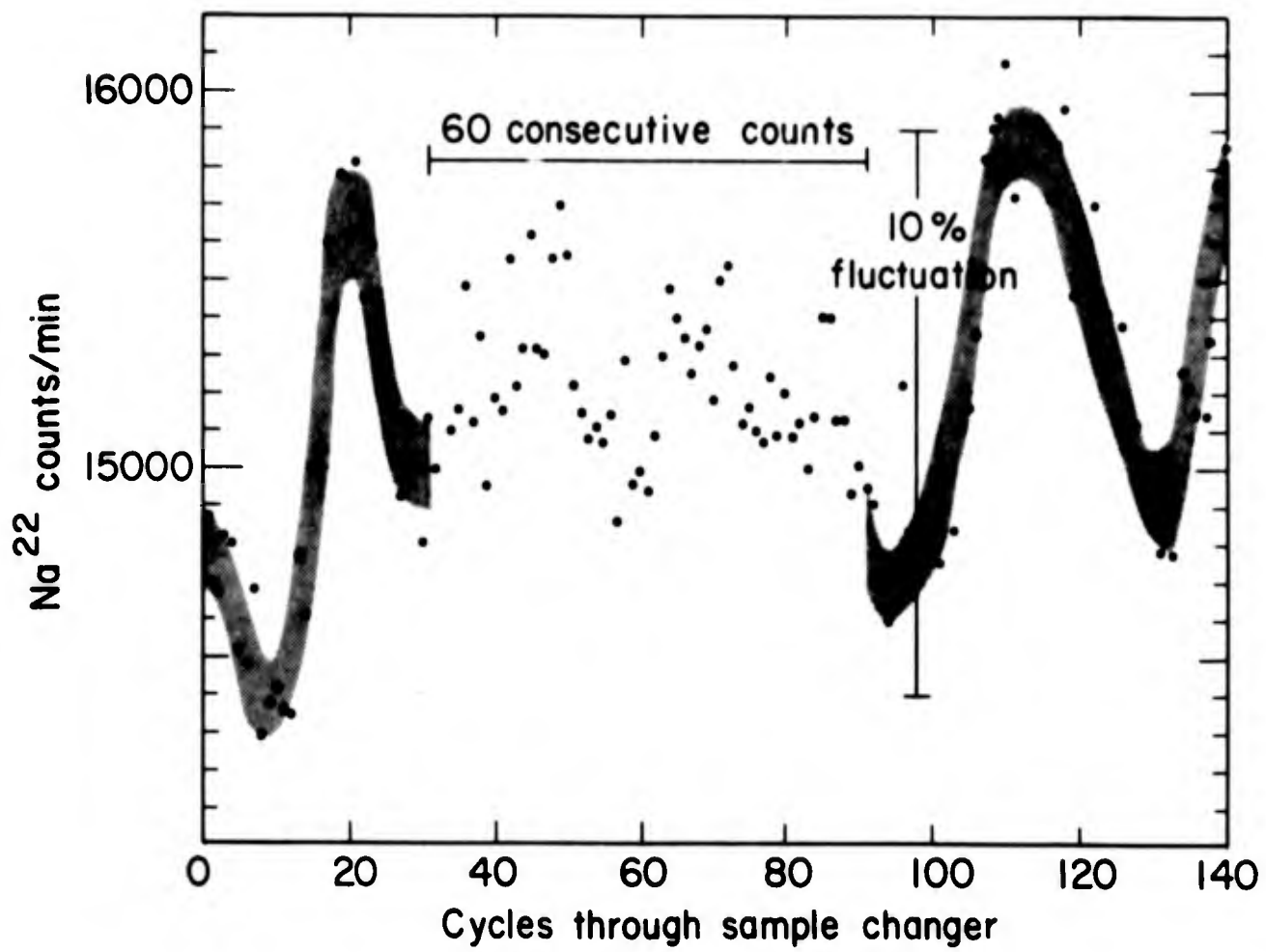
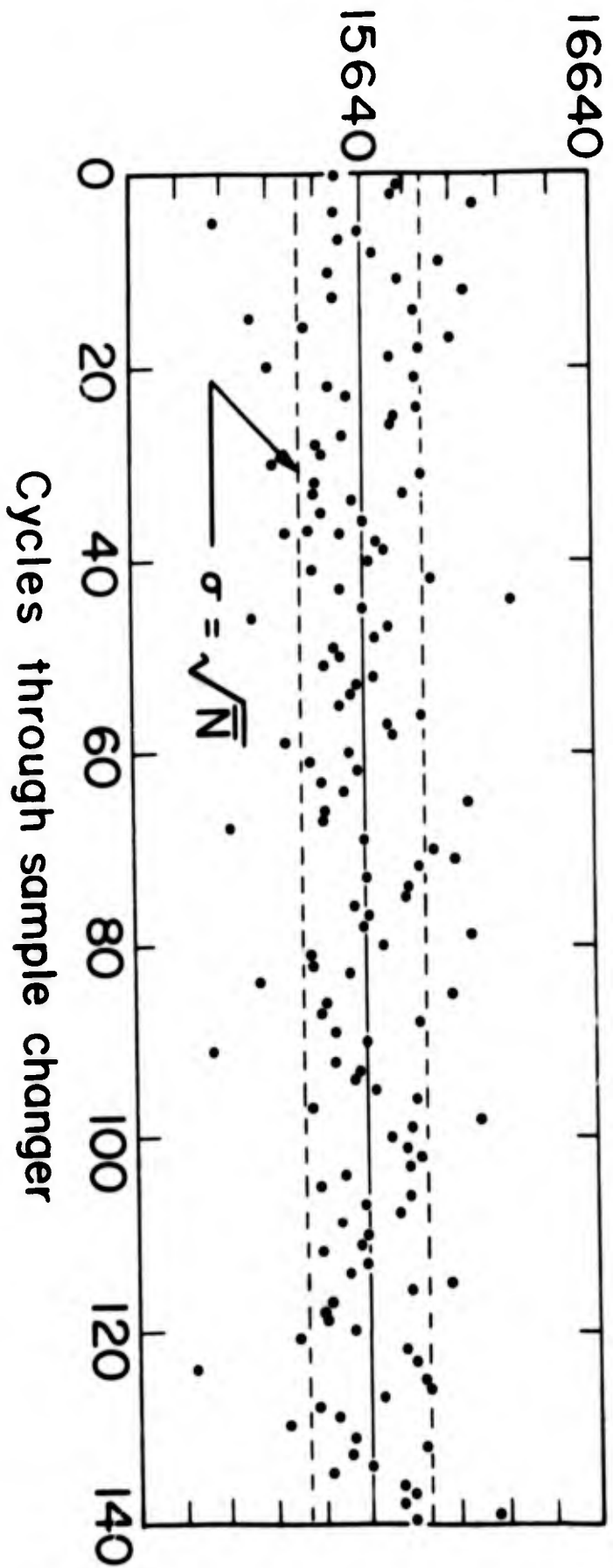


Figure 5.2. Eccentric sample constrained to single orientation. Same situation as Figure 5.1, except that the planchet is keyed throughout the changing cycle and cannot rotate.

Na<sup>22</sup> counts/min



between 100 and 110 was reached. Up to this point the errors appeared to be so random that the experiment was almost abandoned.)

These data were taken with an expensive and highly recommended machine with an automatic sample changer. The changer operation is such that the circular planchets may be rotated by friction in random amounts between counts. This rotation varies from perhaps  $-10^\circ$  to as much as  $30^\circ$  per counting cycle.

To prove that sample rotation was responsible, the changer was modified to allow positive angular location of the planchets during the entire changing cycle. When the same sample was recounted, it yielded the convincing straight line of Figure 5.2, which is now within counting statistics.

It must be emphasized that accurate relocation of the sample is not a solution to the problem, and only serves to obscure the fact that a problem exists. While any one sample may thus be counted reproducibly, the recorded count is a function of the geometry of the particular sample and its orientation with respect to the counter. This means that there is no reliable way of intercomparing samples, and therefore no standardization is possible.

The traditional solution to this problem is an increase in the source-to-window distance, which decreases the effects of eccentricity but which also decreases the counting rate. Such an approach is not feasible with

samples of low activity. Furthermore, many counters are so designed that increasing this distance involves a major reconstruction of the apparatus. If accurate counting is necessary, another solution must sometimes be sought.

An inquiry to the manufacturer indicated that the detector in question was "state-of-the-art", and had a flatter response than other commercially available detectors. The manufacturer kindly provided an experimentally determined plot of the response, obtained by moving a point radiation source across the counter window face in a grid pattern. This plot showed a definite eccentric peak which bore no evident relation to the detector design or construction.

It appeared that the solution would lie in a counting regime which would minimize the effect of eccentricity, and to this end a mathematical model was built and analyzed numerically. This model is based upon the following considerations:

The response  $I$  of the counter is given by

$$I = \iint \phi(r, \theta) S(r, \theta) dr d\theta$$

where  $\phi(r, \theta)$  is the beta flux reaching the window at  $(r, \theta)$  from the source. It is determined by geometry only, and is

$$\phi(r, \theta) = \phi^0 [a^2 / (a^2 + \rho^2)]^{3/2}$$

where  $a$  is the perpendicular distance from the source to the window,  $\phi^0$  the flux at this closest point and unit distance, and  $\rho$  the projected distance from the source to the window at  $(r, \theta)$ .

$S(r, \theta)$  is the "sensitivity surface" of the counter, and is given in general form by

$$S(r, \theta) = 1 - \sum_i b_i z_i^n$$

where the  $b_i$  are coefficients, and the  $z_i$  are coordinates. The sum is the measure of deviation of the detector from an ideal, uniformly flat sensitivity. The surfaces considered were: the tilted plane ( $z_i = \bar{x}$ ), the dihedral ( $z_i = |\bar{x}|$ ), the cone ( $z_i = \bar{r}$ ), the paraboloid of revolution ( $z_i = \bar{r}^2$ ), the parabolic trough ( $z_i = \bar{x}^2$ ), and various combinations of these.  $\bar{x}$  and  $\bar{r}$  are respectively the distances measured from the axis or the center of symmetry of the sensitivity surface, which is in general displaced from the center of the counter by an eccentricity  $E$ .

Of these surfaces, the paraboloid and the trough are at once plausible and provide the best fit to reality. It is felt that the paraboloid is suitable to describe end-window counters in which the sensing element is a hanging wire with central symmetry, whereas the trough is representative of counters having horizontal wires cutting secantly across the window.

These two surfaces (with a cone for comparison) are shown in Figure 5.3, which is a plot of the response  $I$  of the counter as a point source of eccentricity  $R$  is rotated  $180^\circ$  beneath it. The vertical lines in the Figures are terminated at the bottom by the average response  $\langle I \rangle$ , and at the top by the central response  $I^\circ$ , which is the count that would be given by the same sample if its eccentricity were

zero. We will return to the significance of these later.

Figure 5.4 provides a feel for the relative effects of the parameters  $b$  and  $R$ , and is drawn for a trough of zero eccentricity. This surface, though not eccentric, nevertheless has sufficient asymmetry to produce major counting fluctuations, as indicated by the 1% arrow.

When  $E > 0$  and  $R > E$ , the two minima of Figure 5.4 are no longer the same depth, and a characteristic shape appears as shown in Figure 5.5. In Figure 5.6 are plotted some experimental data which have essentially this same curve. (Admittedly, there is a certain subjectivity which enters into drawing the second minimum in the data, but this is influenced by much experience with the peculiarities of other runs, and is felt to be valid.)

A contour map of the response  $I$  for a trough with  $b=0.2$  is shown in Figure 5.7, and compared with an ideal flat response. Lest it be felt from looking at the plot that  $b=0.2$  is an extreme value, recall that 10% fluctuations were observed in Figure 5.1. These require a  $b$  approaching 0.2 for the  $R$  value (about 0.3) of the sample of Figure 5.1. This suggests that there is much yet to be learned about building flat detectors.

If it is clear that a problem exists and has been adequately described, we can turn to methods of ameliorating it. Table 5-1 summarizes some results obtained from the model, in the form of

Figure 5.3. Response of various eccentric sensitivity surfaces to rotation of eccentric samples.  $1^\circ$  is the "best" value obtainable with an eccentric counter. The "trough" and "paraboloid" sensitivities are representative of real counters. The "cone" may not be.

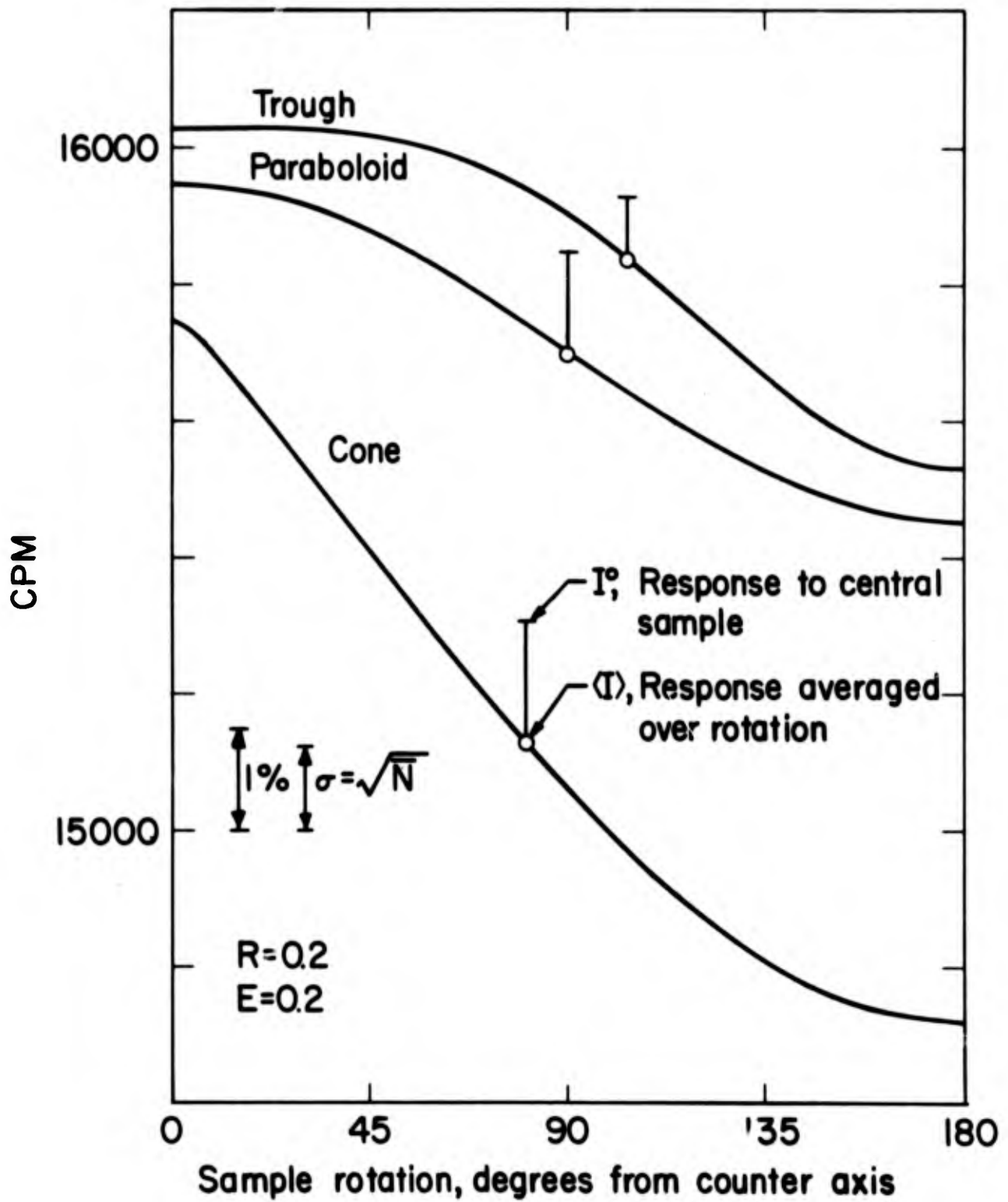


Figure 5.4. Response of non-eccentric trough to eccentric sample rotation. Variable counts arise even when the trough axis is a diameter.

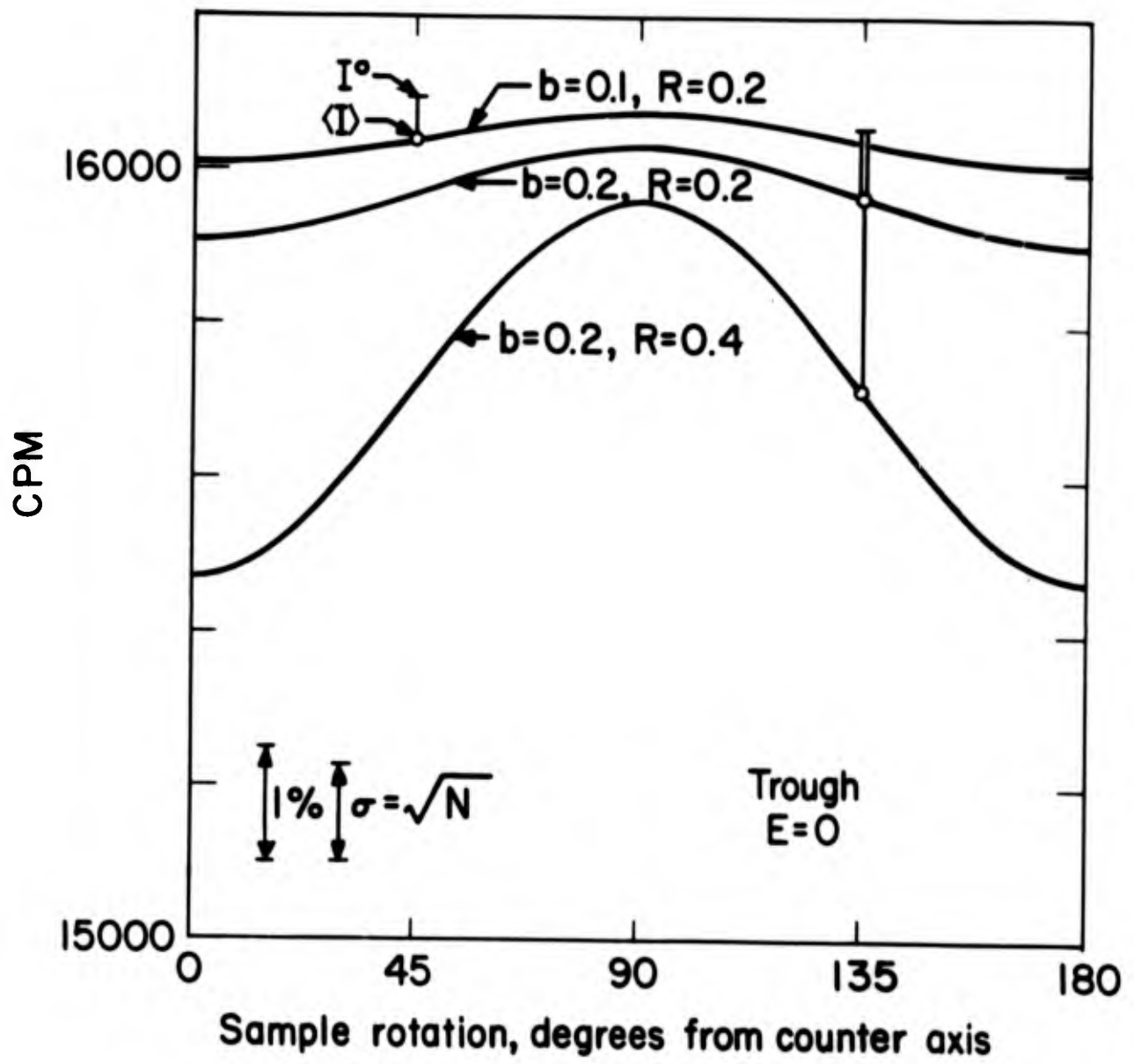


Figure 5.5. Response of eccentric trough. When the trough axis is a secant of the detector, an asymmetric response develops.

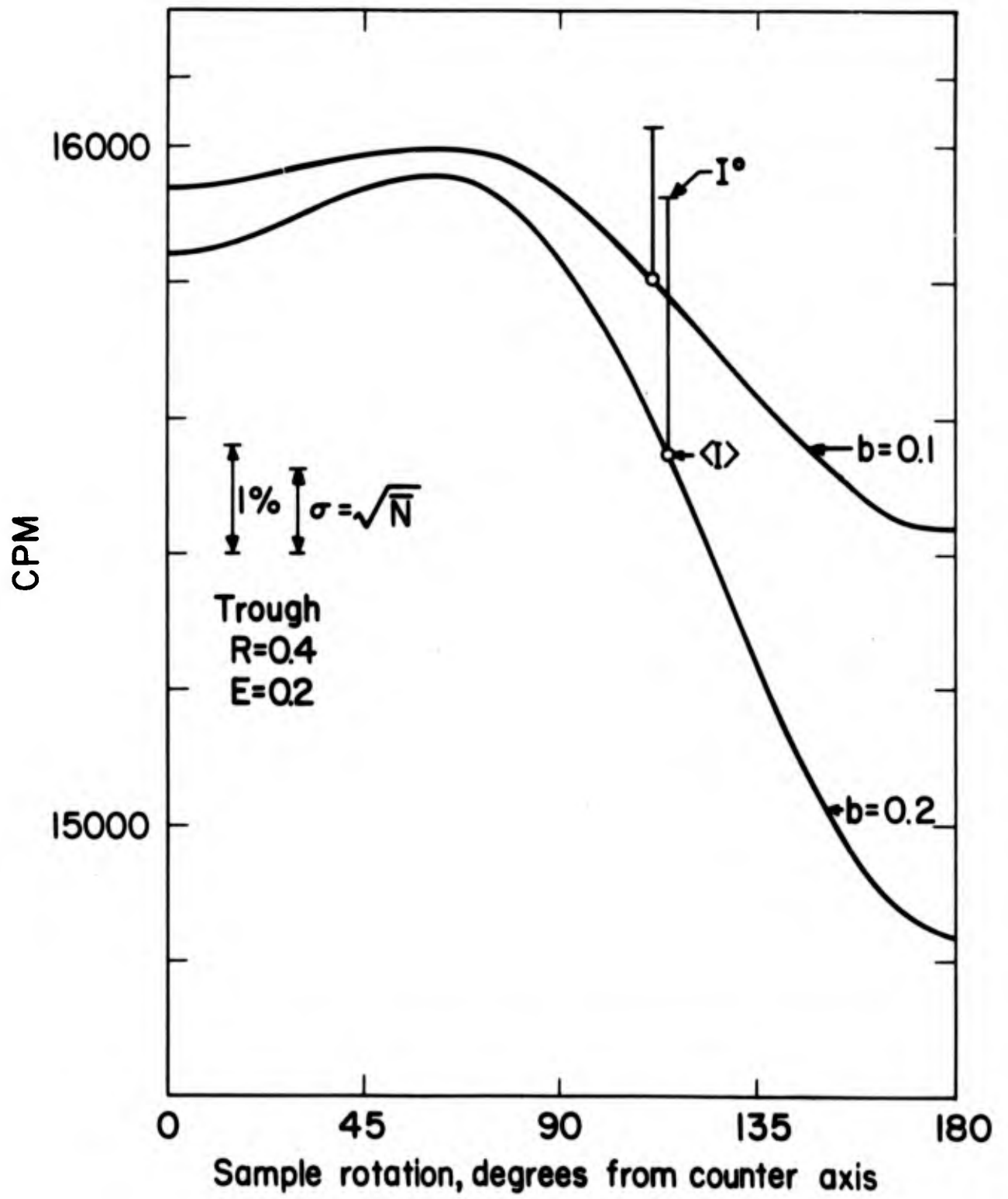


Figure 5.6. Experimental data. This is held to be circumstantial evidence for a detector with an eccentric trough sensitivity.

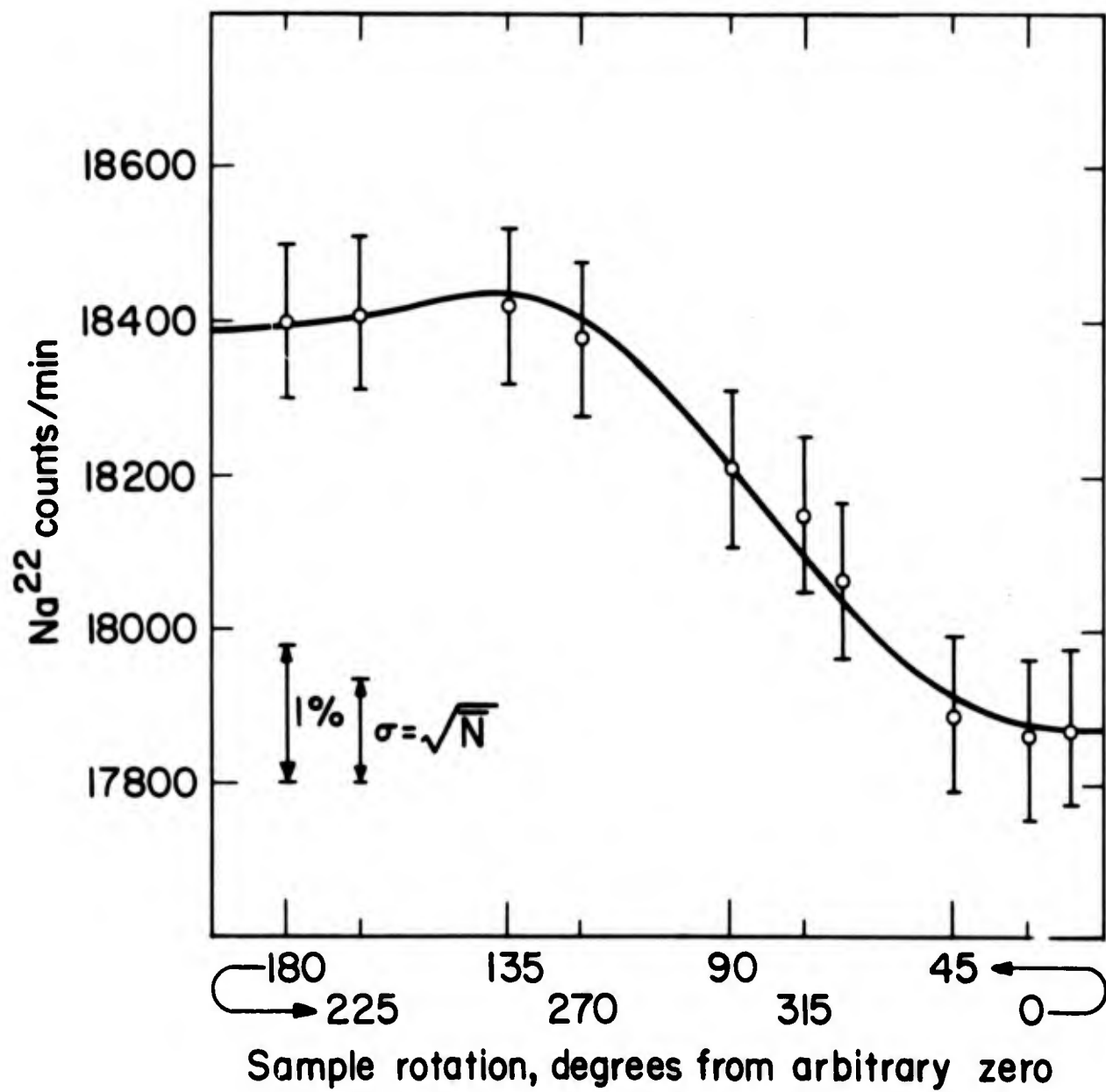
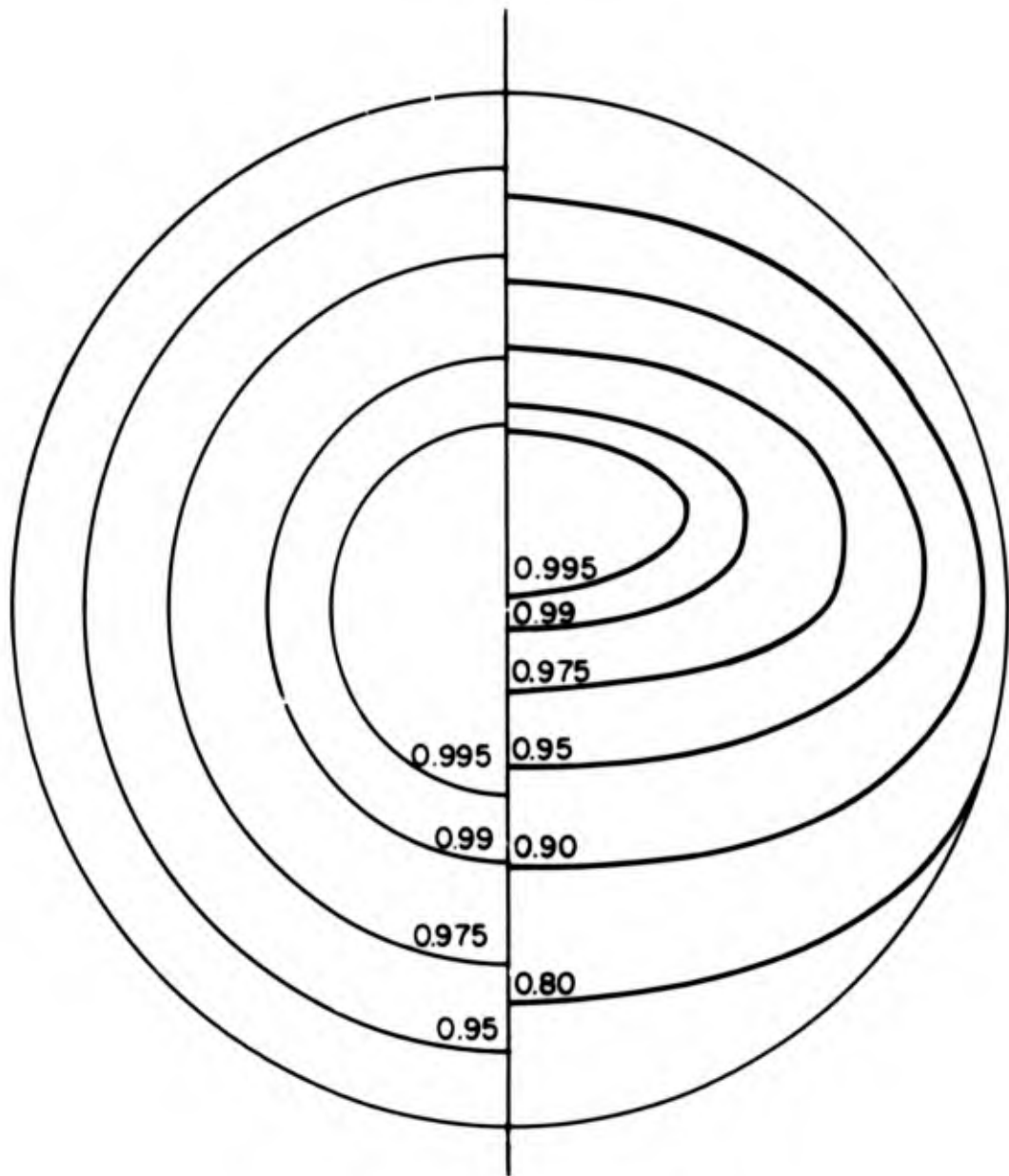


Figure 5.7. Response contour map for an ideal flat sensitivity surface (left) and for an eccentric trough (right). The radial decrease in response is an effect of geometry.



SENSITIVITY SURFACE

FLAT ← | → TROUGH

$b=0.2$

$E=0.2$

$$\eta = I^0 / \langle I \rangle$$

and

$$\delta = \left( \frac{\text{maximum count}}{\text{minimum count}} - 1 \right) 100$$

It will be noted that  $\delta$  is a function of all parameters, while  $\eta$  depends chiefly upon  $R$ .

( $R$ ,  $E$ , and  $a$  are expressed as fractions of the window radius.  $a$  was chosen to be 0.08, as this was the value for the machine in question.)

$I^0$  is the number which we obtain from a counter with an accurately centered sample (regardless of the defects of the particular detector), and is thus the best estimate which can be obtained from the counter. It is the number to which we should like to correct a given count or set of counts  $I$ . To do this, we need to know at least  $\langle I \rangle$  and  $R$ .

It will be noticed that for  $R = 0.2$ , there is little advantage in knowing  $\eta$ , since  $\langle I \rangle$  is within 0.5% of  $I^0$  for almost all cases. This is true even though  $\delta$  ranges above 6%. But there is an advantage to knowing  $\langle I \rangle$  even in this case.

For the paraboloid surface,  $\langle I \rangle$  is the average of any pair of diametral counts, and will be accurately given by any counting system which counts the sample in such 180° pairs. In particular, two diametral counts will give a more reliable estimate of  $\langle I \rangle$  than will three random counts. (The author has had considerable success in manual counting using an end-window detector with four 90° counts, obtaining 0.5% accuracy from (known) samples even though the  $\sigma$  for the

set of four was 9 times the expected deviation.)

For a trough configuration,  $\langle I \rangle$  is no longer given by diametral pairs, and the above expedient is not available. In this case, the properties of the sensitivity surface of the counter can be estimated (e.g., by counting a series of samples of known eccentricity  $R$  and interpolating into  $\delta$  of Table 5-1). Then, if a sufficient number of counts are made on an unknown sample to allow a separation of  $\sigma$  and  $\delta$ , from the  $\delta$  so obtained can be gotten an  $\eta$ , and thence a better estimate of  $I^\circ$ .

The pains necessary in this latter case are seldom justified. An alternative, which seems to have been inadequately explored, is counting the sample on a turntable rotating coaxially with the detector at perhaps 10 rpm. This will provide  $\langle I \rangle$  directly, and is in many cases an adequate approximation to  $I^\circ$ .

## CONCLUSIONS

The questions raised earlier can now be answered. It is clear that only limited confidence can be placed in uncorrected counts of eccentric samples. The average value of a set of such counts will always underestimate the true value, while the maximum count will occasionally overestimate it. Finally, knowledge of the individual counter can be an excellent guide to corrections, and if, in addition, an estimate of sample eccentricity can be made, a reliable count may be obtained from Table 5-1.

Table 5-1. Correction factors for eccentric sources.

Sensitivity Surface	Counter Eccen- tricity  E	$\delta = \%$ Fluctuation				
		$\eta = 1^\circ / \langle I \rangle$				
Amplitude b	Sample Eccentricity R:	0.2	0.4	0.6		
Paraboloid	.0	0. 1.0052	0. 1.0216	0. 1.0527		
	.1	.2	1.57 1.0052	3.12 1.0216	4.61 1.0529	
		.4	3.18 1.0052	7.32 1.0218	9.34 1.0533	
		-----	-----	-----	-----	
	.2	.0	0. 1.0091	0. 1.0376	0. 1.0911	
		.2	3.17 1.0091	6.30 1.0378	9.33 1.0917	
		.4	7.50 1.0093	12.91 1.0385	19.12 1.0937	
	Trough	.0	0.34 1.0036	1.32 1.0138	3.37 1.0347	
		.1	.2	1.56 1.0036	3.48 1.0138	6.06 1.0347
			.4	3.17 1.0036	7.30 1.0139	9.68 1.0348
			-----	-----	-----	-----
		.2	.0	0.77 1.0052	3.04 1.0216	6.75 1.0527
.2			3.15 1.0052	7.00 1.0217	12.19 1.0530	
.4			6.46 1.0053	12.44 1.0221	19.72 1.0539	

## THE MAKING OF BUBBLES

As discussed previously, bubbles form two types of drops. It is convenient to divide the possible size range of bubbles into two classes corresponding to the two kinds of droplets. This can be easily done, since, as we have seen, bubbles smaller than 300 microns make an entirely negligible number of film drops, whereas bubbles larger than 2 mm produce no jet drops which remain airborne long enough to reach the collection apparatus.

Clearly two ways of producing bubbles are called for; since it is well to examine the intermediate range also, a third method is needed.

### FILM-DROP BUBBLES

The one requirement for film drop production is film cap area. The diameter of the bubble itself is unimportant, and all that is needed is a single capillary with a large orifice. Various orifices used included glass and polyethylene tubing, and hypodermic needles of stainless steel and platinum.

The problem is not at the orifice, but at the surface. If the solution is capable of forming a film (as it must be

In this case), rising bubbles will coalesce when they reach the surface to form one or more slowly growing large bubbles. There is visible in this coalescence process an interesting difference between "surface contamination" and "bulk contamination". If the rising bubbles collect appreciable amounts of surfactant from the solution, their surfaces are separately stabilized, and they do not coalesce upon contact with each other. While they form a connected raft, they only infrequently break at the inner septa to form larger bubbles, but rupture at the evaporating upper surface. If, on the other hand, the solution itself is relatively clean, the contamination which the bubble picks up in its travel will be small, and most of the film-forming material will be concentrated in the film cap already present. In this case, a bubble breaks as soon as it contacts another interface, and only a single large bubble is evident. Each bubble brings a little more surfactant with it; breaking inside the larger bubble, it ejects a portion of this material upward. The ejected drops frequently impinge on the inner surface of the large bubble, stabilizing it further with added film-forming material, and increasing its life by replenishing liquid lost by drainage.

#### GAS SOURCE

A filter on the laboratory air line revealed so much foreign material that no attempt was made to purify the air sufficiently for bubble-making. An additional difficulty,

shared with bottled gasses of all varieties, is exercising sufficient control over the flow at the low rates used. A harmonious solution to these two problems was provided by the electrolytic generation of oxyhydrogen. A generator was constructed in the following manner:

The plunger was removed from a 5-ml hypodermic syringe, and replaced with a Teflon plug with two platinum lead-throughs supporting 3 by 5 cm platinum gauze electrodes. These were spotwelded into concentric cylinders and separated by Teflon insulators. The plug was held into the barrel by a screw cap, and the lead-throughs were sealed (to 3 atm) by 2-mm soft rubber spheres. The screw cap compressed the sealing spheres into conical seats, exerting a high radial pressure around the lead-throughs.

A one ampere current through 0.05 molar potassium sulfate electrolyte generated about 0.191 microliters of gas per second, with no appreciable evolution of heat. The system required refilling every few days, which was done with filtered distilled water (since the electrolyte was not consumed).

A one ampere rectifier driven by a variable transformer, and an ammeter, completed the gas generator. The variac gave smooth and reproducible control over flows ranging from 0.004 to 0.4 microliters per second at pressures between zero and 3 atmospheres gauge.

Early designs used glass plumbing with standard taper joints. This proved most unsatisfactory, being inflexible

and impossible to seal. Ultimately all plumbing was done with Luer fittings (standard hypodermic taper) and Teflon "needles" with Kel-F hubs manufactured by The Hamilton Company. In response to an inquiry, Hamilton agreed to make this tubing with Luer hubs on both ends. It is now a standard item, and makes a simple, inert, and easily cleaned piping system for microplumbing which is pressure tight to 100 psi, and can be assembled with fingertips.

The first gas generator used polyethylene insulators to separate the electrodes. Polyethylene is slowly attacked by atomic oxygen, producing unknown oxygenated compounds in the effluent gas--although in extremely small quantities. The Teflon separators show no sign of such attack.

At first, the electrodes were platinized to reduce the overvoltages normally present for both oxygen and hydrogen on smooth platinum. This proved to be a mistake, since the mechanical agitation of bubble formation loosened small bits of the platinum black. These were carried along with the gas stream. The first connecting tube was eventually darkened with these particles; even though the gas was washed by bubbling through distilled water, an occasional piece of platinum would plug the capillary tip. When this occurred, pressure in the system would increase until the Nernst-law voltage rose so high that gas production essentially stopped, or a Luer fitting gave way and the system was completely emptied of gas and liquid. This problem was oversolved by abandoning fine capillaries, and

reverting to smooth platinum electrodes.

#### JET-DROP BUBBLES

To make jet drops, large numbers of small bubbles are wanted, in quantities far beyond the capability of capillary tips, and smaller in size than is convenient for capillaries or possible with glass frits. Since a desirable bubble size distribution is obtained from the platinum gauze electrodes, these were put directly into the micro-ocean, and bubbles made by direct electrolysis of the solution under investigation.

Passing current through the micro-ocean immediately introduces the possibility of creating artifacts by electrode processes, and it adds the requirement that the solution have sufficient ionic strength to be conductive. Complex reactions are possible at electrodes in solutions of dilute organic material, and the possibility cannot be overlooked that these occurred. On the other hand, every feature of the results which changes radically between the film drops and the jet drops is smoothly connected by the small capillary bubbles, indicating that bubble size--and not the manner of production--is the important variable.

Electrolysis of chloride solutions (such as sea water) produces chlorine even though the potential of the chlorine-chloride couple ( $E^\circ = -1.360$ ) is well below the water-oxygen couple ( $E = -0.815$ ) (Latimer, 1952). This is because the latter has a much higher overvoltage on smooth

platinum than does the chlorine reaction. Noticeable amounts of chlorine are evolved from 0.5 molar sodium chloride, and this could conceivably influence the results from sea water. There is no indication that it has done so.

Direct electrolysis produces about  $10^5$  bubbles per second, ranging from 10 to 300 microns in diameter, with some variation noticeable as the surface tension of the electrolyte is changed. Thus, adding  $10^{-8}$  molar sodium lauryl sulfate produced a visible reduction in average bubble size--even though the surface tension change was too small to be detected by capillary rise or maximum bubble pressure methods.

#### CAPILLARY BUBBLES

A glass capillary, drawn out in an ordinary flame, and then redrawn to a hair in a 1/8 inch yellow flame, can be made to produce nearly microscopic bubbles--but only one at a time. By cutting back the tip with a clean pair of scissors, successively larger bubbles can be obtained, until trial and error finds the correct location for any size sought. However, there are two serious limitations on this method of making intermediate bubbles; these are low flow rate and the ease of plugging of the narrow tip.

Professor Kelly kindly pointed out that one might invert the meteorologists' device for making uniform water drops in air--which is a capillary jet vibrated at ca. 4000 cycles (Wolf, 1961). This process generally produces

several streams of drops of different diameters, traveling in different directions, but remarkably uniform in both size and spacing in any one stream. Drop diameter can be accurately measured by microscopic examination under stroboscopic illumination.

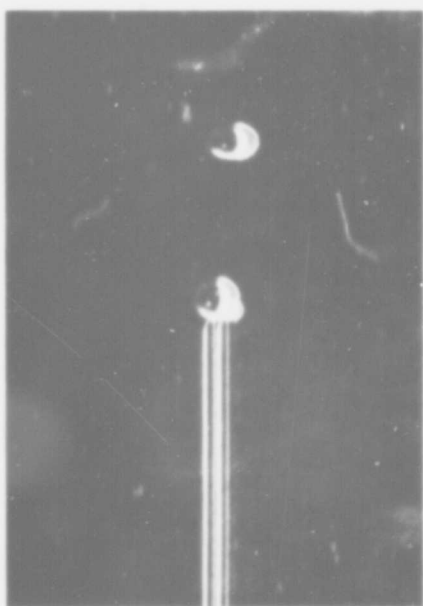
A vibrating capillary for making bubbles was built as follows: A glass tube, passing through a rubber O-ring seal which acted also as an oscillation node, was inserted through the base of the container.

Outside the container, this tube was coupled by light but rigid aluminum tubing to a loudspeaker driver, powered by a 10-watt amplifier fed from an audio generator. The high damping of the water lowers the resonant frequency by an order of magnitude from the air case, and oscillation frequencies are near 300 cycles.

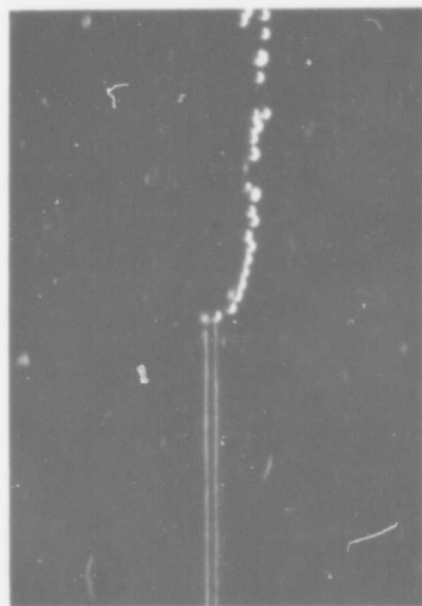
Inside, the tube was drawn into a long thin whip, but no redrawing of the tip was necessary. The whip was long enough to be capable of more than one resonance, although in general only the first harmonic (which had one node part way down the whip) was excitable because of the damping forces. Asymmetries in construction frequently led to elliptical oscillations instead of linear, and there was a range of frequencies near resonance which induced a variety of tip paths. These were sometimes used to produce changes in bubble production.

Figure 5.9-a shows a typical bubble produced with the tip at rest. (The close spacing of the moving bubble and

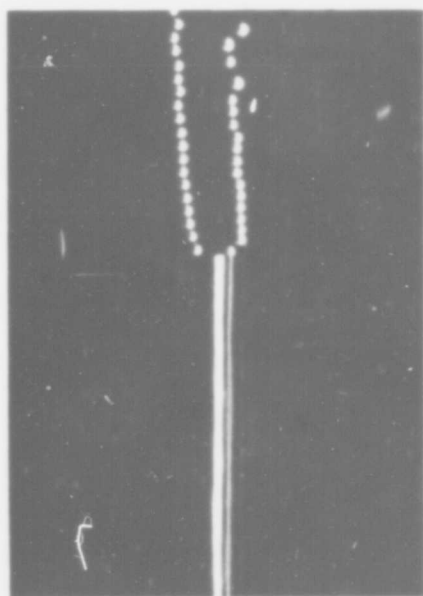
Figure 5.8. Bubbles generated by capillary whip. 2  $\mu$ -sec exposure. Diameters computed from flow rate and oscillation frequency.



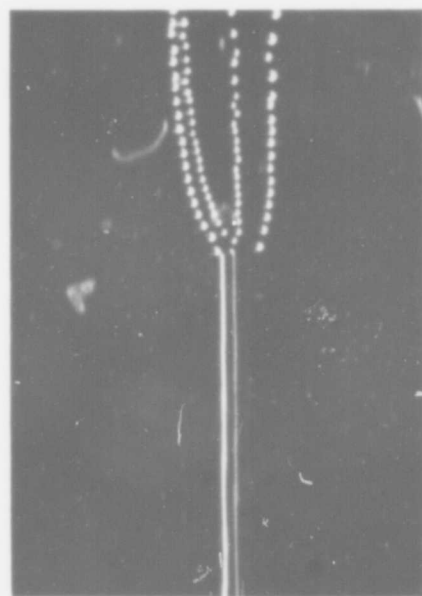
(A)  $f = 3.5 / \text{sec}$   
 $D = 1.28 \text{ mm}$



(B)  $f = 285 / \text{sec}$   
 $D = 294 \mu$



(C)  $f = 560 / \text{sec}$   
 $D = 296 \mu$



(D)  $f = 1140 / \text{sec}$   
 $D = 268 \mu$

the resting one is illusory, as the stationary one did not detach until the moving bubble had risen well beyond the region photographed.) In 5.8-b the capillary is vibrating, and the flow rate is such that a single stream of bubbles is produced at one end of the tip path. The more typical case is shown in 5.8-c, with two parabolic horns of very similar bubbles rising from the ends of the tip path. In 5.8-d is shown a higher flow rate, which forces bubbles off at the midpoints of the swing, generating a larger number of slightly smaller bubbles.

The configurations photographed do not show the full extent of patterns. Stable modes with three, five, and six "horns" have been observed, sometimes fixed in space and sometimes slowly rotating. Also easily obtained is a mode in which the tip oscillation is nearly circular (just below a true resonant frequency). In this mode, bubbles are emitted sideways with such acceleration that to the eye they seem to appear in a circle about 3 cm in diameter, slightly lower than the tip. These are small, numerous and randomly distributed around the circle of appearance. They cannot be easily enumerated or sized. An additional complication is that a vortex is generated in the center of the tip path which collects a large bubble and releases it periodically, along with a bevy of satellite bubbles, all of which are many times larger than the peripheral bubbles. Thus, the size spectrum is not as uniform as for the well-defined modes.

It will be noticed from Figure 5.8 that the size of the bubbles does not appear to be uniform in some of the ascending horns. This is real, and is caused by interactions between bubbles and the wakes of their predecessors, allowing a following bubble to overtake a forward bubble and merge with it. This can be avoided by stirring the liquid gently to disrupt the interaction; essentially monodisperse classes of bubbles can be produced by this method.

Other configurations of tubing employed include the J-shaped form shown in Figure 4.2. This does not give as clearly defined resonances as the simple whip, and generates a much broader spectrum. Nevertheless, it is a spectrum which lies between the film-drop bubbles and the jet-drop bubbles, has comparable flow rates, and is free from tip-plugging problems.

#### ORIFICE PLATES

An attempt was made to generate bubbles from separate but identical orifices. This proved to be an egregious failure, but will be described to discourage its repetition. The orifice plate, kindly supplied by Mr Leo Ghenn of American Viscose Corporation, was akin to a rayon spinneret, and had 27 holes of 0.0017" diameter on a one-inch circle. It was fabricated of Type 403 stainless steel.

When first immersed, this device produced synchronous pulses of 27 identical bubbles, rising uniformly in

symmetric circles. 15 minutes later, there remained no semblance of similarity from one hole to the next. Some holes had stopped, some produced infrequent large bubbles, some emitted copious streams of small bubbles. The range of sizes was somewhat greater than that obtained from an ordinary glass frit.

There are two causes for the failure of a multiple orifice device. The first is variable corrosion at the orifices (although Type 403 stainless should not have been attacked so quickly!). A second, more fundamental, cause is that a critical factor affecting bubble size is the molecular condition of the edge from which the bubble must be torn loose, and this is a region subject to rapid contamination which is variable from hole to hole. It appears unlikely that any multiple-orifice design will consistently yield reproducible bubbles in a real liquid.

## A CASCADE AEROSOL IMPACTOR

### SAMPLE COLLECTION

A consideration felt to be crucial when working with trace quantities is the elimination of all contact with unnecessary surfaces, since selective adsorption may take place at every new surface introduced. Any transfer of sample from collector to processing vessel may result in a partial separation of the original material.

With this in mind, a sample collecting scheme which did not require removing the sample from its point of capture was deemed necessary.

For jet drops above  $50 \mu$ , which are ejected several cm vertically, the simplest collector is a horizontal surface. It is convenient to use a small disc of glass or plastic backed up by a resistance element furnishing sufficient power to evaporate the drops as they hit. This builds up an adherent deposit of dry salt, and relatively large samples can be collected without backdrop into the parent liquid.

For film drops and small jet drops, the aerosol impactor was employed.

## CAPTURE BY IMPACTION

The collection and size classification of aerosol particles is most easily accomplished with a cascade impactor. In this device, air is drawn through a succession of orifices of diminishing diameter, each producing a jet of air which impinges upon a collection plate which deflects it radially through a right angle. The particles, being denser than the airstream and possessing greater inertia, do not follow the streamlines of the airflow. If the forward momentum of a certain sized particle is sufficient to overcome the sideward air drag, it will hit the collecting slide; if not, its momentum will be increased in the following jet, until eventually it is captured.

This process (in the absence of gravitational settling and electrostatic attraction--which cannot in practice be neglected) can be shown (Ranz & Wong 1952) to depend upon a single "impaction parameter"  $\psi$ . (A factor of  $10^6$  is included so that the particle diameter  $d$  may be written in microns with all other variables in cgs units.) We have:

$$\psi = \rho v d^2 / 18 \mu D \times 10^6$$

$\psi$  may be interpreted as the ratio of two forces, of which the first is that required to stop a particle of diameter  $d$  and density  $\rho$  traveling at velocity  $v$  in a distance  $D/2$ :

$$f_1 = \pi \rho d^3 v^2 / 6D \quad .$$

The second is the stopping force available from air drag:

$$f_2 = 3\pi \mu v d \quad .$$

A second interpretation of  $\psi$  is that it is the ratio of the distance the particle will travel in still air with initial velocity  $v$  to the diameter  $D$  of the impactor orifice.

It proves convenient to work with  $\sqrt{\psi}$ , which is then a linear function of the particle diameter  $d$ .

Making simplifying assumptions about the nature of the velocity field in the region where the jet is deflected allowed Ranz & Wong to compute collection efficiencies for several basic impactor designs. Of these, the circular jet shows the sharpest cut-off range. If there is a lower diameter  $d$  which is not collected by a given impactor stage, particles of diameter  $2d$  will be collected with 100% efficiency. Thus, a two-fold range in particle diameters is the smallest which can be expected using impaction techniques.

The efficiency of collection also depends upon a dimensionless ratio  $K$  of the linear dimensions of the device. These dimensions were optimized by Mitchell & Pilcher (1959), who give recommended jet-to-collector distances ( $=0.375 D$ ) and wall clearance ( $>1.3$  cm). Their value of  $K$  was such that 50% collection efficiency was achieved with  $\sqrt{\psi}=0.29$  with a wall loss of less than 1%.

Commercially available impactors are designed for flow rates above 12 l/min. This flow would have emptied the air space in which aerosol was generated entirely too rapidly, and the Mitchell & Pilcher design was scaled down to flow rates ranging from 0.5 to 4 l/min. The scaling proceeds as

follows:

Writing the orifice velocity  $v$  (cm/sec) in terms of the volume flow  $F$  (l/min) and jet diameter  $D$  (cm)

$$v = 10^3 F / 60\pi D^2$$

and inserting this into (1), there results

$$d^2 = (6 \times 18 \times 10^6 \pi \mu \gamma / \rho F) D^3.$$

If the 50% collection efficiency values are denoted by a subscript 50,

$$d_{50} = k_{50} (D^3 / \rho F)^{1/2}$$

where

$$k_{50} = \gamma_{50}^{1/2} (6 \times 18 \times 10^6 \pi \mu)^{1/2} = 72.0.$$

This relationship gives the jet diameter for a given particle diameter. The two-fold theoretical range of particle diameters collected on a single stage sets a convenient minimum between collected diameters. The low limit of the collection range is determined by the smallest jet, which becomes a limiting orifice when the flow rate is high enough for  $v$  to exceed the velocity of sound in air. On the other hand, the flow must be rapid enough to collect the largest desired particles from the essentially non-moving air above the micro-ocean. (An additional consideration is that the flow range should be at least 4 to 1, in order to shift the collected fraction by one whole stage. At worst, this permits idiosyncrasies of a particular stage to be detected more easily; at best it provides a certain degree of confidence in the reliability of the design and manufacture, particularly in the smaller

sizes where calibration is difficult.)

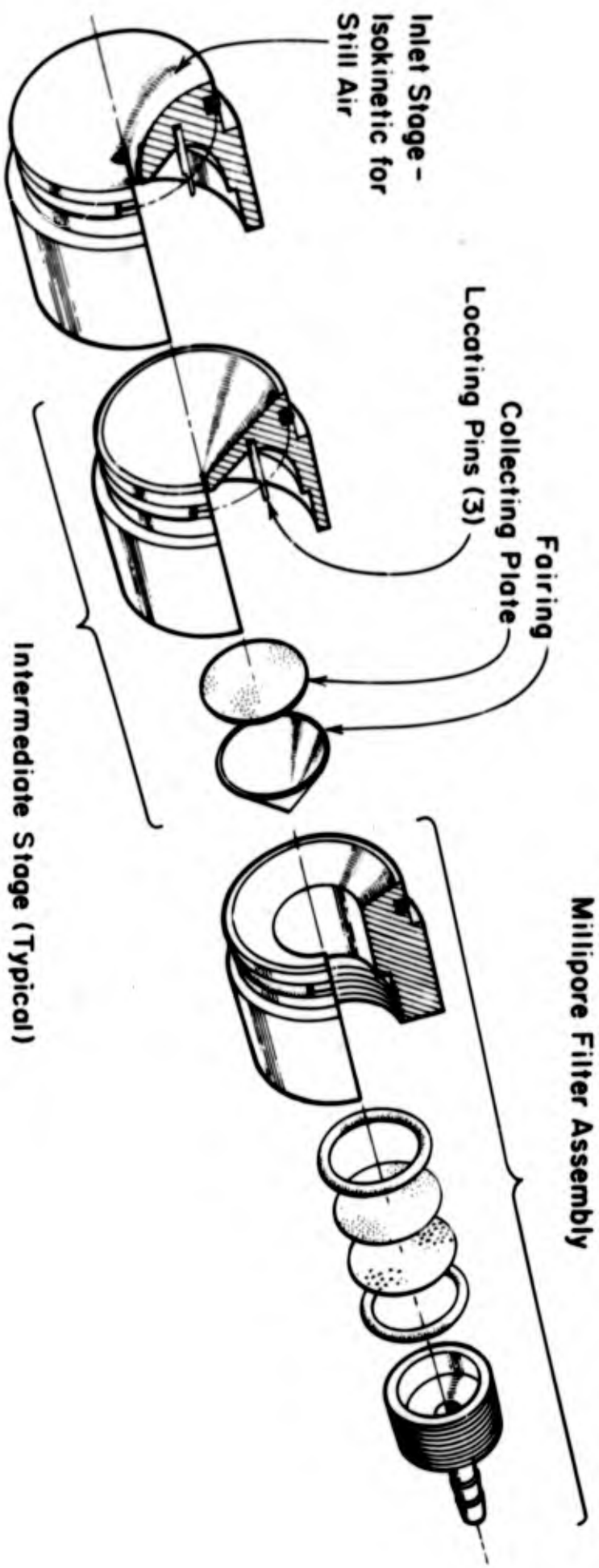
These requirements are met by a flow of 4 l/min (lower flow collected few large drops) and a lower size limit of 1  $\mu$  (which begins to approach sonic velocity in the orifice). Thus both operational limits are set.

The 1- $\mu$  stage was backed up by an 0.45- $\mu$  membrane filter, which did not fit as neatly in the scale-of-two sequence as its nominal size might suggest, since it collected smaller particles also.

The orifice dimensions of the impactor are shown in Table 5-2, along with cut-off diameters  $d_{50}$  for various flow rates. Figure 5.9 is an exploded view of the impactor, showing its inherent simplicity. It was constructed of polyvinyl chloride for ease of machining and corrosion resistance in salt air. (Later, in an attempt to defeat an electrostatic problem, the impactor was plated with chemically deposited copper, 0.0005" nickel, and a rhodium protective coat. The rhodium did not prevent formation of nickel chloride, nor did the conductive surface eliminate the electrostatic problem. In retrospect, PVC appears to have been an excellent construction material.)

The collection slides are located by steps in the three stainless steel pins, and are held in place by the PVC fairing cone which snaps into the locating steps. The fairings serve to reduce turbulence and thereby decrease wall loss.

**Figure 5.9. Aerosol impactor. Any number of intermediate stages may be assembled.**



Millipore Filter Assembly

Intermediate Stage (Typical)

Inlet Stage -  
Isokinetic for  
Still Air

Fairing  
Collecting Plate  
Locating Pins (3)

Table 5-2. Cut-off diameters  $d_{50}$  ( $\mu$ ) for aerosol impactor.

Jet Diam. (cm)	Flow rate X density of particles (l/min)(gm/ml)					
	0.5	1.0	2.0	3.0	4.0	5.0
.0364	.707	.50	.354	.289	.25	(.224)
.0578	1.414	1.00	.707	.578	.50	.448
.0918	2.83	2.00	1.414	1.16	1.00	.896
.1456	5.66	4.00	2.83	2.31	2.00	1.79
.231	11.3	8.00	5.66	4.62	4.00	3.58
.366	22.6	16.0	11.3	9.25	8.00	7.16
.582	45.2	32.0	22.6	18.5	16.0	14.3
.925	90.4	64.0	45.2	37.0	32.0	28.6

The O-rings prevent leakage and also provide sufficient friction to hold the stages together without need for further support.

#### BLOW-OFF

If a stage is overloaded, the excess material is likely to be blown off. This frequently happens when the orifice is small, and, consequently, the impaction area is also small. This is a serious problem when collecting dry samples, although it may be minimized by careful design. If the radial velocity of the airstream drops with sufficient rapidity while there is still some component toward the collector plate, the blown material is redeposited in a halo around the central spot. Liquid material seldom leaves the collector unless it is driven to the edge. Particles which are slightly damp seem to adhere most tenaciously. Fortunately, salt particles fall in this latter category, and, although blow-off halos were frequently observed, redeposition appears to be quantitative. (If blow-off had occurred, the particle size distributions would not be uniform for runs which had total particle numbers varying over three orders of magnitude, and which left deposits ranging from invisible amounts up to thick central hills surrounded by bright halos.)

## COLLECTORS

The preferred collection plate material is artists' matte acetate, which is ordinary cellulose acetate sheet with one surface roughened to take ink. It holds water droplets well and is easy to write on for sample identification.

After collection, samples were sprayed with Krylon lacquer, saturating the salt deposit to prevent flaking and loss of sample in handling. (The lacquer coat weighed ca. 0.2 mg/cm<sup>2</sup>.)

## CALIBRATION

The calibration of an impactor is never an easy task. The method adopted, involving neutron activation of nanogram amounts of iodine, appears not to have been used before and will be described in detail.

But first let us dispose of some "simpler" methods. Lacking a means of generating drops of known size, the first method attempted to use pollen grains, which are remarkably uniform in size and easily available (Hugh Graham Laboratory, P.O.Box 14197, Dallas, Texas). The flow rate through the impactor can be adjusted to compensate for the density (paper mulberry and ragweed pollen, 14  $\mu$  and 19  $\mu$  respectively, have a density between 1.30 and 1.32, as determined by centrifugation in liquids of known density). Using only a single particle size, one can trace out the entire efficiency curve of one stage by varying the flow

rate.

Unfortunately, triboelectrification during separation of the pollen grains from each other left large residual charges. Electrostatic attraction was sufficient to cause the pollen to adhere to the impactor surface, and none would enter the inlet orifice. Grounding the impactor and the vessel in which the pollen was suspended had no effect, and the experiment was abandoned.

Another calibration method considered would have measured the blot size of dye drops collected upon the uniform surface of membrane filters. Surprisingly, the correlation between blot diameter and drop diameter seems to be unknown and cannot be established without drops of known diameter.

The method used was to collect drops of saturated sodium iodate solution for perhaps 4 minutes, until there were some thousands of distinct droplets on the collector stages of interest (16-, 8-, and 4- $\mu$ ). The collectors were 22 mm glass cover slips stuck to one inch glass discs with a drop of water. (This prevented the cover slips from picking up iodate contamination from the three locating pins, which touched only the larger disc.)

The collected droplets--or a representative area thereof--were photographed at a magnification of 25X and the photographs counted with the aid of a bacteria colony counter. (Since large crystals of  $\text{NaIO}_3$  are birefringent, it was hoped that the dried drops would be seen as luminous

spots in a field darkened by the crossed polarizers of a petrographic microscope. This effect was observed in less than 10% of the drop residues.) However, the salt is hygroscopic, so that the apparent size of the drops could be increased many times by breathing lightly upon the slide. Since no effort was made to use the photomicrographs for size information, but only for numbers, the droplets were photographed wet, making the 4- $\mu$  drops easily visible.

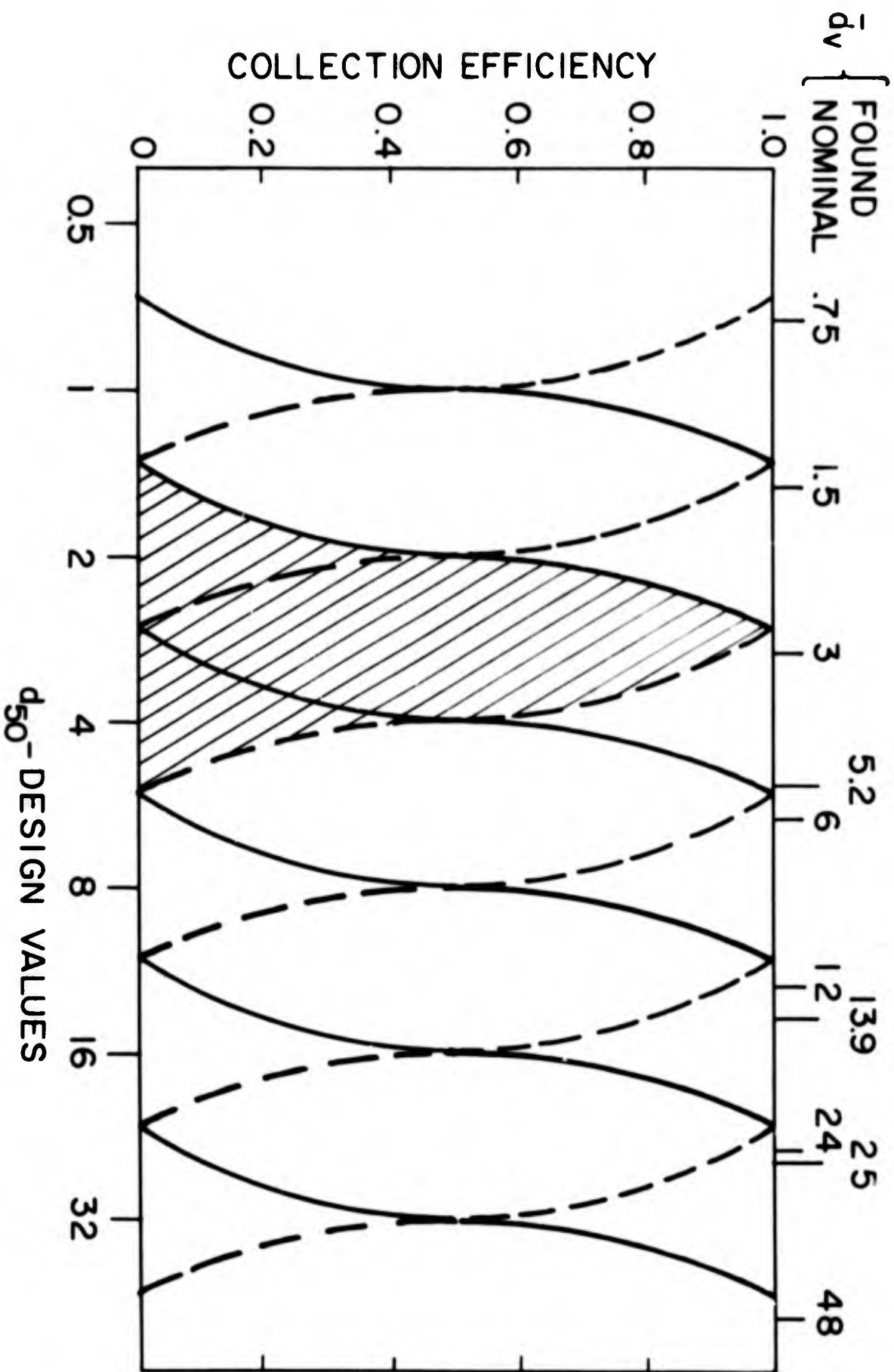
After being photographed, the cover slips were immediately sealed into containers suitable for neutron irradiation, and processed in the MIT Reactor. The resulting 25-minute I-131 was estimated according to the procedure of Duce (1964). (The author is grateful to Dr Duce and Lester Walters for their kind assistance in this determination.) The iodine content was compared with that of a known volume of the bulk liquid, and a direct measure of the total volume collected per stage thus obtained. If the number of particles on the stage is known, the volume-average diameter  $\bar{d}_v$  is easily calculated.

The volume-average diameter of the drops is a function of the particle size distribution which is sampled, and hence not a number characteristic of the sampling device alone. However, for present purposes, it is this number which is most useful. It has been seen in Chapter IV that the size distribution of drops from breaking bubbles is remarkably invariant with respect to both solution and bubble parameters, so that the volume-average diameter

obtained in this calibration is representative of the experimental data. The instrument has been calibrated in the same manner in which it is used, which is a guarantee against systematic errors.

The efficiency curves of Figure 5.10 were taken from the data of Ranz & Wong (1952) and Mitchell & Pilcher (1959), and it is hoped that they are representative of this impactor. The "nominal"  $\bar{d}_v$  values at the top of the graph are obtained by averaging the results of all collections, basing the calculations upon the design values of  $d_{50}$ . The "found" values of  $\bar{d}_v$  are those obtained from the calibration. While the agreement between the nominal and found values is not exceptional, the uncertainties are such that one does not know whether to believe the calibration or the design. The design values have been used throughout this work because of the convenience of the power-of-two series, and the results show no obvious bias from this treatment. The calibration is taken as a reassurance that no gross errors of design or construction were committed.

Figure 5.10. Assumed collection efficiency of the aerosol impactor. The shaded area represents the material collected on the 2- $\mu$  stage. Three  $\bar{d}_v$  values found by calibration are shown at the top of the graph.



## A CONTINUOUS STILL FOR HIGH PURITY WATER

A number of writers (Kitchener 1958, Schenkel & Kitchener 1958, Franks 1961) have stressed the special precautions necessary for work with surface phenomena, and of these none are more fundamental than purity of the solvent. With such warnings in mind, a 1 liter/hr still was built following the designs of Ballentine (1954) and Franks (1961).

## DESIGN

Tap water is run into a constant-head device (where a portion is wasted) and thence through the cooling jacket of the condenser. Flow control, which is critical, is achieved both by changing the pressure head and by a capillary constriction in the tubulation. These are adjusted until the coolant leaving the condenser is at 90°C.

This preheated water flows into a second constant-head device, and thence through a solenoid valve into the first distillation stage. Since internal pressure at the first stage may be 50 cm of water, the first stage pressure head is set at 100 cm. The first stage is a 4-liter reaction kettle, heated by a 1-kw Vycor immersion heater, and

equipped with conductimetric level controls which shut off either the solenoid valve or the heater as appropriate.

Alkaline permanganate is continuously added to the feed to oxidize organic material. The first stage water reaches a steady-state concentration of permanganate and the  $MnO_2$  reaction product, since approximately one third of the input water is drained off by a siphon.

(A word of warning about the alkaline permanganate oxidation: the oxidation of iodide to iodine is rapid; of iodine to iodate, slow. This can result in iodide in the feed being converted into iodine, escaping into the vapor phase, and redissolving in the product.)

The second stage is a 1-liter flask of 50% phosphoric acid, which is itself non-volatile and will trap volatile basic substances which may have escaped from the first stage. Steam is introduced below the surface, and since the acid mixture has a concentration-dependent boiling point, the level is controlled by a thermostatic switch (which, being encased in Teflon, is also an efficient "boiling chip"). Below  $106^\circ C$  (high water) the first stage heater is shut off; above  $120^\circ C$  (low water), the second stage.

Following the second stage is a 5-foot Vigreux column which serves more as a spray trap than as a reflux column. Separating this column from the condenser is a short inclined section maintained at  $150^\circ C$  to act as a film breaker. Preventing the existence of a continuous liquid film between input and output is as removing all liquid

drops entrained in the vapor phase.

The condenser is a straight quartz tube, 8 mm X 80 cm. At its output end is a water-trapped vent for uncondensed steam, and a Soxhlet head which collects the product and directs it either into a system which measures both conductivity and surface tension, or, if the product meets these tests, into a Vycor receiver.

The entire system is flushed by filtered nitrogen, insuring a product free of CO<sub>2</sub> and, more importantly, keeping out atmospheric dust when the system is shut down. If air is admitted, sufficient surface active material enters on dust motes to contaminate the system for several days.

The surest test of cleanliness is the presence of a smooth meniscus above the water level in the receiver. Contamination is revealed by an unwettable zone whose position appears to be a compromise between a hydrophobicity which drives it to the Vycor, and the periodic washing from the walls as the Soxhlet empties. Only when this zone is absent can the surface tension be expected to rise to the desired value (71.8 dynes/cm at 25°C).

## RESULTS

It required several weeks of "steaming out" before the glass had leached sufficiently for the conductivity monitor to come on scale at 10  $\mu$ mhos/cm. After 2 years' operation, and if the product is collected at 90°C, the conductivity is consistently below 0.10  $\mu$ mhos/cm ( $> 10$  megohm-cm). (The

theoretical limit for pure water is 0.055  $\mu\text{mhos/cm.}$ )

This still will satisfactorily remove ions, organic material, and particulate material present in the feed. However, enough colloidal silica sloughs off of the walls to be visible in the receiver as a grey fog by the forward scattered light of a microscope illuminator. No way is known of preventing this sloughing, but if necessary the particles can be removed by filtration.

When 300  $\mu$ -curies of Na-22 were put in the first stage, and a liter of product collected and evaporated, no activity above background was observed. Such sodium (and presumably other metals) as are found in the product are leached from the glassware, for which there is no recourse but replacement by quartz.

**BLANK PAGE**

CHAPTER VI

FLOW PATTERNS AROUND RISING BUBBLES

I have remarked that people working with  
computing machines frequently rediscover  
old mathematics.

Gilbert King  
Comp. Sem. Proc. 1949

## INTRODUCTION

The rise of a bubble through a liquid can produce appreciable concentration gradients by virtue of the shearing motion of the liquid. Appreciable electric potentials can also arise from greater adsorption of an ion with a high diffusion coefficient under the non-equilibrium conditions of the moving bubble. Thus a separation of charge and a fractionation of ions may occur at the bubble surface, giving rise to electric fields which are not due to equilibrium double layer formation, and to surface concentrations other than those expected from thermodynamic equilibrium, caused entirely by differences in the diffusion coefficient (Haydon 1964).

For Reynolds numbers much larger than 1, the problem is very complex and has not been solved. This investigation was undertaken mainly in order to find the flow pattern surrounding the bubble. From this pattern, the diffusion of various ions to the surface can be obtained, as can the rate at which the slower ions are swept past the bubble surface.

It is conceivable that a numerical solution to these problems can be obtained up to a Reynolds number ( $Re$ ) of 200 (the point at which a bubble visibly loses its sphericity) by the methods employed herein. Such calculations should cover both fluid and solid interfaces, and in particular

should be valid through the important transition region from liquid to solid, as a motion-preventing monolayer is accumulated.

This work represents the first stage of such a program, covering the range  $5 \leq Re \leq 100$  for a solid interface, and giving a detailed description of the near-surface flow.

A more ambitious attempt would include the effects of the presumed variation of viscosity near the surface (Lyklema & Overbeek 1961), but neither experiment nor theory can furnish much of a guide at this time.

#### THE HARD SPHERE AS A MODEL OF AN OCEAN BUBBLE

To ask about the mechanisms whereby bubbles collect, alter, and transport material from ocean to atmosphere involves one immediately in the egg-or-chicken question: Which came first, the bubble surface or the bubble? To grow bubbles on a capillary tip is one thing; to form them by enveloping air in a breaking wave is something quite different, and the answers obtained depend on the model used.

In the first case, the interface is "new", and not in equilibrium with the liquid phase. Neither of these conditions obtains in the second case. A "new" interface is fluid and free to flow. This influences both the hydrodynamics of its movement and the diffusion to its surface. An "old" interface, already bearing surface-active material, will behave like a solid sphere. In short, the

"new" bubble will rise approximately 1.5 times as fast as the "old" bubble (Lamb, Sec 337). Thus one must postulate which sort of bubble is to be examined, and justify this choice, before asking further questions of the model.

In the purest water which the author succeeded in making, it was noted that bubbles newly formed at a capillary tip rose at terminal velocity for about 15 cm, and then abruptly decelerated to a second terminal velocity. This can only indicate a rapid transition from free interface to solid interface, and must arise from the accretion of surfactant material onto the bubble surface (this is discussed in detail by Levich, Sec. 83). Though the water was "pure", it was in contact with Lucite and in diffusion contact with Cambridge air (although shielded from direct fallout). Evidently there is sufficient soluble plasticizer in Lucite, or sufficient rubber, chocolate, or soap in the Cambridge atmosphere to contaminate a liter of water rather quickly.

If "clean" water, under favorable conditions, causes bubbles to behave like solid spheres within a few centimeters, then it is probably safe to assume that any bubble formed in the ocean, regardless of the mechanism, will behave like a solid sphere from the outset. Having chosen this model, we have answered an important part of the question, "How does a bubble collect material from the sea?" We are restricted to asking, "What secondary material can a bubble be expected to accumulate?" E.g.: In considering the

organic matter-phosphate ion relationship, we have started by assuming that the bubble is covered with organic material, and are faced with determining whether the phosphate accompanied the organic at this point, or whether the phosphate is swept out of solution as the bubble rises.

#### METHOD OF ATTACK

The hydrodynamics of greatest interest in this connection occur immediately next to the bubble surface. Although there is a known corpus of boundary layer theory which deals with near-surface phenomena, it is not applicable at the low  $Re$  numbers considered here.

Instead, the full, non-linear, steady-state Navier-Stokes equation is solved over a sufficiently large radius surrounding the bubble to reach a region of potential flow in which the solution is known and analytic. Interpolation will then give answers near the surface which depend only upon the accuracy with which the difference equation represents the differential equation. These answers will bridge the gap between boundary layer theory at the high end of the  $Re$  range and viscous flow at the low end.

#### APPROXIMATING THE NAVIER-STOKES EQUATION

To extend the known region from  $Re=40$  to  $Re=100$ , we begin by writing N-S in polar coordinates, and splitting it

into two simultaneous differential equations in the stream function  $\Psi$  and the vorticity  $\omega$ . It is reduced to dimensionless form by

$$r=r'/a, \quad \Psi=\Psi'/Ua, \quad \omega=\omega'a/U, \quad Re=2Ua/\nu$$

where  $a$  is the sphere radius,  $U$  the free stream velocity, and  $\nu$  the kinematic viscosity. Jenson (1958) credits Southwell (Relaxation Methods) with observing that this equation is not adequately approximated by a polynomial in  $r$ , and suggested the substitution  $r=e^z$  and a numerical solution in uniform increments of  $z$ . The resulting differential equations are (see Shafrir & Neiburger 1964)

$$E^2 \Psi = e^{2z} \chi$$

$$E^2 \chi = Re e^z \sin \theta \left[ (\partial \Psi / \partial z) (\partial / \partial \theta) - (\partial / \partial \theta) (\partial / \partial z) \right] \chi (2e^{2z} \sin^2 \theta)^{-1}$$

wherein

$$E^2 = (\partial^2 / \partial z^2) - (\partial / \partial z) + \sin \theta (\partial / \partial \theta) \left[ (\sin \theta)^{-1} (\partial / \partial \theta) \right]$$

and

$$\chi = \omega e^z \sin \theta$$

The fourth order difference equations used to approximate these differential equations make use of the grid point pattern of Figure 6.1, in which the points are labeled with their corresponding subscripts. Expanding the differentials and collecting terms, we obtain

$$\Psi_0 = [C_{-2\theta} \Psi_{-2\theta} + C_{-\theta} \Psi_{-\theta} + C_0 \Psi_0 + C_{2\theta} \Psi_{2\theta} \\ + C_{-2z} \Psi_{-2z} + C_{-z} \Psi_{-z} + C_z \Psi_z + C_{2z} \Psi_{2z} - \chi e^{2z}] / C_0$$

$$\chi_0 = [Q_{-2\theta} \chi_{-2\theta} + Q_{-\theta} \chi_{-\theta} + Q_0 \chi_0 + Q_{2\theta} \chi_{2\theta} \\ + Q_{-2z} \chi_{-2z} + Q_{-z} \chi_{-z} + Q_z \chi_z + Q_{2z} \chi_{2z}] / Q_0$$

The coefficients C and Q are given by

$$C_{\pm 2z} = (\pm \delta z - 1) / 12 \delta z^2$$

$$C_{\pm 2\theta}(\theta) = (\pm \cot \theta \delta \theta - 1) / 12 \delta \theta^2$$

$$C_{\pm z} = (4 \pm 2 \delta z) / 3 \delta z^2$$

$$C_{\pm \theta}(\theta) = (4 \pm 2 \cot \theta \delta \theta) / 3 \delta \theta^2$$

$$C_0 = 5(1/\delta \theta^2 + 1/\delta z^2) / 2$$

where  $\delta z^2$  is written for  $(\delta z)^2$ . Writing

$$S = Re / 2e^z \sin \theta$$

$$\Psi_x'(\theta, z) = (8(\Psi_{+x} - \Psi_{-x}) - (\Psi_{+2x} - \Psi_{-2x})) / 12 \delta x$$

we have further

$$Q_{\pm 2z}(\theta, z) = C_{\pm 2z} \mp S \Psi_0'$$

$$Q_{\pm 2\theta}(\theta, z) = C_{\pm 2\theta} \mp S \Psi_z'$$

$$Q_{\pm z}(\theta, z) = C_{\pm z} \pm 3S \Psi_0'$$

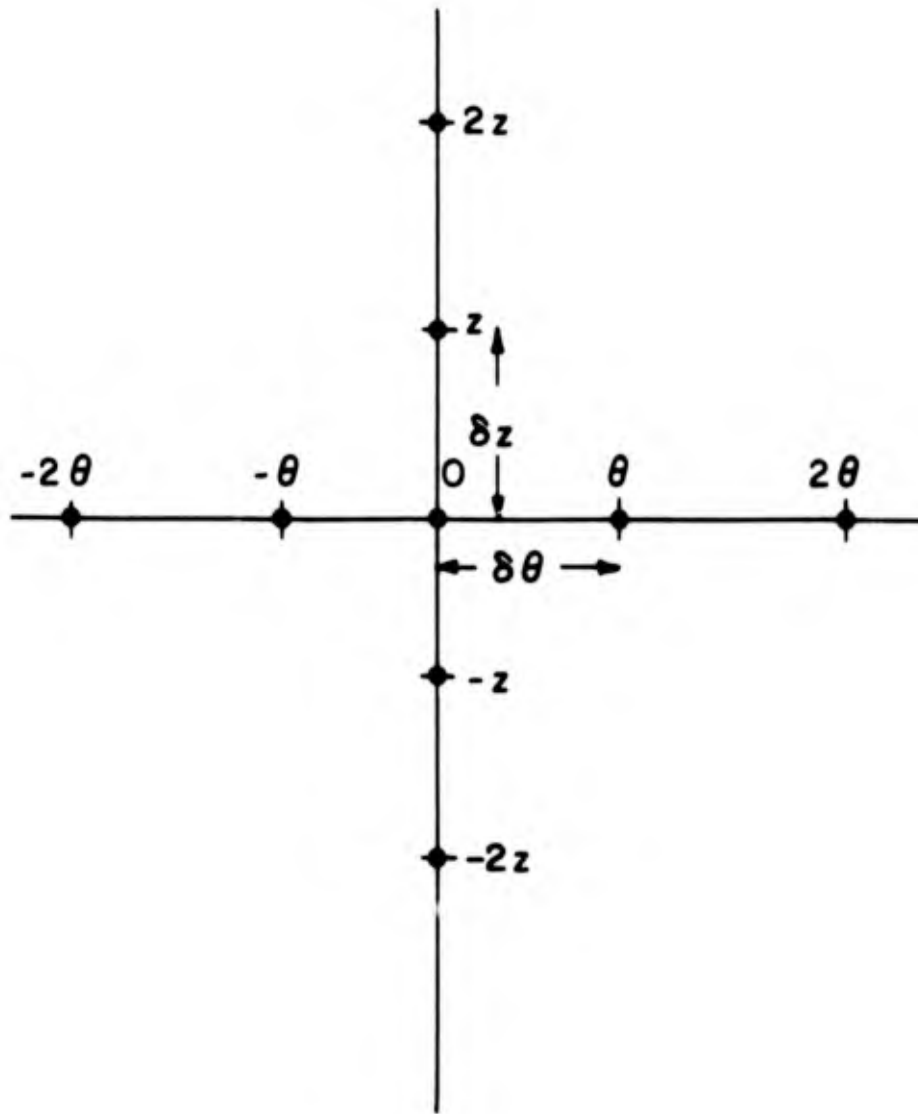
$$Q_{\pm \theta}(\theta, z) = C_{\pm \theta} \pm 3S \Psi_z'$$

$$Q_0(\theta, z) = C_0 + S(\Psi_0' - \cot \theta \Psi_z')$$

## THE COMPLETE SOLUTION

Certain questions about details of the full solution have not been satisfactorily resolved at the time of writing. In particular, the vorticity boundary conditions in the wake, which are not known from theory, affect the computed drag coefficients. It is hoped that a boundary

Figure 6.1. The coordinate system employed.



condition algorithm can be developed which will give results in accord with experiment (the present method is not adequate above  $Re=40$ ), and it would be premature to present the best solution obtained to date. However, there are some features of the results which are not likely to change qualitatively, and which are not obvious from published work. These are: (1) The pressure distribution in the wake appears to be independent of  $Re$  above  $Re=20$ . (2) The velocity distribution at the equator has an upper envelope (outside of the velocity maximum which marks the edge of the incipient boundary layer). This envelope is approached soon after the velocity maximum, and the point of contact moves in toward the sphere as  $Re$  increases.

Furthermore, the details of flow next to the surface do not seem to be greatly affected by the vorticity boundary condition. These will be given, somewhat tentatively, in the expectation that the values will not change by more than 10%.

#### INTERPOLATION TOWARD THE SURFACE

The  $\Psi$  grid must be interpolated near the surface to obtain the streamlines, which are contours of equal  $\Psi$ . This is done by beginning with the viscous flow equation, from which we obtain

$$\Psi \doteq r^2 - 3r/2 + 1/2r$$

to within a constant multiplier at any given angle.

Near the surface we can set  $r=1+\theta$ , and find that first order terms vanish, leaving

$$\Psi = 3\theta^2/2$$

Now, earlier in the solution we set  $r=e^z$ , from which fact we can identify  $\theta$  with  $z$ . To a first approximation  $\Psi=Az^2$ , and for interpolation we employ

$$\Psi = Az^2 + Bz^4$$

and fit the polynomial through the points closest to the surface.

This procedure is followed for every  $\theta$  for which there are points, and also for an additional cut which begins at the front stagnation point and goes at  $45^\circ$  through the points  $(r,\theta) = (1,1)$  and  $(2,2)$  in order to pick up an early value near the axis. Figure 6.2 diagrams the interpolation scheme, and is interpreted thus:  $\Psi = \Psi(z)$  is fitted through the origin,  $\Psi(2)$  and  $\Psi(3)$ , and then inverted to give  $z=z(\Psi)$ .  $z_i = z_i(\Psi_i)$  is then solved for a family of  $\Psi_i$ 's near the surface. This process provides the  $z$  coordinate for each  $\Psi_i$  at each value of  $\theta$ , through which a streamline may be drawn.

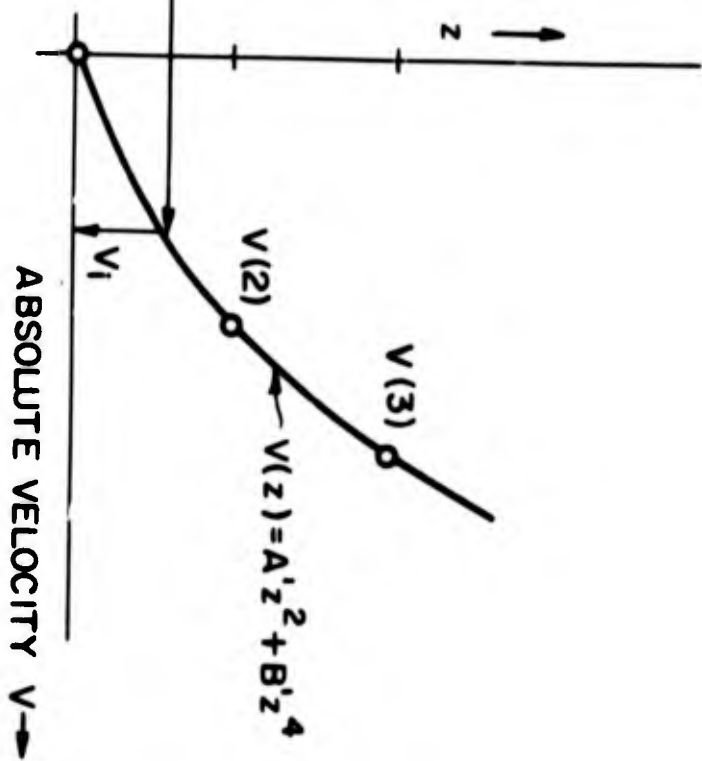
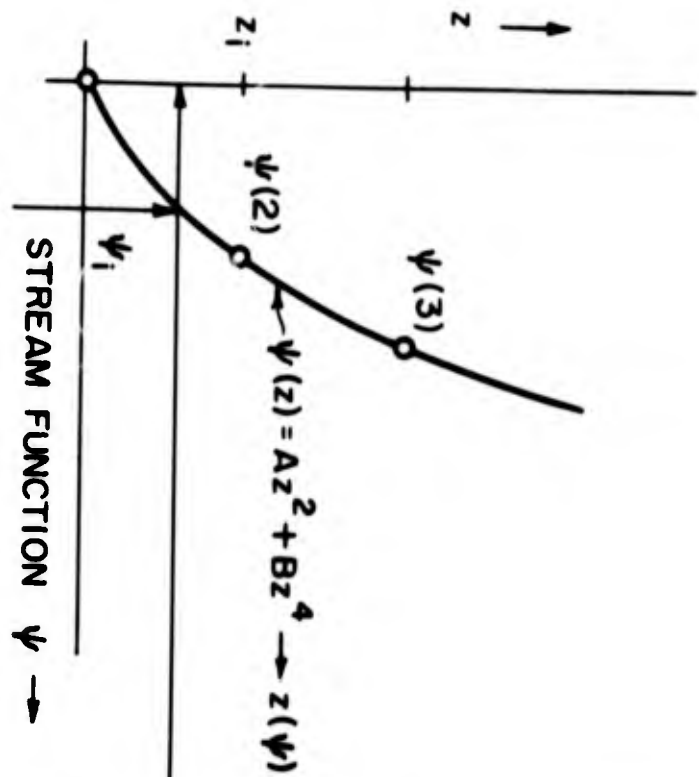
The absolute velocity  $V$  along the stream lines (available from the earlier solution and at the same grid points) is approximated just as is  $\Psi$ , so that

$$V(z) = A'z^2 + B'z^4$$

which is solved for the family  $V_i = V(z_i)$ .

From the computed distance between points along the stream line and the interpolated velocity, a dimensionless transit time  $t$  is obtained. The relation between  $t$  and the

Figure 6.2. Near-surface interpolation scheme. Enter the  $\Psi$  field at  $\Psi_i$  to obtain a  $z_i$ ; enter the  $V$  field at  $z_i$  to find  $V_i$ .



real time  $t'$  is

$$t' = ta/U .$$

#### RESULTS: NEAR-SURFACE FLOW AND TRANSIT TIME

The stream lines and the transit time are shown in Figure 6.3. The bar below the curves is the distance traveled in a scale time of  $10^3$ , in the region of closest approach to the sphere. Flow is much more rapid forward and aft of this region, where the path is farther from the sphere surface.

Only a single stream line is shown for each  $Re$  number. However, if the exponent of  $\Psi$  is taken as  $n$ , the approximate values of the exponents of  $z$  and  $t$  become, respectively,  $(n-1)/2$  and  $(-n-2)$ , at the point of closest approach to the surface. In this manner, Figure 6.3 represents, with sufficient accuracy for present purposes, the answers obtained over the range  $3 \leq n \leq 8$ . (Closer to the surface, computational noise sets a limit upon the interpolation; farther away, the approximating equation is inadequate.) This range may be confidently extended inwards to the sphere surface.

The diagram is misleading in that the separation between the wake and the stagnation region is not the impermeable barrier it appears to be in Figure 6.3. There is undoubtedly eddy diffusion across this zero-velocity surface, and a time-dependent solution would show that the surface itself is not immobile.

Figure 6.3 is plotted in  $\log r$  and  $\theta$ , but in Cartesian coordinates, so that the right edge is the front axis of the sphere, the left edge the rear axis, and the surface of the sphere is toward the bottom of the graph. Thus, the distance from a streamline to the surface is given directly by the ordinate.

#### CONCLUSIONS

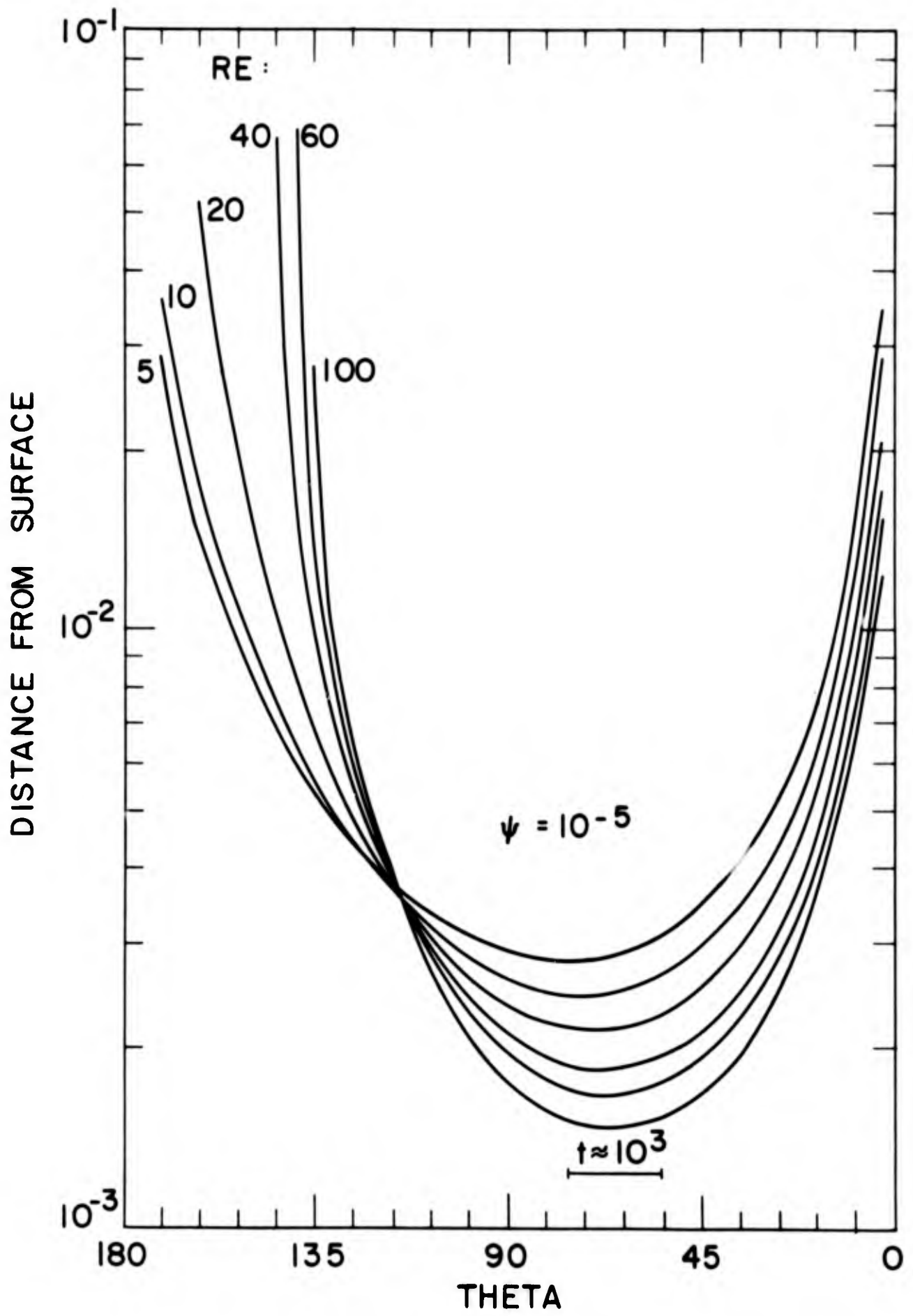
The near-surface flow details of Figure 6.3 give streamlines and transit times which are within the region of molecular diffusion to the surface. They form a basis for examining the collection of material by bubbles in a region of Re numbers which cannot be approximated by either viscous flow equations or by boundary layer theory.

As an aid in interpreting these curves, it can be shown that the dimensionless radius  $R$  of the tube far in front of the sphere, which opens up to become a streamline  $\Psi$ , is

$$R = \sqrt{2\Psi}$$

Thus, if molecular diffusion (not particulate impaction) is the mechanism by which material reaches the surface, the tube swept clean by the bubble is very much smaller than the bubble itself. Bubbles would appear to be much better scavengers of small particulate matter, than they are of dissolved ions.

Figure 6.3. Near-surface stream lines and transit times.



## REFERENCES FOR CHAPTER VI

- Haydon, D. A., 1964: In Prog. Surf. Sci. 1, Ed.: J. F. Danielli, K. G. A. Parkhurst, A. C. Riddiford. Academic Press, New York, p 139.
- Jenson, V. G., 1959: Proc. Roy. Soc. Lon. A 249, 346.
- Lamb, H., 1932: Hydrodynamics, 6th ed., Dover, New York.
- Levitch, V. G., 1962: Physico-chemical Hydrodynamics, Prentice Hall, Englewood Cliffs.
- Lyklema, J., & Overbeek, J. Th. G., 1961: J. Coll. Sci. 16, 501, 595.
- Shafrir, U., & Nelburger, M., 1964: Univ. Calif. Occas. Pap. Vol 1, U.C. Press, Berkeley.

VII

Small bubbles are a subject in themselves.

Garrett Birkhoff

## ACKNOWLEDGEMENTS

I should like to take this opportunity to thank a number of people who (in their separate capacities) have contributed to this work.

Chronologically these begin with Dr Ambrose Nichols and S. B. Weiland, because of whom I am a chemist, and Sam Hinton and Dr Norris Rakestraw, who lured me into oceanography.

William Fahle of Rohr Aircraft gave me parting words of encouragement which have been a stimulus when lesser incentives flagged.

The Chemistry Department at MIT was kind enough to allow me to do interdepartmental thesis research work in the Department of Geology and Geophysics. I am also grateful to the Departmental Secretaries who indefatigably saw to it that the proper forms were properly processed.

Prof. John Winchester's interest in the possibility of ion fractionation in sea foam formed the basis of this work. Prof. Dayton Carritt called my attention to the work of Dr Edward Baylor of Woods Hole Oceanographic Institution, who then suggested the phosphate problem to me. Discussions with Dr Duncan Blanchard raised questions as fast as they answered them throughout the course of the work. Stimulating conversations with Drs Gordon Riley and Peter Wangersky of Bingham Oceanographic Laboratory enabled me to avoid many unforeseen pitfalls.

My triumvirate of Supervisors were unanimous in leaving me to my own devices, except when I needed encouragement or assistance, which they invariably provided, and for both of these attributes I am grateful. Prof. George Scatchard did his skeptical best to see that this attempt at applying physical chemistry to the ocean was more than superficial. Prof. Isadore Amdur deserves particular thanks for his unflinching support of unpopular causes.

For laboratory assistance, I am indebted to Miss Mary Untz and to Alfredo Gonzales. Ken Harper's Geology Shop was exceedingly helpful about building equipment which worked.

The MIT Computation Center made available the necessary computer time, and various staff members from both the Computation Center and Project MAC have been more than helpful.

Financial support from the National Science Foundation (3 years of graduate fellowships) and from the Office of Naval Research (Project NR 083-157) is gratefully acknowledged, as is the cooperation of the Geology Department in the person of Dr Shrock.

Last but not least, I wish to express my appreciation to the several members of the Geochemistry Laboratory of the Department of Geology and Geophysics for many helpful discussions, with particular thanks to Lester Walters and Dr Robert Duce.

Miss Ellen Rice read the manuscript, and did what she could to recast it into English.

## APPENDIX A

## PARTICLE DIAMETERS FROM Na-COUNTS

The volume-average diameter  $\bar{D}_v$  and the surface-average diameter  $\bar{D}_s$ , are obtained from the volume (Na-count) curve. The assumptions involved are (1) each impactor stage collects diameters over a range from  $a$  to  $2a$ , and (2) in this range, a linear approximation is an adequate representation of the volume distribution curve. (Some attempt to follow the sudden valley in the volume curve is necessary, but the data do not warrant a better approximation than linearization in this way.)

$\bar{V}$  and  $\bar{S}$ , the average volume and diameter of a particle on a given stage, are then given by

$$\bar{V} = (\pi/6)\bar{D}_v^3 = (\pi/6) \int_a^{2a} wD^3 dD / W$$

$$\bar{S} = \pi\bar{D}_s^2 = \pi \int_a^{2a} wD^2 dD / W$$

where  $w$  is the weighting function and  $W$  its integral. From the second assumption

$$w(x) = V^0 + v'x$$

where  $V^0 = V(a) - v'a$  and  $v' = (V(2a) - V(a))/a$ . Hence the denominator is just the simple average, and

$$aW = \int_a^{2a} w(x) dx = (V(2a) + V(a))/2$$

which leads to

$$\bar{D}_v^3 = \frac{1}{aW} \int_a^{2a} (V^0 + v^1 x) x^3 dx = a^3 [26V(a) + 49V(2a)] / 20W$$

and

$$D = \frac{1}{aW} \int_a^{2a} (V^0 + v^1 x) x dx = a^2 [11V(a) + 17V(2a)] / 12W$$

## APPENDIX B

## THE DATA-PROCESSING PROGRAM EMPLOYED

The main program consists of two lines of MAD, and does nothing but call INPUT6, which must be a subroutine because of its additional entry point PANIC. PANIC is a return from a rewritten floating point trap (FPT) which allows a dump at the point of failure instead of an EXIT.

"INSERT FILE" is an MIT CTSS addition to MAD, and allows the logical insertion of the 850-card FUZZ file (Appendix C) at this point.

INPUT6 reads data cards, computes elapsed time, corrects for source-to-window distance errors, gets the variance of the counts of each sample, subtracts background, and calls FRAC6.

FRAC6 solves a pair of simultaneous equations to separate two isotopes, computes numerous ancillary relations, and above all, obtains the variance of each of its answers.

The programs have been in continuous development and have not been cleaned up for publication. They harbor minor bugs, and compute many numbers which are no longer germane.















APPENDIX B.1 (Added in proof) TABULATION OF EXPERIMENTAL DATA

Sample	Sodium cpm H	Phosphate, cpm P	Excess Phosphate cpm P <sub>2</sub>	Fractionation F	Volume collected, μl V	Number of Particles N
Run 10						
A	297± 1.4	5936± 63.3		1.000± .017	25.000± .168	
32	3 .2	4421 43.9	4358.0± 44.2	70.187 5.497	.177 .014	3.06E 07±1.01E 03
16	1 .3	5767 55.2	5752.2 55.6	302.705 171.751	.063 .028	6.89E 05 5.08E 03
8	1 .3	11119 74.6	11101.7 74.8	628.150 183.512	.075 .022	7.60E 04 9.39E 04
4	1 .3	6971 62.9	6926.0 63.2	155.495 20.885	.189 .025	1.73E 06 1.21E 06
2	10 .2	3277 24.9	3086.3 25.3	17.212 .414	.802 .016	6.30E 07 1.03E 07
1	5 .3	1094 10.8	984.6 11.1	10.007 .512	.460 .023	2.17E 08 2.41E 07
h	9 .1	1714 24.4	1540.3 24.7	9.860 .236	.732 .012	4.40E 09 4.37E 08
Sum	31 .7	34364 125.9		55.955 1.402	2.498 .055	
Run 11						
A	317± 5.1	4601± 54.6		1.000± .028	25.000± .568	
32	42 1.4	4707 73.6	6097.8± 77.4	11.002 .451	2.209 .083	3.82E 04±6.19E 03
16	27 1.2	5812 69.2	5421.7 71.7	14.875 .738	2.123 .099	2.62E 05 3.93E 04
8	31 2.2	11316 124.8	10568.9 129.8	15.145 .738	4.060 .186	4.47E 06 8.70E 05
4	419 12.0	63037 709.1	57756.8 740.0	10.499 .384	33.040 1.082	3.46E 08 7.10E 07
2	749 28.6	157463 1626.0	146590.5 1692.2	14.483 .642	59.081 2.448	2.77E 09 6.87E 08
1	86 2.0	9641 164.2	8396.2 168.6	7.746 .273	6.763 .193	2.77E 09 3.47E 08
h	52 1.1	5400 153.1	4646.5 154.7	7.168 .293	4.094 .110	2.13E 10 1.86E 09
Sum	1426 31.2	260177 1795.2		12.570 .382	111.369 2.695	
Run 12						
A	214± 2.6	2923± 23.8		1.000± .021	25.000± .428	
32	155 1.4	2588 42.7	477.6± 55.9	1.226 .029	12.025 .180	2.08E 05±1.34E 04
16	160 1.7	2220 45.6	34.5 60.5	1.016 .028	18.684 .304	2.49E 06 1.58E 05
8	84 .9	1205 23.1	62.6 30.8	1.055 .028	9.768 .155	8.86E 06 4.42E 05
4	136 1.0	2193 19.6	332.1 36.0	1.179 .022	15.904 .224	1.37E 08 7.88E 06
2	150 1.2	2066 29.5	22.3 44.9	1.011 .022	17.465 .252	1.13E 09 5.72E 07
1	6 .4	136 9.5	49.7 11.2	1.575 .154	.739 .050	2.94E 08 2.40E 07
h	8 .2	155 6.1	51.3 6.9	1.496 .075	.884 .027	5.08E 09 8.07E 08
Sum	699 2.9	10563 76.3		1.108 .019	75.469 .515	
Run 13						
A	213± 2.6	2923± 23.8		1.000± .021	25.000± .428	
32	155 1.4	2588 42.7	477.6± 55.9	1.226 .029	12.025 .180	2.08E 05±1.34E 04
16	160 1.7	2220 45.6	34.5 60.5	1.016 .028	18.684 .304	2.49E 06 1.58E 05
8	84 .9	1205 23.1	62.6 30.8	1.055 .028	9.768 .155	8.86E 06 4.42E 05
4	136 1.0	2193 19.6	332.1 36.0	1.179 .022	15.904 .224	1.37E 08 7.88E 06
2	150 1.2	2066 29.5	22.3 44.9	1.011 .022	17.465 .252	1.13E 09 5.72E 07
1	6 .4	136 9.5	49.7 11.2	1.575 .154	.739 .050	2.94E 08 2.40E 07
h	8 .2	155 6.1	51.3 6.9	1.496 .075	.884 .027	5.08E 09 8.07E 08
Sum	699 2.9	10563 76.3		1.108 .019	75.469 .515	
Run 14						
A	194± 2.2	2350± 38.0		1.000± .028	25.000± .405	
32	115 1.5	1280 68.6	-120.8± 76.3	.914 .054	9.912 .174	1.72E 05±1.29E 04
16	61 1.6	700 40.3	-43.2 47.3	.942 .063	7.885 .230	9.47E 05 7.71E 04
8	47 4.4	521 50.1	-30.4 73.8	.912 .123	6.066 .566	5.80E 06 1.37E 06
4	92 1.0	1020 50.9	-102.2 56.9	.909 .050	11.912 .188	1.05E 08 1.61E 07
2	106 3.4	1215 20.9	-67.8 53.2	.947 .040	13.610 .471	8.84E 08 9.69E 07
1	41 1.4	470 21.0	-33.2 28.8	.934 .055	5.340 .190	2.40E 09 2.55E 08
h	38 2.4	473 35.8	8.7 46.7	1.019 .101	4.929 .308	2.72E 10 5.00E 09
Sum	501 6.7	5680 116.6		.933 .029	59.653 .890	
Run 15						
A	154± 1.6	2243± 37.8		1.000± .028	25.000± .363	
32	399 3.8	10772 142.4	4961.7± 191.2	1.854 .048	43.174 .608	7.47E 05±4.53E 04
16	114 1.1	2852 48.8	1193.1 61.1	1.719 .048	18.492 .266	2.05E 06 8.86E 04
8	25 .5	624 21.2	262.3 23.7	1.726 .077	4.027 .094	3.35E 06 1.67E 05
4	152 1.7	3851 63.7	1842.2 81.1	1.743 .049	24.620 .373	2.51E 08 2.28E 07
2	324 3.0	8805 115.5	4083.4 154.6	1.865 .047	52.623 .726	3.77E 09 2.31E 08
1	76 .9	1853 25.6	738.1 36.1	1.662 .044	12.427 .192	5.32E 09 2.29E 08
h	87 1.0	1996 28.0	730.9 40.4	1.578 .042	14.105 .221	8.04E 10 4.49E 09
h	160 1.9	2285 39.9		.982 .028	25.925 .402	
Sum	176 5.5	30753 204.8		1.794 .038	169.467 1.096	
Run 16						
A	154± 1.6	2243± 37.8		1.000± .028	25.000± .363	
32	399 3.8	10772 142.4	4961.7± 191.2	1.854 .048	43.174 .608	7.47E 05±4.53E 04
16	114 1.1	2852 48.8	1193.1 61.1	1.719 .048	18.492 .266	2.05E 06 8.86E 04
8	25 .5	624 21.2	262.3 23.7	1.726 .077	4.027 .094	3.35E 06 1.67E 05
4	152 1.7	3851 63.7	1842.2 81.1	1.743 .049	24.620 .373	2.51E 08 2.28E 07
2	324 3.0	8805 115.5	4083.4 154.6	1.865 .047	52.623 .726	3.77E 09 2.31E 08
1	76 .9	1853 25.6	738.1 36.1	1.662 .044	12.427 .192	5.32E 09 2.29E 08
h	87 1.0	1996 28.0	730.9 40.4	1.578 .042	14.105 .221	8.04E 10 4.49E 09
h	160 1.9	2285 39.9		.982 .028	25.925 .402	
Sum	176 5.5	30753 204.8		1.794 .038	169.467 1.096	
Run 17						
A	153± 4.2	2273± 122.1		1.000± .085	25.000± .974	
32	37 1.1	713 33.9	167.9± 49.9	1.308 .108	3.988 .161	6.92E 04±1.20E 04
16	5 .4	182 22.3	103.1 23.5	2.306 .356	.868 .066	9.01E 04 1.34E 04
8	5 .2	154 12.9	86.6 14.0	2.276 .260	.746 .042	7.25E 05 1.57E 05
4	20 2.3	319 38.2	23.5 54.3	1.080 .191	3.252 .387	3.20E 07 2.06E 07
2	82 3.2	1451 85.6	235.5 109.6	1.194 .102	13.368 .646	1.05E 09 2.92E 08
1	26 1.0	450 24.7	66.9 34.4	1.184 .110	3.993 .201	1.74E 09 2.58E 08
h	27 1.0	470 41.4	72.5 50.1	1.182 .133	4.376 .200	2.48E 10 4.15E 09
h	156 4.4	2215 103.8		.958 .078	25.433 .999	
Sum	199 4.4	3720 99.5		1.255 .087	30.602 .824	
Run 18						
A	153± 4.2	2273± 122.0		1.000± .085	25.000± .974	
32	10 .5	169 33.8	-6.4± 35.9	.959 .230	1.141 .064	1.97E 04±4.75E 03
16	6 .3	79 16.1	4.9 17.3	1.066 .236	.816 .056	9.66E 04 1.95E 04
8	6 .2	53 20.7	-32.5 21.5	.618 .247	.936 .045	9.51E 05 1.86E 05
4	11 1.5	135 11.8	-31.5 16.9	.811 .092	1.836 .090	1.62E 07 3.38E 06
2	65 1.9	955 58.1	-3.7 86.7	.996 .090	10.546 .426	8.56E 08 2.03E 08
1	24 .7	338 16.1	-24.3 29.1	.933 .077	3.980 .159	1.78E 09 2.18E 08
h	32 .9	426 61.1	-42.4 68.7	.909 .144	5.153 .206	3.00E 10 4.46E 09
Sum	153 2.4	2135 96.6		.940 .072	24.407 .516	
Run 19						
A	142± 3.5	1297± 46.8		1.000± .062	25.000± .871	
32	150 3.5	3796 131.6	2426.0± 148.0	2.771 .168	17.608 .597	3.05E 05±4.44E 04
16	115 2.9	2964 110.0	1915.8 122.1	2.828 .178	20.202 .718	2.57E 06 3.23E 05
8	34 1.3	1137 38.0	826.4 41.9	3.665 .243	5.979 .246	5.10E 06 5.84E 05
4	138 3.7	3427 119.8	2163.4 136.2	2.713 .168	24.353 .886	2.38E 08 4.68E 07
2	158 4.0	4252 146.4	2805.5 163.6	2.939 .180	27.888 .986	1.81E 09 2.32E 08
1	35 1.3	973 36.6	853.9 40.8	3.067 .210	6.116 .272	2.60E 09 2.55E 08
h	34 3.2	943 33.8	636.1 46.8	3.075 .344	5.909 .588	3.29E 10 9.52E 09
Sum	663 8.0	17491 262.9		2.886 .138	108.055 1.767	

Sample	Sodium cpm N	Phosphate, cpm P	Excess Phosphate cpm P <sub>2</sub>	Fractionation P	Volume collected, ml V	Number of Particles N
Run 20						
A	142± 1.6	750± 14.1		1.000± .030	25.000± .385	
32	17 ± .8	228± 52.7	2215.9± 52.8	34.616± 1.917	1.430 ± .068	2.51E 04± 5.02E 03
16	1 ± .5	1095 15.4	1090.1± 15.7	234.941 14.611	.152 ± .094	1.52E 04 1.03E 04
8	1 ± .5	3581 48.8	3577.1 48.9	883.296 587.220	.134 ± .089	1.30E 05 2.83E 05
4	1 ± .5	1534 26.1	1529.7 26.2	393.480 281.209	.129 ± .092	1.02E 06 2.43E 06
2	1 ± .6	850 18.0	842.5 18.3	111.124 47.368	.252 ± .107	1.78E 07 3.58E 07
1	1 ± .6	98 11.2	93.7 11.6	22.588 15.714	.143 ± .098	6.73E 07 1.16E 08
h	1 ± .6	96 9.3	88.6 9.9	13.269 6.177	.238 ± .108	1.44E 09 2.91E 09
h	141 1.4	880 18.9		1.171 ± .038	24.797 ± .370	
Sum	18 1.5	9535 81.3		97.595 8.202	2.499 ± .250	
Run 21						
A	127± 4.1	1042± 55.1		1.000± .088	25.000± 1.161	
32	597 19.4	74151 3606.9	69237.4± 3621.2	15.092± 1.286	78.574 ± 3.595	1.38E 06± 2.67E 05
16	323 10.5	36441 1680.0	33783.7 1690.3	13.712 ± 1.169	63.751 ± 2.924	7.68E 06 1.16E 06
8	119 5.7	15140 703.9	14159.7 700.1	13.437 ± 1.405	23.527 ± 1.357	2.05E 07 3.08E 06
4	921 29.7	99170 4571.1	91591.6 4601.6	13.086 ± 1.095	181.796 ± 8.296	1.89E 09 3.37E 08
2	1671 53.9	143281 6593.9	129539.7 6463.4	10.627 ± .872	329.640 ± 15.035	2.30E 10 4.37E 09
1	181 5.9	32795 1561.1	31301.9 1564.6	21.969 ± 1.861	35.809 ± 1.646	1.46E 10 2.09E 09
h	78 2.6	18851 871.5	18210.7 872.7	29.454 ± 2.474	15.353 ± .707	7.64E 10 1.07E 10
h	123 4.0	878 48.4		.866 ± .077	24.310 ± 1.110	
Sum	3891 15.9	419829 9159.6		13.118 ± .890	728.451 ± 17.928	
Run 22						
A	138± 2.1	750± 28.8		1.000± .058	25.000± .528	
32	15 ± .9	1038 23.4	957.7± 24.1	12.928 ± .974	1.771 ± .108	3.07E 04± 8.03E 03
16	1 ± .5	499 12.2	494.5± 12.5	102.890 58.033	.161 ± .090	1.59E 04 7.91E 03
8	1 ± .5	847 22.4	840.1 22.6	115.013 62.957	.244 ± .090	2.59E 05 4.19E 05
4	1 ± .6	385 14.4	378.1 14.7	53.994 23.515	.236 ± .102	1.87E 06 2.64E 06
2	3 ± .5	382 12.8	367.7 13.1	26.281 5.260	.481 ± .093	3.42E 07 3.46E 07
1	2 ± .6	162 12.3	153.2 12.8	18.179 6.897	.295 ± .109	1.40E 08 1.27E 08
h	3 ± .7	250 17.1	233.8 17.6	15.435 4.036	.536 ± .134	3.29E 09 3.68E 09
h	143 1.9	577 22.9		.740 ± .043	25.809 ± .520	
Sum	25 1.7	3564 44.9		25.587 ± 1.991	3.724 ± .277	
Run 27						
A	132± 4.3	3548± 147.9		1.000± .075	25.000± 1.161	
32	0 ± .2	28 4.4	17.0± 6.9	2.565 ± 1.298	.051 ± .024	
16	-0 ± .1	2 1.1	0. 0.	0. 0.	.000 ± .003	
8	0 ± .6	7 .9	-7 15.5	.904 ± 1.899	.052 ± .109	
4	4 ± .3	180 10.4	68.3 14.9	1.613 ± 1.180	.785 ± .068	
2	15 ± .5	590 25.2	200.8 35.0	1.516 ± .115	2.743 ± .128	
1	3 ± .3	138 6.4	49.6 11.0	1.564 ± .174	.620 ± .057	
h	5 ± .2	185 9.4	58.2 12.5	1.459 ± .121	.894 ± .045	
h	17 ± .6	582 24.6	127.0 38.2	1.279 ± .098	3.207 ± .157	
Sum	177 4.5	5259 152.9		1.110 ± .073	6.352 ± 1.188	
Run 28						
A	174± 3.0	3851± 132.0		1.000± .054	25.000± .601	
32	2452 29.0	72457 820.3	18107.3± 2325.1	1.333 ± .055	235.225 ± 4.888	4.07E 06± 3.62E 05
16	1564 24.1	45103 617.3	10423.1 1557.2	1.301 ± .056	225.145 ± 5.160	2.78E 07 2.11E 06
8	1118 17.9	32795 479.8	8015.0 1133.9	1.323 ± .058	160.869 ± 3.755	1.57E 08 1.13E 07
4	3163 41.7	94402 923.4	24290.4 2983.0	1.346 ± .056	455.164 ± 9.790	4.24E 09 4.42E 08
2	740 12.8	22565 482.1	6171.5 840.5	1.376 ± .065	106.425 ± 2.585	5.69E 09 3.83E 08
1	161 3.8	5169 174.6	1610.6 237.1	1.453 ± .082	23.105 ± .676	9.83E 09 7.57E 08
h	193 7.9	6794 183.9	2521.8 303.8	1.590 ± .099	27.732 ± 1.237	1.59E 11 2.59E 10
Sum	9390 61.0	279285 1560.2		1.342 ± .053	1233.664 ± 12.997	
Run 30						
A	75± 6.3	3844± 453.6		1.000± .205	25.000± 2.964	
32	3 ± .5	237 33.6	100.2± 45.5	1.731 ± .459	.594 ± .113	1.03E 04± 8.41E 03
16	3 ± .6	288 34.9	121.4 51.5	1.728 ± .447	1.085 ± .213	1.48E 05 1.21E 05
8	5 ± .9	456 54.0	211.5 79.7	1.865 ± .699	1.590 ± .332	1.68E 06 1.34E 06
4	21 1.8	2079 241.7	1018.9 300.1	1.961 ± .400	6.896 ± .821	6.79E 07 4.54E 07
2	22 2.1	2296 267.1	1175.0 330.3	2.048 ± .428	7.290 ± .928	4.68E 08 2.03E 08
1	8 1.1	869 101.9	453.0 131.4	2.089 ± .484	2.704 ± .435	1.21E 09 3.05E 08
h	13 2.0	1571 188.8	924.5 234.1	2.431 ± .597	4.202 ± .750	2.52E 10 1.74E 10
h	77 6.5	3780 448.5		.955 ± .196	25.731 ± 3.056	
Sum	74 3.8	7796 425.5		2.056 ± .335	24.361 ± 1.568	
Run 31						
A	83± .7	4745± 56.5		1.000± .021	25.000± .317	
32	8 ± .8	19741 461.6	19305.± 464.1	45.352 ± 5.214	1.529 ± .171	2.65E 04± 1.27E 04
16	1 ± .3	5308 77.3	5276.0± 79.3	163.964 89.728	.171 ± .093	1.70E 04 1.16E 04
8	1 ± .2	4043 56.7	3933.1 38.0	80.326 15.902	.265 ± .052	2.83E 05 3.26E 05
4	1 ± .2	1561 35.5	1492.1 37.0	22.508 3.460	.366 ± .035	3.06E 06 1.89E 06
2	1 ± .2	860 21.9	829.4 25.0	28.045 10.984	.161 ± .063	6.68E 06 7.22E 06
1	0 ± .3	247 2.6	231.2 14.8	15.573 14.295	.084 ± .077	9.19E 06 7.22E 06
h	1 ± .3	225 9.7	183.6 18.7	5.490 2.154	.213 ± .084	3.88E 07 7.78E 07
h	77 ± .7	2191 30.5		.498 ± .011	25.175 ± .288	1.39E 09 2.94E 09
Sum	12 1.0	31986 471.4		47.402 ± 4.267	2.791 ± .246	
Run 32						
A	10± 2.3	1546± 78.6		1.000± .078	25.000 ± .788	
32	20 ± .7	700 22.0	405.7± 29.6	2.381 ± .176	3.167 ± .139	5.48E 04± 1.04E 04
16	33 ± .6	1263 31.8	777.9± 42.4	2.604 ± .165	7.841 ± .221	1.17E 06 1.54E 05
8	17 ± .5	701 24.8	453.8± 29.3	2.838 ± .206	3.992 ± .151	3.61E 06 3.59E 05
4	3 ± .2	148 5.8	100.5 ± 7.4	3.120 ± .324	.766 ± .062	5.05E 06 7.38E 05
2	1 ± .4	27 4.4	16.4 7.4	2.592 ± 1.536	.167 ± .095	8.89E 06 6.74E 06
1	1 ± .4	8 3.3	1.6 7.0	1.077 ± .955	.126 ± .099	6.13E 07 1.39E 08
h	0 ± .4	13 3.0	11.5 6.2	8.393 ± 29.357	.025 ± .087	1.16E 08 5.66E 08
h	103 1.7	1613 41.4		1.053 ± .067	24.772 ± .690	
Sum	73 1.3	2859 46.7		2.616 ± .158	16.084 ± .348	
Run 33						
A	102± 6.9	1615± 151.7		1.000± .164	25.000± 2.399	
32	26 1.7	4011 365.5	3602.4± 369.6	9.810 ± 1.589	4.221 ± .403	7.31E 04± 3.00E 02
16	72 4.7	11164 1017.3	10034.8 1028.4	9.883 ± 1.598	17.689 ± 1.659	2.68E 06 1.37E 04
8	75 5.3	20533 1906.9	19749.5 1913.7	17.686 ± 2.887	18.324 ± 1.789	1.84E 07 6.22E 04
4	19 1.9	13599 1235.6	13293.8 1236.4	44.592 ± 7.891	4.721 ± .563	3.18E 07 9.90E 04
2	2 ± .3	1517 139.2	1478.1 139.5	38.495 ± 9.011	.610 ± .118	3.14E 07 1.28E 05
1	1 ± .5	115 10.6	104.3 12.9	10.603 ± 7.358	.168 ± .115	7.29E 07 7.93E 05
h	1 ± .3	103 10.6	87.9 11.9	6.874 ± 2.585	.232 ± .081	1.38E 09 2.28E 07
Sum	196 7.6	51443 2520.2		16.636 ± 2.190	45.765 ± 2.545	
Run 34						
A	97± 2.8	1800± 79.7		1.000± .075	25.000± 1.029	
32	4 ± .6	620 30.9	553.7± 33.2	9.305 ± 1.771	.617 ± .110	
16	(.08) ± .4	906 47.0	0. 0.	(.668) ± .7	.020 ± .102	
8	-1 ± .5	925 36.0	0. 0.	0. 0.	-.157 ± .125	
4	1 ± .4	882 35.2	866.7 ± 35.9	56.449 ± 26.076	.217 ± .099	
2	3 ± .8	339 15.7	291.8 ± 21.4	7.123 ± 2.203	.662 ± .200	
1	1 ± .6	98 7.6	70.6 ± 14.1	3.606 ± 1.603	.376 ± .164	
h	1 ± .3	70 4.0	42.5 ± 7.3	2.568 ± .602	.376 ± .084	
Run 35						
>16	8± 1.0	1578± 68.3	1425.5± 71.2	10.479± 1.484	2.088± .264	
8	(.0465) ± .6	1375 54.2	0. 0.	(1594) ± .7	.012 ± .165	
<8	9 1.1	2284 94.0	2124.3 96.5	14.333 ± 2.054	2.213 ± .287	
h	97 2.8	1816 90.7		1.012 ± .079	24.921 ± 1.027	

## APPENDIX C

## FUZZ--AN ERROR PROPAGATION MODE FOR MAD

FUZZ is an example of the flexibility of MAD as described in the Appendices to the MAD Manual. To the author's knowledge, it is the most ambitious extension undertaken, consisting of some two dozen operators defining a double-word Mode 6 (with the second word carrying the variance through all defined operations). Working with double-word arithmetic has uncovered several bugs in the MAD compiler. The fatal bugs have been fixed at MIT, some non-fatal ones remain (particularly in the integer arithmetic set, which fails to examine both active machine registers) and must be written around.

A write-up of FUZZ is available from the MIT Computation Center as Memo CC-249, but the program itself has not been published elsewhere.

Also included are SS and SSS, required double-word versions of the MAD subscripting routines .03311 and .MTX respectively, together with SIN6 and COS6, versions of SIN and COS which return error estimates.



```

FDP      8
STG      LOC+2
TRA      LOC+2
PZE
CLA      LOC-5
      8-13
STO      LOC+2
TRA      LOC+3
PZE      LOC-1
STG      A
CLA      LOC-3
FDP      LOC+2
STG      LOC+2
TRA      A+1
CLA      LOC-8
FDP      KCA
KCA
FDP      LOC-10
CLA      LOC-5
OUT      ACO
JMP      8-12,8T,8-39
END
MODE STRUCTURE 6/1 TO 6
JMP      8+2,AC,8+1
JMP      8+32,MB,8+10
JMP      8+10,8T,8+1
JMP      8+28,AT,8+1
JMP      8+9,MB,8+1
STO      T
JMP      8+5
STG      T
JMP      8+3
STO      DT
DT      DT+1
CLA      B
ORA      -2330000000000K
FAD      LOC+2
STO      LOC+2
TRA      PZE
CLA      A
FDP      LOC-6
      -1.
PSJ      LOC-8
STO      A+1
FDP      LOC-10
KCA
FDP      LOC-12
CLA      LOC-8
ACO
OUT

```

```

STO      LOC+2
TRA      LOC+2
PZE      LOC+2
STG      LOC+2
TRA      LOC+2
PZE      B
      -2330000000000K
FAD      -2330000000000K
STO      LOC+2
TRA      LOC+2
PZE      LOC-10
CLA      LOC-2
FDP      LOC+2
STO      LOC+2
TRA      LOC+2
PZE      LOC-6
CLA      -1.
PSB      LOC-8
STO      LOC-15
CLA      LOC-15
JMP      8-26
JMP      8+1,8T,8-46
KCA
JMP      8-43
END
MODE STRUCTURE 6/6 TO 6
JMP      8+2,AC,8+1
JMP      8+6,MB,8+10
JMP      8+35,8T,8+1
JMP      8+22,AT,8+1
JMP      8+5,MB,8+1
STO      T
JMP      8+5
STG      T
JMP      8+3
STO      DT
DT      DT+1
CLA      A
FDP      B
STG      LOC+2
TRA      LOC+2
PZE      LOC-1
XCA      B+1
FDP      A+1
FAD      B
FDP      B
XCA      B
CLA      LOC-8
OUT      ACO
STO      LOC+2
TRA      LOC+2
PZE

```



```

STO      LOC+2
TRA      LOC+2
PZE      B
CLA      -1.
XCA      A
CLA      -POWER0...
STO      LOC+2
TRA      LOC+2
PZE      XCA
XCA      LOC-2
PMP      LOC-12
XCA      A+1
LDB      LOC-7
STO      LOC-8
PMP      A
LDB      LOC-10
OUT      ACB
STO      LOC+3
TRA      LOC+3
PZE      B
LDB      B
PMP      LAC+2
TRA      LOC+2
PZE      B
CLA      -1.
XCA      LXC-10
CLA      -POWER0...
STO      LOC+2
TRA      LOC+2
PZE      XCA
XCA      LOC-2
PMP      LOC-12
XCA      LOC-19
LDB      LOC-7
STO      LOC-8
PMP      LOC-23
LDB      LOC-10
OUT      ACB
END

JMP      MAKE STRUCTURE 0.P.1 TO 6
        0+2.AC.0+1

```

```

JMP      0+4.MB.0+22
JMP      0+11.BT.0+1
JMP      0+04.AT.0+1
JMP      0+6.MB.0+6
JMP      0+9.BT.0+1
T
0+12
T
0+10
BT
BT+1
0+7
XCA      LOC+2
TRA      LOC+2
PZE      LOC-1
STO      LOC+2
TRA      LOC+2
PZE      LOC-3
JMP      0+7
B
B
STO      LOC+2
TRA      LOC+2
PZE      B
CLA      -1
A
-Power1...
LOC+2
LOC+2
LOC-2
LOC-12
A+1
LOC-7
LOC-8
A
LOC-10
ACB
STO      LOC+3
TRA      LOC+3
PZE      B
CLA      -1
SUB
XCA
XCA
CLA
TSX
TSX
STO      LOC+2
TRA      LOC+2
PZE      XCA
XCA      LOC-2
PMP      LOC-12
XCA      A+1
LDB      LOC-7
STO      LOC-8
PMP      A
LDB      LOC-10
OUT      ACB
STO      LOC+3
TRA      LOC+3
PZE      XCA
XCA      LOC-2
PMP      LOC-12
XCA      LOC-19
LDB      LOC-7
STO      LOC-8
PMP      A
LDB      LOC-10
OUT      ACB
STO      LOC+3
TRA      LOC+3
PZE      B
LDB      B
PMP      LOC+2
TRA      LOC+2

```



```

RCA AC
OUT
END
NODE STRUCTURE .ABS-6 TO 6
JMP ++12.BT,++1
JMP ++1.AC,++2
JMP ++6.MB,++2
JMP ++3.MB,++7
STO T
++3
T
T
JMP ++3
DT
STO BT+1
CLA B
LDG B+1
GSP
OUT
END
NODE STRUCTURE .RMB-6 TO 6
JMP ++12.BT,++1
JMP ++1.AC,++2
JMP ++6.MB,++2
JMP ++3.MB,++7
STO T
++3
T
JMP ++3
DT
STO BT+1
CLA B
LDG B+1
GSP
OUT
END
NODE STRUCTURE 4...BTM-6
JMP CLA
LDG B+1
TBA FF
OUT
END
NODE STRUCTURE 0...BIF-6 TO 2
JMP ++1.AC,++6
JMP ++6.MB,++1
JMP ++13.AT,++1
STO T
++10
JMP ++12.BT,++7
JMP ++1.MB,++6
JMP ++1.AT,++3
RCA ++6
STO T
++3

```

```

++1.AC,++2
++6.MB,++2
++3.MB,++7
T
++3
T
JMP ++3
DT
STO BT+1
CLA B+1
OUT
RCA AC
OUT
END
DEFINE UNARY OPERATOR .PS... PRECEDENCE HIGHER THAN .MDT.
NODE STRUCTURE .PS-6 TO 0
JMP ++13.BT,++1
JMP ++1.AC,++2
JMP ++6.MB,++2
JMP ++3.MB,++7
T
++3
T
JMP ++3
DT
STO BT+1
CLA B+1
TBA -SORT...
OUT
RCA AC
++3
END
DEFINE UNARY OPERATOR .PR... PRECEDENCE HIGHER THAN .MDT.
NODE STRUCTURE .PR-6 TO 0
JMP ++15.BT,++1
JMP ++1.AC,++2
JMP ++6.MB,++2
JMP ++3.MB,++7
T
++3
T
JMP ++3
DT
STO BT+1
CLA B+1
TBA -SORT...
RCA AC
OUT
RCA AC
STO LOC+2
TBA LOC+2
PZE
TBA -SORT...
RCA AC
STO LOC-2

```



```

*SS
FAP TWO-DIMENSIONAL MATRIX SUBSCRIPTION ROUTINE FOR DOUBLE WORDS
  REM CALLING SEQUENCE
  CLA 1
  LDQ J
  TSX (SS+4)
  TAY A+ADIM
  REM A IS THE BASE ADDRESS A10)
  REM ADIM IS THE DIMENSION VECTOR ADDRESS
  COUNT 24
  LBL S5,X
  ENTRY SS
  STO J
  CLA 2,4
  ONE
  XCA
  CAL 1,4
  PDC 0,1
  VJM -3,1,15
  LLS 15
  ADD J
  SUB ONE
  ALS 1
  ADD -2,1
  TRA 2,4
  PZE 1
  BSS 1
  SYN 0
  END

```

```

  ADD
  SUB
  STA
  PAD
  VEMD
  2,4
  -1
  0+1,1,1
  TXL
  STO
  LDQ
  VJM
  LLS
  TAY
  ALS
  ADD
  TRA
  BSS
  SYN
  END

  LOOP
  VEMD
  OUT
  BADD
  TEMP
  END

  COMPUTE END OF DIM VECTOR
  PLUS ONE, AND
  STORE IT.
  ZERO TO INITIALIZE SUM.
  SUM(I,J) J=1...N
  SUM(I,J)-1
  INCREMENT K.
  TEST FOR (N-1) MULTIPLICATIONS.
  WHICH GETS N(I).
  (SUM(I,J)-1)*N(I) K=2...N
  INCREMENT J, AND START ON NEXT INDEX.
  ZOSUM
  ZOSUM+8
  RETURN.

```

```

*SSS
FAP N-DIMENSIONAL MATRIX SUBSCRIPTION ROUTINE
  FOR DOUBLE WORDS
  FOR A11,12,13) IN AN N1 X N2 X N3 MATRIX
  WITH A11,1,1)=A(B), SSS RETURNS A LINEAR
  SUBSCRIPT..
  2*((I1-1)*(A2+12-1))+(N3+15-1)))+8
  WHICH HAS THE NET RESULT OF GETTING
  ALTERNATE WORDS FROM CORE.
  COUNT 30
  LBL S55,X
  ENTRY SSS
  CLA 1,4
  ARS 18
  SUB -1
  STA NADD
  SUB -1
  STA BADD
  CLS 00
  PAC .1

```

```

  GET ADR. OF DIM. VECTOR
  AND
  FROM IT, THE ADR. OF N
  WHICH IS STORED.
  AS IS THE ADR. OF B
  FETCH (N)
  AND PUT IT IN IR 1.

  OUT
  EXTERNAL FUNCTION (R)
  INSERT FILE FUZZ
  E=O SIN6.
  ANGLE =DA, R(1)
  ERROR =VA, R(1)
  T = SIN.(ANGLE)
  U = COS.(ANGLE)
  T=O OUT
  E=O COS4.
  ANGLE =DA, R(1)
  ERROR =VA, R(1)
  T = COS.(ANGLE)
  U = SIN.(ANGLE)
  TRIG(1) =DA, T
  TRIG(1) =VA, (U+U)
  F=M TRIG(1)
  D=M TRIG(1)
  MODE NUMBER 6 X, TRIG
  E=M

```

ONE(11).BA.1.  
ONE(11).VA.0.

```

STO DT
STO DT+1
CLA A
FSB B
OUT AC
FSB A
CMS A
OUT AC
END
MODE STRUCTURE 6..DIF.0 TO 2
JMP ++1.AC,++6
JMP ++4.MD,++1
JMP ++14.BI,++1
STO T
JMP ++8
JMP ++8.AI,++3
JMP ++1.MD,++6
JMP ++8.BI,++1
STO T
JMP ++3
STO DT
STO DT+1
CLA A
FSB B
OUT AC
KCA A
FSB A
CMS A
OUT AC
END
MODE STRUCTURE 6..DIF.6 TO 2
JMP ++1.AC,++6
JMP ++3.MD,++1
STO T
JMP ++8
JMP ++8.AI,++1
JMP ++9.BI,++4
JMP ++1.MD,++5
STO T
JMP ++3
STO DT
STO DT+1
CLA A
FSB B
OUT AC
FSB A
CMS A
OUT AC
END
D*N ZERO(11)
MODE NUMBER 6 ZERO
ZERO(11).BA.0.
ZERO(11).VA.0.
D*N ONE(11)
MODE NUMBER 6 ONE

```

## APPENDIX D

## MODEL OF ECCENTRIC RADIOACTIVE SOURCE AND DETECTOR

This is an on-line program, allowing man-machine interaction at various points.

SHARP evaluates the sensitivity, flux, and response, at each point, and sums the response into a total. (Summation is preferable to integration because of the high pole directly above the source, which cannot be analytically treated. Even a Fourier integration returns position-dependent answers.)

BELKMN rotates the source under the detector and monitors the user's wishes concerning the several parameters. PICS is used for print-out of various intermediate results, and all printing is done with CIRCLE, which creates a circular map of the detector.

```

*****CHECKM *****
INSERT FILE COMMAND
PI = 314159265
SIZE = 11
N = 5
A = 2
INCR = 1
INCY = 1

START

WAR = 0
WIN = 1.0E10
INTEG = 0
PRINT COMMENT SPLAJE TYPE IN NEAT DATA JCI.0
READ DATA
THIS CARD WILL CONTAIN THINGS LIKE ***
R ADO. DIES. N. AND PIC.
DDI2) = SIZE
STEP = (SIZE-1)/10
SCALE = 5.71STEP0.1
RANGE = (SIZE-1)/2
RMAX = (RANGE+STEP+STEP)SCALE
A2 = A/A
E2 = E/E
D2 = D/D
SD = D
PRINT COMMENT S MAPS
PI T SCAL. WHICH
M R MICR. NE. SVES
TIM ROTAT. FOR L. .... N. 1.
A = 01/NL
M R L. G. N. 1.
D = 0.
D2 = 0.
E/L
SIN = SIN(A)
COS = COS(A)
SHARP(1) = 1
O/E
TIM MAPPER FOR VIL-RANGE OF P. 1. 0. RANGE
VS = VILSCALE
J = VILRANGE
J = MAPPER FOR ALI-RANGE OF P. 1. 0. RANGE
KS = VILSCALE
D2 = KS/SVSVS
M R D2. G. R. A. K. T. O. MAPPER
D = SORT(102)
SIN = VS/D
COS = KS/D
SHARP(1) = INC(INCY)
I = I/RANGE
I = I/TOTALS
A = I-INTEG(I)/GAIN(I)G. 4. INTEG-INTEG(I)

```

MAPPER

```

D2 = SDZ
D = SD
TIM MMLZ. FOR I-1. STEP 0. G. SIZE
TIM MMLZ. FOR J-1. STEP 0. G. SIZE
INTEG(I) = INTEG(I)/INTEG
CIRCLE. INTEG. G. SIZE
PIT MAPP. INTEG
PIT NOSP. A. B. C. F. G
T O START
E/L
M R PIC. M. E. N. C. S. P. I. L. S.
M R TOTALS. G. M. A. A. N. D. D. N. E. 0. M. A. X. TOTALS
M R TOTALS. L. O. M. I. N. A. N. D. D. N. E. 0. M. I. N. TOTALS
M R L. E. M. N. 1. TOTALS
CENTR = TOTALS
D = SD
D2 = SDZ
T O ROTAT
E/L
M R L. E. 0. O. R. L. E. N
INTEG = INTEG/TOTALS/2
O/E
INTEG = INTEG/TOTALS
E/L
PIT 5279.208. M. 180. /PI. TOTALS

```

ROTAT

```

ROTAV = INTEG/M
M R A. G. 0. PIT INTEG. SD. M. A. R. M. A. R. /CENTR. L. O. M. I. N. /CENTR. L.
IROTAV. ROTAV/CENTR. L. CENTR. L.
T O START

```

TYPOGRAPHY

```

VS INTEG. S. S. 28. EFFECT OF ROTATION ON COUNT
L27. WITH SOURCE ECCENTRICITY D OF 7.23M MM/
2510. MAXIMUM F. 0. 0. 9. 5. /510. MINIMUM F. 0. 0. 9. 5. /
3510. M. R. T. A. V. F. 0. 0. 9. 5. /510. CENTR. F. 0. 0.
V/S MAPP = 51.30. RELATIVE COUNTS VS. SAMPLE POSITION.
1. MULTIPLY COUNTS BY 0.11048
V/S NOSP = 55.14. SOURCE DIST A OF 7.23M MM/55.
1. COMPARE COEF. F OF 7.27/55. 14. 0. 0. 0. 0. ECC. E OF 7.23M MM/
2510. PLANE COEF. C OF 7.27/55. 14. 0. 0. 0. 0. 0.
351M MM/55. 14. THROUGH COEF. G OF 7.23M
E/M

```





## BIBLIOGRAPHY

- Allan, R. S., G. E. Charles, & S. G. Mason, 1961: The approach of gas bubbles to a gas/liquid interface. *J. Coll. Sci* 16, 150-165.
- Arnold, J. D., & C. Y. C. Pak, 1962: Protein-protein interaction at the air-water interface. *J. Coll. Sci.* 17, 348-362.
- Ballentine, R., 1954: High efficiency still for pure water. *Anal. Chem.* 26, 549-550.
- Bateman, H., 1962: Partial Differential Equations of Mathematical Physics, Chap. 10, Dover, New York.
- Baylor, E. R., W. H. Sutcliffe, Jr., & D. S. Hirschfeld, 1962: Adsorption of phosphate onto bubbles. *Deep sea Res.* 9, 120-124.
- Baylor, E. R., & W. H. Sutcliffe, Jr., 1963: Dissolved organic matter in seawater as a source of particulate food. *Limn. & Oceanog.* 8, 369-371.
- Blanchard, D.C., 1963: The electrification of the atmosphere by particles from bubbles in the sea. Progress in Oceanography 1, Chapter 2, 71-202, Pergamon Press, New York.
- Blanchard, D.C., 1964: Sea-to-air transport of surface active material. *Science* 146, 396-397.
- Briggs, D. R., 1940: The metaphosphate protein reaction. *J. Biol. Chem.* 134, 261-272.
- Day, J. A., 1964: Production of droplets and salt nuclei by the bursting of air-bubble films. *Quart. J. Roy. Meteor. Soc.* 90, 72-78.
- Dean, G. A., 1962: The iodine content of some New Zealand drinking waters with a note on the contribution from sea spray to the iodine in rain. *New Zealand J. Sci.* 6, 208-214.
- DeVries, A. J., 1958: Foam Stability. *Rubber Chem. & Tech.* 31, 1142-1205.
- Drabikowski, W., 1963: Formation of complexes of adenosine triphosphate and orthophosphate with protein. *Lodz. Towarz. Nauk, Wydział III* 91, 72 pp. CA 60:4383g.

- Duce, R.A., J.T. Wasson, J.W. Winchester, & F. Burns, 1963: Atmospheric iodine, bromine and chlorine. *J. Geophys. Res.* 68, 3943-3947.
- Duce, R. A., J. W. Winchester, & T. W. Van Nahl, 1965: Iodine, bromine, and chlorine in the Hawaiian Marine Atmosphere. *J. Geophys. Res.* 70, 1775-1799.
- Dueul, H., & H. Neukom, 1949: Über die Reaktion von Borsäure und Borax mit polysacchariden. *Makromol. Chem.* 3, 13-30.
- Eagland, D., & F. Francks, 1960: Interfacial hydrolysis of soap and detergent solutions. 3rd Internat. Cong. on Surf. Act. Cologne, Vol. 11, 539-544.
- Duursma, E. K., 1960: Dissolved organic carbon, nitrogen and phosphorus in the sea. *Neth. J. Sea Res.* 1, 1-148.
- Eriksson, E., 1957: The chemical composition of Hawaiian rainfall. *Tellus* 9, 509-520.
- Eriksson, E., 1959: The yearly circulation of chloride and sulfur in nature; meteorological, geochemical and pedological implications. Part I. *Tellus* 11, 375-403.
- Eriksson, E., 1960: The yearly circulation of chloride and sulfur in nature; meteorological, geochemical and pedological implications. Part II. *Tellus* 12, 63-109.
- Facy, L., 1951: Embruns et noyaux de condensation. *J. Sci. de la Meteor.* 3, 62-68.
- Frank, F. C., 1949: The influence of dislocations on crystal growth. *Disc. Farad Soc.* 5, 48-54.
- Franks, F., 1961: A continuously operating still for high purity water for use in surface chemistry. *Chem. & Ind.* (1961), 204-205.
- Fox, S. W., 1960: How did life begin? *Science* 132, 200-208.
- Gast, J. A., & T. G. Thompson, 1959: Evaporation of boric acid from sea water. *Tellus* 11, 344-347.
- Gibbs, J. W., 1878: Collected Works. Yale, New Haven, p 229 ff.
- Glimcher, M. J., & S. M. Crane, 1964: The incorporation of radioactive inorganic orthophosphate as organic phosphate by collagen fibrils in vitro. *Biochem.* 3, 195-202.

- Goetz, A., 1965: The constitution of aerocolloidal particulates above the ocean surface. Proc. Internat. Conf. Cloud Physics, Tokyo & Sapporo, May-June. p 42-44.
- Goodrich, F. C., 1957: Molecular interaction in monolayers. 2nd Internat. Cong. Surf. Act., Vol I, 85-91.
- Guest, W. L., & W. C. M. Lewis, 1939: The effect of electrolytes upon the interfacial tension between water and dekalin. Proc. Roy. Soc. London A170, 501-513.
- Harvey, H. W., 1955: The Chemistry and Fertility of Sea Water. Cambridge Univ. Press, Cambridge. 224 pp.
- Hassid, W. Z., G. T. Cori, & R. M. McReady, 1943: Constitution of the polysaccharide synthesized by the action of crystalline muscle phosphorylase. J. Biol. Chem. 148, 89-96.
- Hunt, J. D., & K. A. Jackson, 1965: Nucleation of solid in an undercooled liquid by cavitation. Paper presented at Internat. Symp. on Nucleation Phenomena, April, Cleveland.
- Isono, K., 1957: On sea salt particles in the atmosphere. Geofis. pur. appli. 36, 156.
- James, J. W., & B. A. Pethica, 1960: Ion exchange at surfaces containing lauryl sulphate. 3rd Internat. Cong. on Surf. Act. Cologne, Vol. II, 227-233.
- Jirgensons, B., 1962: Natural Organic Molecules. Pergamon, N. Y., p 167.
- Judson, C. M., A. A. Lerew, J. K. Dixon, & D. J. Salley: Radiotracer study of sulfate ion adsorption at the air/solution interface in solutions of surface-active agents. J. Phys. Chem. 57, 916-923.
- Junge, C. E., 1953: Die Rolle der Aerosole und der gasförmigen Belmenunger der Luft im Spurenstoffhaushalt der Troposphäre. Tellus 2, 1-26.
- Junge, C. E., & R. T. Werby, 1958: The concentration of chloride, sodium, potassium, calcium, and sulfate in rain over the United States. J. Meteor. 15, 417-425.
- Katchmann, B. J., & J. R. VanWazer, 1954: Soluble and insoluble phosphates of yeast. Biochim. et Biophys. Acta 14, 445-446.
- Ketchum, B. H., N. Corwin, & D. J. Keen, 1955: The significance of organic phosphorus determinations in

- ocean water. *Deep sea Res.* 2, 172-181.
- Kitchener, J. A., 1958: Use of ion exchange resins in preparing water of high purity. *Nature* 182, 1667.
- Kientzler, C. F., A. B. Arons, D. C. Blanchard, & A. H. Woodcock, 1954: Photographic investigation of the projection of droplets by bubbles bursting at a water surface. *Tellus* 6, 1-7.
- Klevens, H. B., 1950: Solubilization. *Chem. Rev.* 47, 1-74.
- Knelman, F., N. Dombrowski, & D. M. Newitt, 1954: Mechanism of the bursting of bubbles. *Nature* 173, 261.
- Köhler, H., and M. Båth, 1952: Quantitative chemical analysis of condensation nuclei from sea water. *Nova Acta Reg. Soc. Scient. Upsaliensis* 15:7, 24 pp.
- Komabayasi, M., 1962: Enrichment of inorganic ions with increasing atomic weight in aerosol, rainwater and snow in comparison with sea water. *J. Meteor. Soc. Japan* 40, 25-38.
- Latimer, W. M., 1952: Oxidation Potentials, 2nd ed. Prentice-Hall, Englewood Cliffs.
- Lewis, G.N., M. Randall, K. S. Pitzer, & L. Brewer, 1961: Thermodynamics. McGraw-Hill, N. Y., Chapter 29.
- MacIntyre, F., 1965: FUZZ--An error-propagation mode for MAD. MIT Comp. Center Memo CC-249.
- McBain, J. W., & C. W. Humphreys, 1932: The microtome method of determination of the absolute amount of adsorption. *J. Phys. Chem.* 36, 300-311.
- Miller, R. B., 1961: The chemical composition of rainwater at Taika, New Zealand. *New Zealand J. Sci.* 4, 844-853.
- Mitchell, R. I., & J. M. Pilcher, 1959: Improved cascade impactor for measuring aerosol particle size. *Ind. Eng. Chem.* 51, 1039-1042.
- Miyake, Y., 1948: The chemical nature of the saline matter in the atmosphere. *Geophys. Mag.* 16, 64-65.
- Miyake, Y., & S. Tsunogai, 1963: Evaporation of iodine from the ocean. *J. Geophys. Res.* 68, 3938-3993.
- Miyake, Y. & S. Tsunogai, 1965: Chemical composition of oceanic rain. *Proc. Internat. Conf. Cloud Physics, Tokyo & Sapporo, May-June.* p 73-78.

- Moore, D. J. 1952: Measurements of condensation nuclei over the North Atlantic. *Quart. J. Roy. Met. Soc.* 78, 596-602.
- Moore, D. J., & B. J. Mason, 1954: The concentration, size distribution and production rate of large salt nuclei over the oceans. *Quart. J. Roy. Meteor. Soc.* 80, 583-590.
- Munckzak, F. 1960: On the appearance of ninhydrin positive substances in the atmosphere. *Tellus* 12, 292-292.
- Nancollas, G. H. & N. Purdie, 1964: The kinetics of crystal growth. *Quart. Rev.* 18, 1-20.
- Naude, C. F., & A. T. Ellis, 1961: On the mechanism of cavitation damage by nonhemispherical cavities collapsing in contact with a solid boundary. *Trans. ASME Ser. D, J. Basic Eng.* 648-656.
- Naudet, M. & P. Desnuelle, 1948: Analyse et fabrication des produits de condensation peptides-acides gras (Lamepons, Maypons). *Oleagineux* 2, 458-463.
- Newitt, D. M., 1954: Bursting of bubbles at an air-water interface. *Nature* 173, 1048.
- Nishisawa, S., M. Fukuda, & N. Inoue, 1954: Photographic study of suspended matter and plankton in the sea. *Bull. Fac. Fish Hokaido Univ.* 2, 36-40.
- Oddie, B. C. V., 1962: The chemical composition of precipitation at cloud level. *Quart. J. Roy. Meteor. Soc.* 88, 535-538.
- Oncley, J. L., 1959: Chemical characteristics of proteins, carbohydrates, and lipids. in J. L. Oncley, ed., Biological Science--A study program. pp 30-49. Wiley, New York.
- Ossipow, L., F. D. Snell, & J. Hickson, 1957: The surface chemistry of alkyl esters of sucrose. 2nd Internat. Cong. on Surf. Act., Vol. 1, 50-55.
- Perlmann, G. E., 1955: The nature of phosphorus linkages in phosphoproteins. *Advances in Protein Chem.* 10, 1-30.
- Ranz, W. E., 1959: Some experiments on the dynamics of liquid films. *J. App. Phys.* 30, 1950-1955.
- Ranz, W. E., & J. B. Wong, 1952: Impaction of dust and smoke particles on surface and body collectors. *Ind. & Eng. Chem.* 44, 1371-1381.
- Randles, J. E. B., 1957: Ionic hydration and the surface potential of aqueous electrolytes. *Disc. Farad. Soc.* 24, 194-199.

Rayleigh, Lord, 1878: On the instability of jets. Proc. Lon. Math. Soc. 10, 4-13.

Rayleigh, Lord, 1892: On the instability of a cylinder of viscous liquid under capillary force. Phil. Mag. S. 5, 34, 145-154.

Rayleigh, Lord, 1891: Some applications of photography. Nature 44, 249-254.

Riley, G. A., 1963: Organic aggregates in seawater and the dynamics of their formation and utilization. Limn. & Oceanog. 8, 372-381.

Rossby, C.-G., & H. Egner, 1955: On the chemical climate and its variation with the atmospheric circulation pattern. Tellus 7, 118-133.

Rossby, C.-G., 1959: Current problems in meteorology. p 44, in B. Bolin, Ed.: The Atmosphere and the Sea in Motion, Rockefeller Inst. Press, N.Y.

Schaefer, V. J., 1952: Continuous cloud chamber. Ind. & Eng. Chem., 44, 1381-1382.

Scheludko, A., D. Eskerova, & D. Platikanov, 1963: The kinetics of the thinning and rupture of thin liquid films. Koll. Zh. 25, 606,612.

Schenkel, J. H., & J. A. Kitchener, 1958: Contamination of surfaces by conductivity water from ion exchange resins. Nature 182, 131.

Sebba, F., 1960: Ion Flotation. Elsevier, Amsterdam.

Shinoda, K., & K. Ito, 1961: Selective adsorption studies by radiotracer technique: The selective adsorption between calcium and sodium ions at the ionized interface. J. Phys. Chem. 65, 1499-1502.

Sugawara, K., 1959: Syn-bubble-bursting fractionation of sea salt. Internat. Oceanog. Cong. Preprints, 875-877.

Sugawara, K., 1961: Effect of sea breeze on the chemical composition of coastal fresh water lakes. Verh. Internat. Verein. Limnol. 14, 889-892.

Suglura, Y., 1965: Effect of organic matter on constitution of sea salt in sea water bubbles. Proc. Internat. Conf. Cloud Physics, Tokyo & Sapporo, May-June. p 47-51.

Sutcliffe, W. H., Jr., E. R. Baylor, & D. W. Menzel, 1963: Sea surface chemistry and Langmuir circulation. Deep-sea Res. 10, 232-243.

- Toba, Y., 1959: Drop production by bursting of air bubbles on the sea surface (2) Theoretical study on the shape of floating bubbles. *J. Ocean. Soc. Japan* 15, 121-130.
- Valko, E. I. & M. B. Epstein, 1957: Comicellization. 2nd Internat. Cong. on Surf. Act., Vol 1, 334-339.
- van Voorst Vader, F., 1960: Simultaneous adsorption of calcium and sodium ions at the surface of surfactant solutions. 3rd Internat. Cong. on Surf. Act. Cologne, Vol 11, 276-282.
- Vegotsky, A. & S. W. Fox, 1959: Pyropolymerization of amino acids to proteinoids with phosphoric acid or polyphosphoric acid. *Federation Proc.* 18, 343.
- Walling, C., E. E. Ruff, & J. L. Thornton, Jr., 1957: The adsorption of cations by anionic foams. *J. Phys. Chem.* 61, 486-489.
- Walton, A. G., 1965: Nucleation of crystals from solution. *Science* 148, 601-607.
- Wilson, A. T., 1959: Surface of the ocean as a source of air-borne nitrogenous material and other plant nutrients. *Nature* 184, 99-101.
- Woodcock, A. H., 1948: Note concerning human respiratory irritation associated with high concentrations of plankton and mass mortality of marine organisms. *J. Mar. Res.* 7, 56-62.
- Woodcock, A. H., 1953: Salt nuclei in marine air as a function of altitude and wind force. *J. Meteor.* 10, 362-371.
- Wolf, W. R., 1961: Study of the vibrating reed in the production of small droplets and solid particles of uniform size. *Rev. Sci. Inst.* 32, 1124-1129.
- Worthington, A. M., & R. S. Cole, 1897: Impact with a liquid surface studied by the aid of instantaneous photography. *Phil. Trans. Roy. Soc. Lon.* A189, 137-148.
- Worthington, A. M., & R. S. Cole, 1900: Impact with a liquid surface studied by the aid of instantaneous photography. *Phil. Trans. Roy. Soc. Lon.* A194, 175-200.

## BIOGRAPHICAL SKETCH

The author was born in [REDACTED] on [REDACTED] to [REDACTED]. It is unclear whether he ever graduated from high school, and if so, from whence. He has worked as a journeyman machinist, lumber dry kiln operator, and machine designer, and at sundry lesser trades. Reaching a point at which the real world became untenable, he retreated to the civilized academic world as a special student at San Diego State College in September 1956, while continuing to hold his night shift job as an engineering loftsmen at Rohr Aircraft Corporation. While at SDSC he was elected to Phi Eta Sigma and served as an officer.

He transferred to the University of California at Riverside as a junior in 1958, and received a Bachelor of Arts, with honors, in chemistry in June 1960. He had been a laboratory teaching assistant and a research assistant while at UCR, and was awarded the Secondo Cassini Memorial Scholarship in 1960.

Accepting a National Science Foundation Fellowship (twice renewed) he entered the Department of Chemistry at MIT in September 1960. While at MIT he taught freshman chemistry voluntarily for one semester (NSF policy on additional emolument to Fellows was then somewhat unclear) and subsequently held a teaching assistantship in the Spring term of 1961. He held a research assistantship in the Department of Chemistry, but conducted his research in the Geochemistry Laboratory of the Department of Geology and Geophysics for the years 1963-1965, under an interdepartmental agreement.

During his NSF Fellowship he spent the summer of 1961 working at the Musee d'Histoire Naturelle (Paris) on the Soret effect with Dr Jacques Chanu, and subsequent summers at MIT.

The author was elected to Sigma Xi while at MIT and has at various times been a student member of the American Geophysical Union and the American Chemical Society.

His hobbies include rock climbing and folk lore.

The  
typography  
and editing of  
this work were performed  
with the use of J. H. Saltzer's  
programs TYPSET and RUNOFF  
on the MIT Computation  
Center's Time  
Sharing  
system.

\* \*

\*

## ERRATA

Pg	Par	Ln	Change from:	to:
17	3	3	, and are ignored	are ignored
21	2	2	0.5 u	0.5 $\mu$
31	1	3	molec/cm	molec/cm <sup>2</sup>
		1		add: = 10 <sup>8</sup> cm <sup>2</sup> /l
33	2	3	1898	1897
45	1	5	1898	1897
54	2	2	2 to 3 u	2 to 3 $\mu$
78	2	10	PO ions	PO <sub>4</sub> <sup>-3</sup> ions
81	4	1	contribution	contribution
92	3	4	nodal point are	nodal point is
94	1	6	Na PO	Na <sub>3</sub> PO <sub>4</sub>
102	4	7	completly	completely
106	3	3	Occasionally	Occasionally
120	2	10	/256	/256 $\lambda$
140	2	5	(F=2.05)	(F <sub>z</sub> =2.05)
148	2	11	enrichment	enrichment
149	3	2	enrichment	enrichment
222	1	13	( $\partial I / \partial \theta$ )	( $\partial \Psi / \partial \theta$ )
223	1	2	$-\chi e^{2z}$	$-\chi_0 e^{2z}$